

---

# Geometric Median Matching for Robust $k$ -Subset Selection from Noisy Data

---

Anish Acharya \*  
UT Austin

Sujay Sanghavi  
UT Austin  
Amazon

Alexandros G. Dimakis  
UC Berkeley  
Bespoke Labs

Inderjit S Dhillon  
UT Austin  
Google

## Abstract

Data pruning – the combinatorial task of selecting a small and representative subset from a large dataset, is crucial for mitigating the enormous computational costs associated with training data-hungry modern deep learning models at scale. Since large-scale data collections are invariably noisy, developing data pruning strategies that remain robust even in the presence of corruption is critical in practice. However, existing data pruning methods often fail under high corruption rates due to their reliance on empirical mean estimation, which is highly sensitive to outliers.

In response, we propose Geometric Median (GM) Matching, a novel  $k$ -subset selection strategy that leverages the GM — a robust estimator with an optimal breakdown point of  $1/2$ ; to enhance resilience against noisy data. Our method iteratively selects a  $k$ -subset such that the mean of the subset approximates the GM of the (potentially) noisy dataset, ensuring robustness even under arbitrary corruption. We provide theoretical guarantees, showing that GM Matching enjoys an improved  $\mathcal{O}(1/k)$  convergence rate, outperforming  $\mathcal{O}(1/\sqrt{k})$  scaling of uniform sampling, even under arbitrary corruption. Extensive experiments across image classification and image generation tasks demonstrate that GM Matching consistently outperforms existing pruning approaches, particularly in high-corruption settings; making it a strong baseline for robust data pruning.

## Contents

<b>1</b>	<b>INTRODUCTION</b>	<b>3</b>
1.1	ROBUSTNESS VS DIVERSITY : . . . . .	3
1.2	OVERVIEW OF OUR APPROACH : . . . . .	3
1.3	CONTRIBUTIONS. . . . .	5
<b>2</b>	<b>RELATED WORK</b>	<b>6</b>
<b>3</b>	<b>PROBLEM SETUP : ROBUST DATA PRUNING</b>	<b>7</b>
3.1	CORRUPTION MODEL . . . . .	7
3.2	PROXY ENCODER . . . . .	9
<b>4</b>	<b>WARMUP: K-SUBSET SELECTION VIA MOMENT MATCHING</b>	<b>10</b>
4.1	VULNERABILITY UNDER GROSS CORRUPTION . . . . .	10

---

\*correspondence to: anishacharya@utexas.edu

<b>5</b>	<b>GEOMETRIC MEDIAN MATCHING</b>	<b>10</b>
5.1	ROBUST MEAN ESTIMATION . . . . .	11
5.1.1	APPROXIMATE GM . . . . .	12
5.2	ROBUST MOMENT MATCHING . . . . .	13
5.3	THEORETICAL GUARANTEE . . . . .	14
5.4	COMPUTATIONAL CONSIDERATIONS . . . . .	15
5.4.1	GM MATCHING SCALING LAW . . . . .	15
5.4.2	COMPUTATIONAL IMPROVEMENTS . . . . .	17
<b>6</b>	<b>EXPERIMENTS</b>	<b>19</b>
6.1	BASELINES . . . . .	19
6.2	APPROXIMATING FROM NOISY DISTRIBUTIONS . . . . .	20
6.3	IMAGE CLASSIFICATION . . . . .	22
6.3.1	EXPERIMENTAL SETUP . . . . .	22
6.3.2	IDEAL (NO CORRUPTION) SCENARIO: . . . . .	23
6.3.3	ROBUSTNESS TO IMAGE CORRUPTION: . . . . .	24
6.3.4	ROBUSTNESS TO LABEL CORRUPTION: . . . . .	25
6.3.5	ROBUSTNESS TO ADVERSARIAL ATTACKS: . . . . .	26
6.3.6	ABLATIONS WITH PROXY ENCODER . . . . .	27
6.4	UNCONDITIONAL IMAGE GENERATION . . . . .	32
<b>7</b>	<b>CONCLUSION AND LIMITATIONS</b>	<b>35</b>
<b>A</b>	<b>NOTATIONS AND ABBREVIATIONS</b>	<b>40</b>
<b>B</b>	<b>ADDITIONAL DEFINITIONS</b>	<b>41</b>
<b>C</b>	<b>LEMMA 3 : VULNERABILITY OF IMPORTANCE SCORE BASED PRUNING</b>	<b>42</b>
C.1	PROOF OF LEMMA 3 . . . . .	42
<b>D</b>	<b>PROOF OF THEOREM 1</b>	<b>43</b>
D.1	BOUNDING ESTIMATION ERROR FROM APPROXIMATE GEOMETRIC MEDIAN . . . . .	43
D.2	CONVERGENCE OF THE GREEDY UPDATES . . . . .	44
<b>E</b>	<b>PROOF OF LEMMA 1</b>	<b>46</b>
<b>F</b>	<b>COMPUTING GEOMETRIC MEDIAN</b>	<b>47</b>

# 1 INTRODUCTION

The recent success of deep learning has been largely fueled by the training of gigantic models on vast amounts of training data (Radford et al., 2018, 2021b; Brown et al., 2020; Touvron et al., 2023; Kaplan et al., 2020; Hestness et al., 2017). However, such large-scale training is usually associated with enormous computational costs, hindering the path to democratizing AI (Paul et al., 2021).

Data pruning – the combinatorial task of reducing a large training set into a small informative subset (Feldman, 2020; Agarwal et al., 2005; Muthukrishnan et al., 2005; Har-Peled, 2011; Feldman & Langberg, 2011), is a promising approach to reduce the enormous computational and storage costs of modern deep learning.

## 1.1 ROBUSTNESS VS DIVERSITY :

Consequently, a large body of recent work has been proposed to solve the **combinatorial subset selection** problem. At a high level, these approaches rely on some carefully designed importance scoring criterion to rank the training samples, retaining a fraction of them as representative samples (super samples) used for training the downstream model. For example, spatial sampling approaches (Xia et al., 2022; Joshi & Mirzasoleiman, 2023; Sorscher et al., 2022; Needell et al., 2014) calculate the importance score of a sample in terms of the distance from the centroid of its corresponding class marginal. Samples closer to the centroid are considered the most prototypical (easy) and those far from the centroid are treated as least prototypical (hard). Canonical scoring criteria have also been developed in terms of gradients (Paul et al., 2021), uncertainty (Pleiss et al., 2020), and forgetfulness (Toneva et al., 2018). Notably, the spatial distance-based score is closely related to the gradient / uncertainty / forgetting-based score. Samples close (far away) to the class centroid are often associated with smaller (larger) gradient norm / lower (higher) uncertainty / harder (easier) to forget (Paul et al., 2021; Sorscher et al., 2022; Xia et al., 2022).

In the ideal scenario i.e. in the **absence of any corruption**, hard examples are known to contribute the most towards downstream generalization performance (Katharopoulos & Fleuret, 2018; Joshi et al., 2009; Huang et al., 2010; Balcan et al., 2007) as they often encode the most discriminative and task-relevant information in the dataset (Xu et al., 2020).

However, in the **realistic noisy scenarios involving outliers**, this strategy often fails since the noisy examples are wrongly deemed informative for training (Zhang & Sabuncu, 2018; Park et al., 2024). To mitigate this issue, existing pruning methods, tailored for such noisy scenarios, aim to retain the most prototypical / easy samples (Pleiss et al., 2020; Jiang et al., 2018; Har-Peled et al., 2007; Shah et al., 2020; Shen & Sanghavi, 2019). Yet, by prioritizing samples far from the decision boundary, these methods overlook less prototypical but uncorrupted and highly informative examples. This bias introduces a fundamental robustness vs. diversity trade-off (Xia et al., 2022), where *emphasizing robustness can lead to a lack of diversity* in the pruned subset. This limitation not only results in suboptimal generalization performance but, in extreme cases, can also lead to degenerate solutions (Sugiyama & Kawanabe, 2012).

Moreover, real-world scenarios frequently deviate from idealized assumptions, making it challenging or infeasible to adapt selection criteria and methodologies to diverse and unpredictable conditions. Consequently, despite its drawbacks in prioritizing informative examples, random sampling remains the industry standard due to its simplicity, efficiency, and ease of implementation.

## 1.2 OVERVIEW OF OUR APPROACH :

To go beyond these limitations, we investigate the  $k$ -subset selection problem under the Gross Corruption Framework (Definition 1), where  $0 \leq \psi < \frac{1}{2}$  fraction of the samples are allowed to be **arbitrarily perturbed**. This allowance for **arbitrary** corruption enables us to capture many practical robustness scenarios – including **corrupt features / labels** and **adversarial attacks**.

We make a key observation that: *existing pruning methods typically use the empirical mean to calculate the centroid of the samples, which then guides the selection process based on how representative those samples are*. However, the **empirical mean is highly susceptible to outliers** – in fact, it is possible to construct a single adversarial example to arbitrarily perturb the empirical mean (Figure 1).

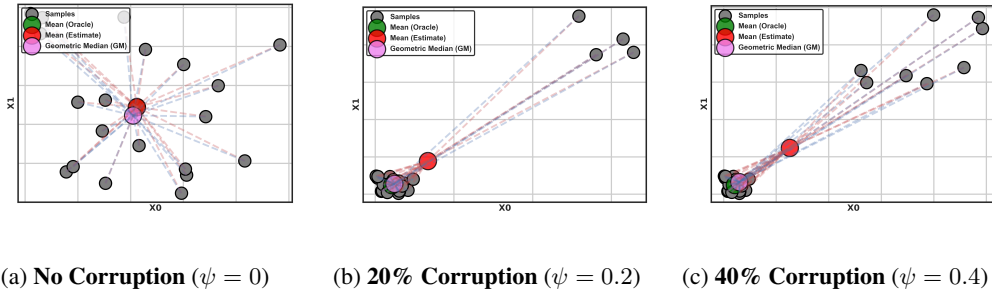


Figure 1: **ROBUST MEAN ESTIMATION**: As the corruption rate  $0 \leq \psi < \frac{1}{2}$  increases (representing the fraction of samples drawn from an adversary-chosen distribution), the empirical mean increasingly deviates from the true uncorrupted mean. In contrast, the geometric median (GM) remains robust and stays closer to the uncorrupted (oracle) mean, demonstrating its resilience to outliers.

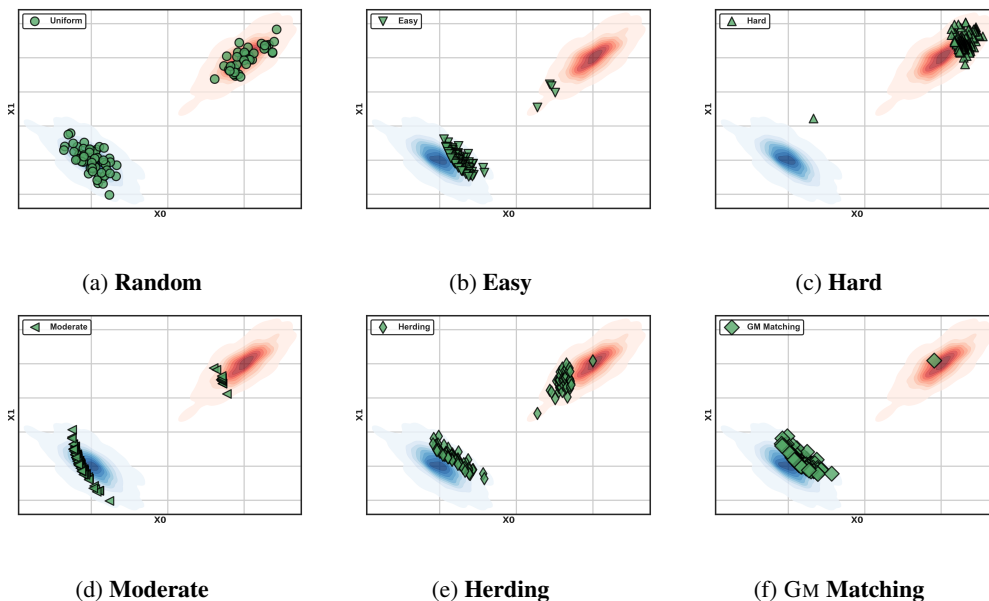


Figure 2: **DATA PRUNING IN THE WILD (Sampling from Noisy Gaussian)**: Subset 10% of the examples from anisotropic Gaussian (blue) where 40% of the samples replaced by an adversarial distribution (red). We compare GM Matching with several spatial sampling algorithms (Section 6.1): Random, Easy, Hard, Moderate, and Kernel Herding. GM Matching yields significantly more robust subset than the other approaches.

As a consequence, in the presence of arbitrary corruption, the conventional distinction between easy (robust) and hard samples breaks down, leading to the selection of subsets that are significantly compromised by corruptions (2).

In response, we propose a novel subset selection strategy that fosters balanced diversity, effectively navigating various regions of the distribution while avoiding distant, noisy points. Specifically, we formulate the subset selection problem as one of minimizing the Maximum Mean Discrepancy (Gretton et al., 2012) between the empirical distribution induced by the selected subset and that of the underlying true (uncorrupted) distribution. Our key idea is to replace the empirical mean with a robust surrogate – Geometric Median (GM)(Definition 4) (Weber et al., 1929; Weiszfeld, 1937) – a classical estimator of the central tendency, inherently robust to outliers.

In particular, we optimize over finding a  $k$ -subset that minimizes the distance between the subset’s empirical mean and the GM of the (potentially noisy) dataset over some appropriate embedding space, using herding (Welling, 2009) style greedy iterative updates. We call our algorithm Geometric Median (GM) Matching as described in Algorithm 1.

---

**Algorithm 1 GEOMETRIC MEDIAN (GM) MATCHING**

---

(initialization)

A finite collection of grossly corrupted (Definition 1) observations  $\mathcal{D} = \{\mathbf{x}_i \in \mathbb{R}^d\}_{i=1}^n$ ; pretrained encoder  $\phi(\cdot) : \mathbb{R}^d \rightarrow \mathbb{R}^s$  e.g. CLIP (Radford et al., 2021b); initial weight vector  $\boldsymbol{\theta}_0 \in \mathbb{R}^s$ ; number of sampling batches  $B$ , population fraction for GM computation  $0 < \gamma_{\text{GM}} \leq 1$ .

(compute embeddings)

$$\Phi = \{\omega_i = \phi(\mathbf{x}_i) \in \mathbb{R}^s : \forall \mathbf{x}_i \in \mathcal{D}\}$$

(pick random  $n_{\text{GM}}$ -subset for GM computation)

$$\Phi_{\text{GM}} \stackrel{i.i.d.}{\sim} \Phi, \text{ where, } n_{\text{GM}} = |\Phi_{\text{GM}}| = \gamma_{\text{GM}}|\Phi| \leq n$$

(compute  $\epsilon$ -approximate geometric median via Algorithm 2)

$$\boldsymbol{\mu}_{\epsilon}^{\text{GM}}(\Phi_{\text{GM}}) = \arg \min_{\mathbf{z} \in \mathbb{R}^s} \sum_{\omega_i \in \Phi_{\text{GM}}} \|\mathbf{z} - \omega_i\|$$

(partition data into batches)

$$\mathcal{D} = \bigcup_{b=1}^B \mathcal{D}_b$$

(initialize subset)

$$\mathcal{D}_S \leftarrow \emptyset$$

**for** batch index  $b = 1, \dots, B$  **do**

(load batch embeddings)

$$\Phi_b = \{\omega_i \in \Phi : \mathbf{x}_i \in \mathcal{D}_b\}$$

**for** iterations  $t = 0, 1, \dots, k/B$  **do**(find embedding closest to  $\boldsymbol{\theta}_t$ )

$$\omega := \arg \max_{\omega_i \in \Phi_b} \langle \boldsymbol{\theta}_t, \omega_i \rangle$$

(update direction parameter)

$$\boldsymbol{\theta}_{t+1} := \boldsymbol{\theta}_t + \left[ \boldsymbol{\mu}_{\epsilon}^{\text{GM}}(\Phi_b) - \omega \right]$$

(update selected subset)

$$\mathcal{D}_S := \mathcal{D}_S \cup \mathbf{x} \text{ where, } \omega = \phi(\mathbf{x})$$

(update the batch embedding set)

$$\Phi_b := \Phi_b \setminus \omega$$

**end****end****return:**  $\mathcal{D}_S$ 

---

Intuitively, GM Matching can be viewed as a robust generalization of Kernel Herding (Chen et al., 2010). By replacing its vulnerable empirical mean with the GM, we inherit the favorable  $\mathcal{O}(1/k)$  convergence of Kernel Herding while adding robustness to adversarial and heavy-tailed noise, bridging moment-matching and robust estimation in a unified framework.

**1.3 CONTRIBUTIONS.**

Overall, our contributions can be summarized as follows:

- We introduce a principled formulation of the  $k$ -subset selection problem under the Gross Corruption model (Definition 1), allowing up to 50% of the data to be arbitrarily corrupted. This generalizes prior noise models such as Huber contamination and Byzantine failure, and captures a wide range of real-world noise scenarios such as label noise, outliers, and adversarial attacks. To the best of our knowledge, this is the first theoretical and algorithmic treatment of robust data pruning under such a general corruption model.
- We demonstrate that state-of-the-art pruning strategies – including those designed for robustness – fail under gross corruption due to their reliance on the empirical mean, which has an asymptotic breakdown point of zero. Through both formal analysis (Section 4.1, Lemma 3) and illustrative examples (Figure 1, Figure 6), we show how even a single adversarial point can arbitrarily skew moment-based selection methods.
- Motivated by this key observation, we propose a robust alternative: Geometric Median(GM) Matching. Our method selects a subset whose empirical mean approximates the Geometric Median (GM) of the full (potentially corrupted) dataset. We formalize this as a robust moment matching objective (14), and solve it via a greedy, herding (Chen et al., 2010) style iterative selection

procedure (Algorithm 1). Unlike prior approaches, GM Matching leverages the optimal 1/2 breakdown point of GM, ensuring robustness even under adversarial perturbations.

- We provide rigorous theoretical analysis showing that GM Matching converges to a bounded neighborhood of the true (uncorrupted) underlying mean at an  $\mathcal{O}(1/k)$  rate (Theorem 1). This matches the best-known rates from Kernel Herding in clean settings, and crucially, continues to hold under arbitrary corruption. As a corollary, we derive bounds on the Maximum Mean Discrepancy (MMD) between the selected subset and the clean distribution (Lemma 1), establishing formal generalization guarantees.
- We propose a practical, batched version of GM Matching that enables efficient computation at scale as outlined in Algorithm 1. Our method incorporates two key engineering strategies: (i) sub-sampling for GM estimation, and (ii) batched greedy selection. We analyze the computational complexity and demonstrate that batching yields near-linear speedups without significantly compromising performance.
- We conduct comprehensive experiments across a range of tasks — including image classification, unsupervised distribution matching, and image generation. Our benchmarks cover diverse noise types: feature corruptions, label noise, and adversarial attacks. In all settings, GM Matching consistently outperforms existing methods, especially under high corruption and aggressive pruning (often by >10%), establishing it as a state-of-the-art robust coreset selection strategy.
- Our analysis and visualizations (Figure 2) highlight how GM Matching balances robustness and diversity — avoiding the degeneracies of “easy-only” pruning while excluding adversarial outliers. This addresses a key open problem in the pruning literature: how to retain task-relevant examples near the decision boundary without being misled by corrupted points.

## 2 RELATED WORK

A large body of recent works have been proposed to solve the data selection problem. At a high level, there are two main directions:

**IMPORTANCE SAMPLING.** One set of data pruning approaches rely on some carefully designed pruning metrics to rank the training samples based on the scores and retain a fraction of them as representative samples, used for training the downstream model. For example, (Xia et al., 2022; Joshi & Mirzasoleiman, 2023; Sorscher et al., 2022) calculate the importance score of a sample in terms of the distance from the centroid of its corresponding class marginal. Samples closer to the centroid are considered most prototypical (easy) and those far from the centroid are treated as least prototypical (hard). While this work primarily focuses on spatial approaches, it is worth mentioning that the canonical importance scoring criterion have been proposed in terms gradient norm (Paul et al., 2021; Needell et al., 2014), uncertainty (Pleiss et al., 2020) and forgetfulness (Toneva et al., 2018; Feldman & Zhang, 2020). Typically, samples closer to the class centroid in feature space tend to have lower gradient norms, exhibit lower uncertainty, and are harder to forget during training. In contrast, samples farther from the centroid generally have higher gradient norms, greater uncertainty, and are easier to forget (Paul et al., 2021; Sorscher et al., 2022; Xia et al., 2022). However, such scoring-based selection methods typically rely on the empirical mean to define centroids, making them brittle under data corruption—a vulnerability that becomes critical in noisy or adversarial settings.

**MOMENT MATCHING METHODS.** A second family of methods tackles data selection as an optimization problem, aiming to match certain statistical moments—such as means, losses, or gradients—between the subset and the full dataset. These techniques, often rooted in coreset construction, select a subset whose empirical properties approximate those of the entire dataset (Chen et al., 2010; Campbell & Broderick, 2018; Dwivedi & Mackey, 2021). A notable extension is gradient-based moment matching (Mirzasoleiman et al., 2020), which seeks to preserve the full dataset’s gradient dynamics within the selected subset, enabling efficient yet faithful training.

**SUBSET SELECTION FROM NOISY DATA.** Despite substantial advances in subset selection algorithms for large-scale datasets, most existing methods are designed for idealized, clean training data. In practical scenarios, however, real-world datasets are often noisy—affected by mislabeled examples, corrupted features, or adversarial attacks. Unfortunately, extending traditional subset selection methods to such noisy settings remains an under-explored challenge. A key limitation of

many classical approaches lies in their dependence on the empirical mean—a statistic known to be highly sensitive to outliers and heavy-tailed distributions. As we formally demonstrate in Lemma 3, this renders them brittle under arbitrary corruption, where even a small fraction of adversarial points can severely skew the selection process. Consequently, any method that uses the empirical mean as a reference—either directly (e.g., centroid-based selection) or indirectly (e.g., gradient- or uncertainty-based ranking)—inherits the same fundamental vulnerability.

Several recent works have attempted to address robustness, but often in narrowly scoped settings. For instance, methods tailored to label noise (Pleiss et al., 2020; Park et al., 2024) typically rely on techniques such as relabeling or sample reweighting, assuming access to a relatively clean subset or side information. These strategies can be effective in controlled scenarios but do not generalize well to broader corruption types such as input perturbations, distribution shift, or structural outliers.

Another class of methods mitigate noise by aggressively pruning away uncertain or atypical examples—often selecting only the most prototypical or easy-to-learn samples (Shah et al., 2020; Toneva et al., 2018; Jiang et al., 2018; Har-Peled et al., 2007). While such selection improves robustness by avoiding noisy outliers, it inadvertently sacrifices diversity, discarding informative hard examples that are essential for learning decision boundaries. This introduces a well-known robustness–diversity tradeoff (Xia et al., 2022; Feldman & Zhang, 2020), where safe selection leads to suboptimal generalization. To balance this trade-off, Xia et al. (2022) proposed a moderation strategy that retains samples closest to the median distance from the class centroid—aiming to avoid both overly hard and overly easy examples. However, this approach still fundamentally relies on spatial distances measured from the empirical mean, making it vulnerable to corruption that distorts this reference point. Furthermore, while a few recent works have studied robust subset selection in a theoretical manner, they are either limited to linear models (Xu et al., 2025) or assume simplified theoretical frameworks (Thompson, 2022; Park et al., 2024), strong assumptions (Qian et al., 2017). These works stop short of providing practical algorithms or generalization guarantees applicable to modern, highly nonlinear deep learning systems.

In contrast, our work introduces a simple, theoretically grounded algorithm for subset selection under arbitrary data corruption, bridging the gap between robustness and diversity. GM Matching generalizes to deep models and real-world noisy data, offering provable guarantees under the Gross Corruption.

**CONNECTION TO KERNEL HERDING.** GM Matching builds upon the classical Kernel Herding framework (Welling, 2009; Chen & Welling, 2010; Bach et al., 2012), which selects representative subsets that match the mean embedding of the data distribution in a reproducing kernel Hilbert space (RKHS). While Kernel Herding offers favorable convergence guarantees  $\mathcal{O}(1/k)$  vs.  $\mathcal{O}(1/\sqrt{k})$  for random sampling; it relies on the empirical mean, making it vulnerable to outliers and adversarial corruption. GM Matching preserves the moment-matching spirit of Kernel Herding but replaces the empirical mean with the geometric median (GM), a robust estimator with a breakdown point of 1/2. This simple substitution significantly improves robustness without compromising convergence. To our knowledge, GM Matching is the first method to combine robust estimation with herding-style greedy selection, enabling provably fast and stable subset selection even under high rates of data corruption.

### 3 PROBLEM SETUP : ROBUST DATA PRUNING

Given a set of  $n$  samples, data pruning (or coresampling) aims to find a  $k$ -subset that is representative of the underlying distribution. If such a subset can be found compute-efficiently, then training a parametric model on the subset typically yields similar generalization performance as training on the entire dataset while resulting in a significant speedup when  $k \ll n$ .

#### 3.1 CORRUPTION MODEL

However, real-world data is often noisy and imperfect due to the difficulty and expense of obtaining perfect semantic annotations, adversarial attacks, or simply measurement noise. To account for such realistic scenarios, we study the **combinatorial  $k$ -subset selection** problem under Gross Corruption (Definition 1) – a strong corruption model (Diakonikolas et al., 2019; Acharya et al., 2022) that

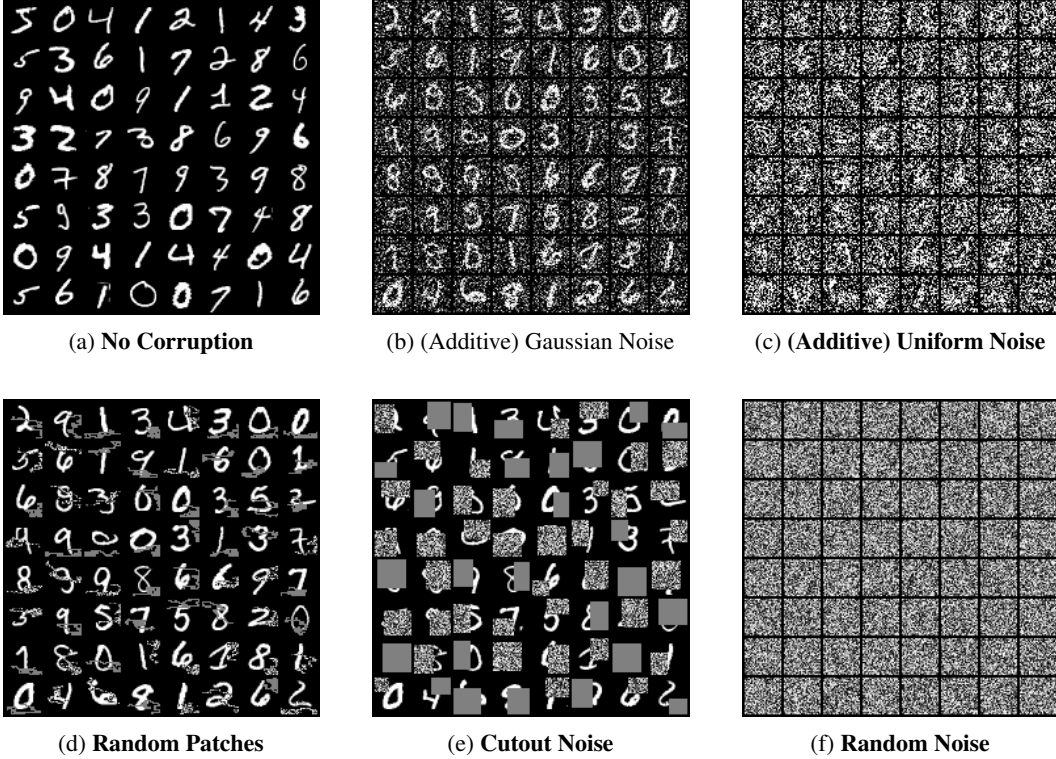


Figure 3: **Image Corruption:** Distinct types of data corruption applied on MNIST images.

generalizes both the **Huber Contamination Model** (Huber, 1992) and the **Byzantine Corruption Framework** (Lampert et al., 1982).

**Definition 1 (Gross Corruption).** *Given observations  $\mathcal{D} = \{\mathbf{x}_i \in \mathbb{R}^d \stackrel{i.i.d.}{\sim} p(x)\}_{i=1}^n$ , an adversary inspects all the samples and arbitrarily perturbs  $\psi \in [0, \frac{1}{2})$  fraction of them. We will refer to such a set of samples  $\mathcal{D} = \mathcal{D}_G \cup \mathcal{D}_B$  as  $\psi$  grossly corrupted, where  $\mathcal{D}_B, \mathcal{D}_G$  denote the sets of corrupt and clean samples respectively.*

Simply put, samples  $\mathbf{x}_i \in \mathcal{D}$  follow a mixture distribution:

$$p^{\text{noisy}}(x) = (1 - \psi)p(x) + \psi q(x) \quad (1)$$

where,  $p(x)$  is the true underlying distribution of interest, and  $q(x)$  is an adversarially chosen **arbitrary** distribution, and  $0 \leq \psi < 1/2$  is the corruption fraction.

The goal of Robust Data Pruning is thus to judiciously select a  $k$ -subset  $\mathcal{D}_S \subseteq \mathcal{D}$  where  $|\mathcal{D}_S| = k$ , that *encapsulates the underlying uncorrupted distribution  $p(x)$  induced by subset  $\mathcal{D}_G$  without any a-priori knowledge about the corrupted samples.*

Let,  $\hat{p}_S$  denote the empirical measure induced by  $\mathcal{D}_S$ . Then, we aim to solve:

$$\min_{\mathcal{D}_S \subseteq \mathcal{D}} \Lambda \left( \hat{p}_S(x) \parallel p(x) \right) \quad (2)$$

for some appropriate divergence measure  $\Lambda$ . As discussed in Section 5, the proposed GM Matching (Algorithm 1) finds the subset by minimizing the **Maximum Mean Discrepancy (MMD)** (Gretton et al., 2012) between  $\hat{p}_S$  and the true underlying uncorrupted distribution  $p$ .

We measure the robustness of subset selection algorithms via breakdown point (Donoho & Huber, 1983; Lopuhaa et al., 1991; Davies & Gather, 2007; Olive, 2001) (Definition 2) – a classic tool in robust optimization to assess the resilience of an estimator.



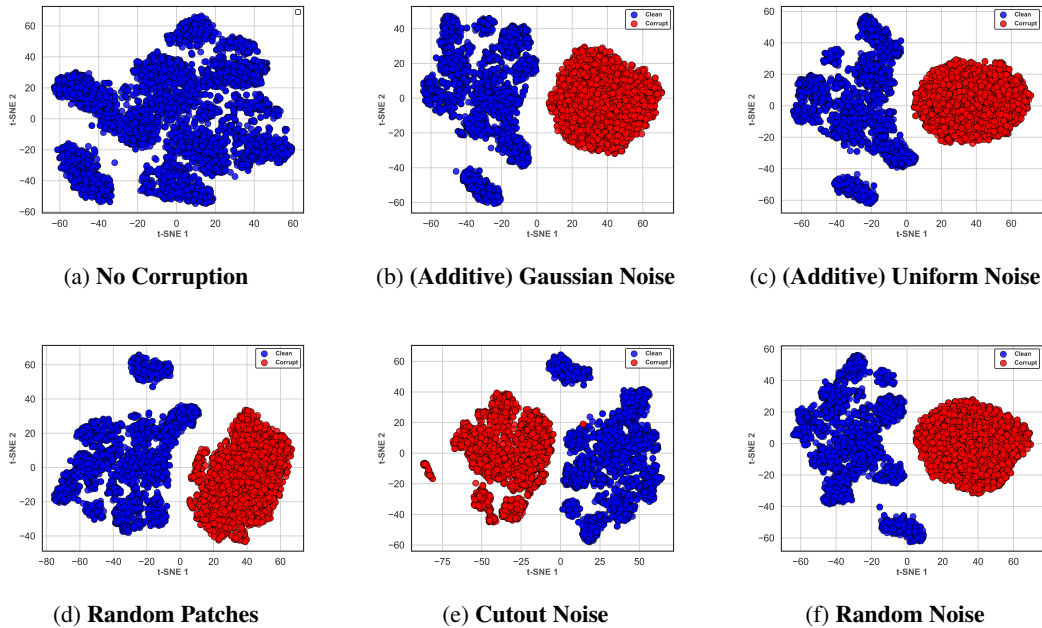


Figure 4: **(PROXY EMBEDDING SPACE)** t-SNE Visualization of CLIP ViT-B/32 Embeddings of a subset of MNIST images from Figure 3: (a) Clean (baseline), and where 45% samples corrupted with (b) Gaussian noise, (c) Uniform noise, (d) Random patches, (e) Cutout noise.

**Definition 2 (Breakdown Point).** *The breakdown point  $\zeta_T$  of an estimator  $T(\cdot)$  is the smallest fraction  $\psi$  of corrupted samples that can cause it to diverge arbitrarily:*

$$\zeta_T = \inf \left\{ \psi \geq 0 : \sup_{\mathcal{D}_B} \left\| T(\mathcal{D}) - T(\mathcal{D}_G) \right\| = \infty \right\} \quad (3)$$

$T(\cdot)$  achieves the **optimal breakdown point**  $\zeta_T^* = 1/2$  if it remains bounded  $\forall 0 \leq \psi < 1/2$ .

### 3.2 PROXY ENCODER

Identifying sample importance is an ill-posed problem without some notion of similarity among the samples. Hence, we will assume access to a *proxy encoder* (Assumption 1).

**Assumption 1 (Proxy Encoder).**  $\phi : \mathbb{R}^d \rightarrow \mathcal{H}$  that maps raw inputs into a separable embedding space (potentially infinite-dimensional), i.e., a Reproducing Kernel Hilbert Space (RKHS) (Hofmann et al., 2008; Sriperumbudur et al., 2010; Vert et al., 2004; Cho & Saul, 2009)  $\mathcal{H}$  with inner product determined by a positive-definite kernel:

$$\omega(\mathbf{x}, \mathbf{x}') = \langle \phi(\mathbf{x}), \phi(\mathbf{x}') \rangle_{\mathcal{H}} \quad (4)$$

We further assume that  $\phi(\cdot)$  is a **characteristic feature map**, i.e. the mapping  $p \mapsto \mu_p = \mathbb{E}_{\mathbf{x} \sim p} [\phi(\mathbf{x})]$  is injective. Simply put, for any two distributions  $p$  and  $q$ :

$$\mu_p = \mu_q \implies p = q. \quad (5)$$

Additionally, we will assume bounded features, i.e.,  $\|\phi(\mathbf{x})\| \leq R \forall \mathbf{x} \in \mathcal{D}$  for some constant  $R$ .

In practice, we instantiate such embeddings with pretrained *foundation models*, e.g., CLIP encoders (Radford et al., 2021a) – explicitly trained via a contrastive objective (Chen et al., 2020) to map semantically similar examples closer together while pushing dissimilar ones apart. To illustrate, Figure 3 shows MNIST samples corrupted with various noise types.

To illustrate, Figure 4 provides a t-SNE visualization (Van der Maaten & Hinton, 2008) of these noisy samples as embedded by a pretrained CLIP ViT-B/32 (Radford et al., 2021a) model. Clearly, the visualization reveals a clear separation between clean and corrupted samples in the embedding space, thereby validating the use of the pretrained CLIP encoder to obtain robust kernel mappings that define a well-behaved RKHS for our application.

## 4 WARMUP: K-SUBSET SELECTION VIA MOMENT MATCHING

In the uncorrupted setting i.e. when  $\psi = 0$ , a natural and theoretically grounded approach for data pruning is to formulate it as a combinatorial MOMENT MATCHING objective:

$$\arg \min_{\substack{\mathcal{D}_S \subseteq \mathcal{D} \\ |\mathcal{D}_S|=k}} \left[ \Delta^2(\mathcal{D}_S, \mathcal{D}) := \left\| \frac{1}{|\mathcal{D}|} \sum_{\mathbf{x}_i \in \mathcal{D}} \phi(\mathbf{x}_i) - \frac{1}{k} \sum_{\mathbf{x}_j \in \mathcal{D}_S} \phi(\mathbf{x}_j) \right\|^2 \right] \quad (6)$$

The goal is to find a  $k$ -subset such that the empirical mean of the subset  $\boldsymbol{\mu}(\mathcal{D}_S)$  closely approximates the empirical mean  $\boldsymbol{\mu}(\mathcal{D})$  of the full dataset where,

$$\boldsymbol{\mu}(\mathcal{D}) = \frac{1}{|\mathcal{D}|} \sum_{\mathbf{x}_i \in \mathcal{D}} \phi(\mathbf{x}_i), \quad \boldsymbol{\mu}(\mathcal{D}_S) = \frac{1}{k} \sum_{\mathbf{x}_j \in \mathcal{D}_S} \phi(\mathbf{x}_j) \quad (7)$$

Note that, (6) is an instance of the famous subset sum problem – known to be NP-hard via a reduction from  $k$ -set cover (Feige, 1998).

Remarkably, although the squared-distance function  $\Delta^2(\mathcal{D}_S, \mathcal{D})$  is *not* submodular in  $\mathcal{D}_S$ , (Mirza-soleiman et al., 2020) showed that *one can transform* (6) into a *submodular set cover* instance. Since submodular set cover can be approximated efficiently by standard greedy algorithms (Nemhauser et al., 1978), an *approximate* solution to (6) follows. In particular, for a desired  $\varepsilon > 0$ , we can choose a fine enough discretization (often implemented as an  $\varepsilon$ -net over the feature space) and guarantee:

$$\Delta^2(\mathcal{D}_S, \mathcal{D}) \leq (1 + \varepsilon) \left\| \boldsymbol{\mu}(\mathcal{D}) - \boldsymbol{\mu}(\mathcal{D}_S^*) \right\|^2 = (1 + \varepsilon) \Delta^2(\mathcal{D}_S^*, \mathcal{D}) \quad (8)$$

where,

$$\mathcal{D}_S^* := \arg \min_{\substack{\mathcal{D}_S \subseteq \mathcal{D} \\ |\mathcal{D}_S|=k}} \Delta^2(\mathcal{D}_S, \mathcal{D}) \quad (9)$$

This guarantee implies that even though the underlying problem is NP-hard, we can efficiently compute a subset  $\mathcal{D}_S$  whose moment matching error is within a  $(1 + \varepsilon)$  multiplicative factor of the optimal error, while maintaining a polynomial (or near-linear) runtime.

### 4.1 VULNERABILITY UNDER GROSS CORRUPTION

Despite strong theoretical guarantees in the uncorrupted setting, the moment matching objective can result in arbitrarily poor solutions under gross corruption ( Definition 1)  $\forall \psi > 0$ . The vulnerability can be attributed to the estimation of target moment via empirical mean – notorious for its sensitivity to outliers. To illustrate, consider a single adversarial sample:

$$\mathbf{x}^B = \left( |\mathcal{D}| \boldsymbol{\mu}^B - \sum_{\mathbf{x} \in \mathcal{D} \setminus \mathbf{x}^B} \phi(\mathbf{x}) \right) \quad (10)$$

This single adversarial sample forces the empirical mean to an arbitrary target  $\boldsymbol{\mu}^B$  chosen by the adversary, implying that the empirical mean can't tolerate even a single grossly corrupted sample, i.e. yields **lowest possible asymptotic breakdown point of 0**.

Consequently, optimizing over (6) no longer guarantees convergence to the true underlying (uncorrupted) moment  $\boldsymbol{\mu}^G = \mathbb{E}_{\mathbf{x} \in \mathcal{D}_G} \phi(\mathbf{x})$ . Instead, the subset selection can be hijacked by a single bad sample, warping the solution towards an adversarial target.

## 5 GEOMETRIC MEDIAN MATCHING

Building on this key observation, our proposal is to solve a robust variant (14) of the moment matching objective (6) instead. *The key idea is to replace the empirical mean with a robust surrogate estimator of the target moment*, mitigating its susceptibility to corrupted samples.

As discussed before, GM Matching involves two key steps:

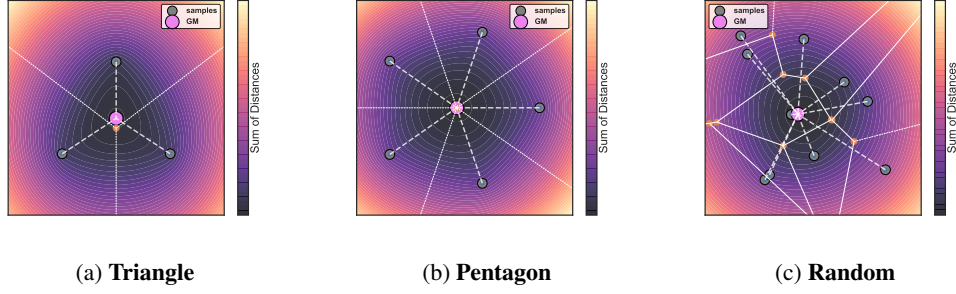


Figure 5: **GEOMETRIC MEDIAN VISUALIZATION:** The plots illustrate the computation of the geometric median (denoted by the pink circle) for three different spatial point configurations: (a) Triangle, (b) Pentagon, and (c) Random. The color gradient represents the sum of distances  $\rho(\mathbf{z})$  from a candidate point  $\mathbf{z}$  to all data points, with darker regions indicating smaller values of  $\rho(\mathbf{z})$ . The white dashed lines show the connections between the geometric median and the data points, emphasizing how the geometric median minimizes the total Euclidean distance to all points. Additionally, the Voronoi regions formed around the data points visually partition the space based on proximity, offering insight into how the geometric median balances contributions from each point. In symmetric configurations such as (a) and (b), the Voronoi structure highlights the symmetry in influence regions, leading to a geometric median located at the center. For the random configuration (c), the irregular Voronoi regions illustrate the varying influence of data points, with the geometric median robustly adapting to minimize the total distance while down-weighting the effect of outlier-like points.

- Find an estimate of the centroid  $\boldsymbol{\mu}$  of training observations such that  $\Delta = \|\boldsymbol{\mu} - \boldsymbol{\mu}^{\mathcal{G}}\|$  remains bounded even when the observations are  $\alpha$ -corrupted (Definition 1).
- Find a subset  $\mathcal{S} \subseteq \mathcal{D}$  such that the empirical mean of the subset  $\approx \boldsymbol{\mu}$ .

In the rest of this section, we discuss these two key ideas in detail.

## 5.1 ROBUST MEAN ESTIMATION

A well-designed robust estimator should guarantee that the estimation error,  $\Delta = \|\tilde{\boldsymbol{\mu}} - \boldsymbol{\mu}^{\mathcal{G}}\| \leq \delta$  remains bounded under the strong gross corruption (Definition 1).

In this context, Geometric Median (GM) (Definition 4) is a well-studied spatial estimator, known for several nice properties like rotation and translation invariance and **optimal breakdown point of 1/2** under gross corruption (Minsker et al., 2015; Kemperman, 1987) (Figure 1,5,6).

**Definition 3 (Convex Hull).** Given a set  $\mathcal{S} \subseteq \mathbb{R}^d$ , the convex hull of  $\mathcal{S}$  is defined as the set of all convex combinations of points in  $\mathcal{S}$ , i.e.

$$\text{conv}(\mathcal{S}) = \left\{ \sum_{i=1}^m \lambda_i \mathbf{x}_i : \mathbf{x}_i \in \mathcal{S}, \lambda_i \geq 0, \sum_{i=1}^m \lambda_i = 1, m \in \mathbb{N} \right\}.$$

Moreover, GM is guaranteed to lie in the relative interior of the convex hull of the majority (good) points i.e.  $\boldsymbol{\mu}^{\text{GM}} \in \text{conv}(\mathcal{D}_{\mathcal{G}})$ , making it an attractive choice for estimating the target mean.

**Definition 4 (Geometric Median).** Suppose, we are given a finite collection of observations  $\{\phi(\mathbf{x}_1), \phi(\mathbf{x}_2), \dots, \phi(\mathbf{x}_n)\}$  defined over Hilbert space  $\mathcal{H} \in \mathbb{R}^d$ , equipped with norm  $\|\cdot\|$  and inner  $\langle \cdot \rangle$  operators. Then, the Geometric Median (Fermat-Weber point) (Weber et al., 1929; Minsker et al., 2015; Cohen et al., 2016)  $\boldsymbol{\mu}^{\text{GM}}$  is defined as:

$$\boldsymbol{\mu}^{\text{GM}} = \arg \min_{\mathbf{z} \in \mathcal{H}} \left[ \rho(\mathbf{z}) := \sum_{i=1}^n \left\| \mathbf{z} - \phi(\mathbf{x}_i) \right\| \right] \quad (11)$$

Note that, in contrast, the empirical mean is the minimizer of the squared Euclidean distances:

$$\hat{\boldsymbol{\mu}} = \arg \min_{\mathbf{z} \in \mathbb{R}^d} \rho(\mathbf{z}), \quad \text{where} \quad \rho(\mathbf{z}) = \sum_{i=1}^n \left\| \mathbf{x}_i - \mathbf{z} \right\|^2 \quad (12)$$

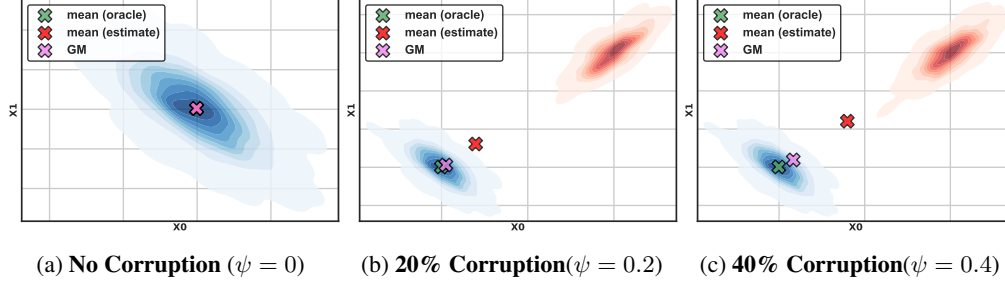


Figure 6: (SAMPLING FROM NOISY GAUSSIAN) ROBUST MEAN ESTIMATION: As we progressively increase  $0 \leq \psi < 1/2$  (fraction of corrupt samples in the data); while the empirical mean drifts away, GM remains close to the uncorrupted mean; demonstrating its resilience to outliers.

---

**Algorithm 2 (WEISZFELD, 1937) COMPUTING  $\epsilon$ -APPROX. GM**

---

**Input:**

Observations  $\{\mathbf{x}_i \in \mathbb{R}^d\}_{i=1}^n$ , initial guess  $\mathbf{z}^{(0)} \in \mathbb{R}^d$ , convergence threshold  $\epsilon > 0$ , and regularization parameter  $\delta > 0$ .

**Initialization:**

Initialize  $\mathbf{z}^{(0)}$  (e.g., as the arithmetic mean of  $\{\mathbf{x}_i\}$ ), set iteration counter  $k \leftarrow 0$ .

**while** not converged (i.e.,  $\|\mathbf{z}^{(k+1)} - \mathbf{z}^{(k)}\| \geq \epsilon$ ) **do**

    (compute update step)

$$\mathbf{z}^{(k+1)} \leftarrow \frac{\sum_{i=1}^n \frac{\mathbf{x}_i}{\|\mathbf{x}_i - \mathbf{z}^{(k)}\| + \delta}}{\sum_{i=1}^n \frac{1}{\|\mathbf{x}_i - \mathbf{z}^{(k)}\| + \delta}}$$

    (update iteration counter)

$k \leftarrow k + 1$

**end**

**Return:**  $\mathbf{z}^* \leftarrow \mathbf{z}^{(k)}$

---

ensuring computational simplicity, as a closed-form solution exists  $\hat{\mu} = \frac{1}{n} \sum_{i=1}^n \mathbf{x}_i$ , which follows from the first-order optimality conditions of convex quadratic minimization.

However, this also makes the empirical mean sensitive to outliers, as extreme values have a disproportionately large effect on the sum of squared distances. On the other hand, the linear penalty in the GM computation ensures that the objective is less influenced by outliers, as deviations are not amplified quadratically.

### 5.1.1 APPROXIMATE GM

Note that the geometric median optimization problem is inherently non-smooth due to the presence of the Euclidean norm  $\|\mathbf{x}_i - \mathbf{z}\|$ , which leads to non-differentiability at points where multiple distances are equal, making gradient-based optimization difficult.

Moreover, while a closed-form solution exists for  $d = 1$ , (Bajaj, 1988) showed that for dimensions  $d \geq 2$ , in general, the geometric median does not admit a closed-form solution expressible in radicals, rendering its exact computation algebraically intractable.

However, since the problem is convex, iterative algorithms can be used to approximate the geometric median efficiently to arbitrary precision. As a result, a long line of research has focused on developing efficient approximation methods, and several algorithms have been proposed (Weiszfeld, 1937; Vardi & Zhang, 2000; Cohen et al., 2016) to compute  $\epsilon$ -approx GM instead.

We call a point  $\mu_\epsilon^{\text{GM}} \in \mathcal{H}$  an  $\epsilon$  accurate GM if:

$$\sum_{i=1}^n \left\| \mu_\epsilon^{\text{GM}} - \phi(\mathbf{x}_i) \right\| \leq (1 + \epsilon) \sum_{i=1}^n \left\| \mu^{\text{GM}} - \phi(\mathbf{x}_i) \right\| \quad (13)$$

In this work, we adopt the celebrated Weiszfeld algorithm (Algorithm 2) – an iterative procedure for approximating the geometric median by leveraging a re-weighted averaging scheme.

## 5.2 ROBUST MOMENT MATCHING

Leveraging the breakdown and translation invariance properties of GM, we aim to solve for the following objective:

$$\arg \min_{\substack{\mathcal{D}_S \subseteq \mathcal{D} \\ |\mathcal{D}_S|=k}} \left( \Delta_{\text{GM}}^2 := \left\| \boldsymbol{\mu}_\epsilon^{\text{GM}}(\mathcal{D}) - \frac{1}{k} \sum_{\mathbf{x}_i \in \mathcal{D}_S} \phi(\mathbf{x}_i) \right\|^2 \right) \quad (14)$$

where,  $\boldsymbol{\mu}_\epsilon^{\text{GM}}(\mathcal{D})$  denotes the GM of the noisy dataset in RKHS, and  $\phi(\cdot) : \mathbb{R}^d \rightarrow \mathcal{H}$  denotes the feature map. In essence, our goal is to find a  $k$ -subset  $\mathcal{D}_S$  such that the empirical mean of the subset  $\boldsymbol{\mu}(\mathcal{D}_S)$  approximately matches  $\boldsymbol{\mu}_\epsilon^{\text{GM}}(\mathcal{D})$ .

The optimization problem above is combinatorial in nature and, in general, NP-hard following the same line of argument as Section 4. To tackle it, we adopt a herding-style greedy minimization procedure (Chen et al., 2010), which iteratively builds the subset by adding one sample at a time.

Starting with a suitably chosen  $\boldsymbol{\theta}_0 \in \mathcal{H}$ ; we repeatedly perform the following updates, adding one sample at a time,  $k$  times:

$$\mathbf{x}_{t+1} := \arg \max_{\mathbf{x} \in \mathcal{D}} \langle \boldsymbol{\theta}_t, \phi(\mathbf{x}) \rangle \quad (15)$$

$$\boldsymbol{\theta}_{t+1} := \boldsymbol{\theta}_t + \left( \boldsymbol{\mu}_\epsilon^{\text{GM}}(\mathcal{D}) - \phi(\mathbf{x}_{t+1}) \right) \quad (16)$$

We refer to the resulting end-to-end robust data pruning approach as GM Matching (Algorithm 1).

From a mathematical perspective, the objective function (14) can be viewed as a measure of the discrepancy between the robust target moment and the empirical mean of the selected subset. Note that this herding approach bears resemblance to greedy matching pursuits and the Frank-Wolfe algorithm (Bach et al., 2012) for convex optimization over the convex hull of  $\{\phi(\mathbf{x}) | \mathbf{x} \in \mathcal{D}\}$ .

The first update selects the next sample that is most aligned with the current residual direction. The inner product serves as a proxy for the reduction in the objective function if  $\mathbf{x}$  was added to the subset. Once a new sample is selected, the residual is updated to reflect the remaining discrepancy between the target robust moment and the accumulated contribution of the selected samples.

Notably, the herding style updates make GM Matching an infinite memory, deterministic process; since at any iteration  $t = T$ ,  $\boldsymbol{\theta}_T$  encapsulates the entire sampling history:

$$\boldsymbol{\theta}_T = \boldsymbol{\theta}_0 + T \boldsymbol{\mu}_\epsilon^{\text{GM}}(\mathcal{D}) - \sum_{t=1}^T \phi(\mathbf{x}_t) \quad (17)$$

Let,  $\boldsymbol{\theta}_0 = \boldsymbol{\mu}_\epsilon^{\text{GM}}$ , then, at each iteration  $t = T$  GM Matching is performing the following greedy update:

$$\mathbf{x}_{T+1} = \arg \max_{\mathbf{x} \in \mathcal{D}} \left[ \langle \boldsymbol{\mu}_\epsilon^{\text{GM}}(\mathcal{D}), \phi(\mathbf{x}) \rangle - \frac{1}{T+1} \sum_{t=1}^T \omega(\mathbf{x}, \mathbf{x}_t) \right]$$

Conceptually,  $\boldsymbol{\theta}_T$  represents the vector pointing towards under-sampled regions of the target distribution induced by  $\mathcal{D}$  at iteration  $T$ . Greedy updates in the direction that reduces the accumulated error encourage the algorithm to explore underrepresented regions of the feature space, **promoting diversity**. In other words, the algorithm’s greedy selection strategy aligns each new sample with  $\boldsymbol{\theta}$ , effectively *herding* new points to fill the gaps left by earlier selections.

Moreover, by matching the GM rather than the empirical mean, the algorithm imposes larger penalties on outliers, which lie farther from the core distribution, **prioritizing samples near the convex hull of uncorrupted points**  $\mathcal{C}_{\mathcal{G}} = \text{conv}\{\phi_{\mathcal{B}}(\mathbf{x}) | \mathbf{x} \in \mathcal{D}_{\mathcal{G}}\}$ . As a result, the algorithm promotes diversity in a balanced manner, effectively exploring different regions of the distribution while avoiding distant, noisy points, thus **mitigating the robustness vs. diversity trade-off** discussed in Section 1.

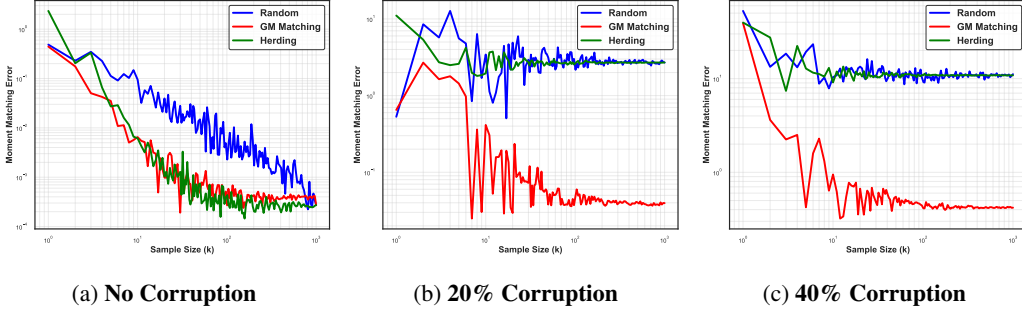


Figure 7: **SAMPLING CONVERGENCE (RECOVERING ANISOTROPIC GAUSSIAN)**: Comparison of convergence rates for Mean Discrepancy, defined as  $\Delta^2 = \|\boldsymbol{\mu}(\mathcal{D}_S) - \boldsymbol{\mu}(\mathcal{D}_G)\|^2$ , as a function of subset size  $k = |\mathcal{D}_S|$  under varying corruption rates. Without corruption, both Herding and GM Matching achieve a quadratic improvement ( $1/k$ ) over random sampling ( $1/\sqrt{k}$ ). In the presence of corruption, GM Matching demonstrates superior robustness, maintaining convergence while Random and Herding do not converge.

### 5.3 THEORETICAL GUARANTEE

In this section, we theoretically characterize the proposed GM Matching algorithm.

Our convergence analysis leverages two key properties of GM – its robustness under gross corruption and the fact that it is guaranteed to lie in the interior of the convex hull of the majority (good) samples (Boyd & Vandenberghe, 2004). These properties allow us to bound the estimation error of the  $\epsilon$ -approximate GM with respect to the true (uncorrupted) mean, and to further analyze how the error diminishes as we select more samples.

First, we exploit the robustness property of GM to get an upper bound on the estimation error w.r.t the underlying oracle mean (Acharya et al., 2022; Chen et al., 2017).

Next, we use the property that GM is guaranteed to lie in the interior of the convex hull of the majority of the samples (Boyd & Vandenberghe, 2004).

Combining these two results, we establish the following convergence guarantee:

**Theorem 1.** *Suppose that we are given a set of grossly corrupted samples  $\mathcal{D} = \mathcal{D}_G \cup \mathcal{D}_B$  (Definition 1), an  $\epsilon$  approx. GM( $\cdot$ ) oracle  $\boldsymbol{\mu}_\epsilon^{\text{GM}}(\cdot)$  (11) and bounded, characteristic feature map  $\phi(\cdot) : \mathbb{R}^d \rightarrow \mathcal{H}$  (Assumption 1). Then, GM Matching guarantees that the mean of the selected  $k$ -subset  $\mathcal{D}_S \subseteq \mathcal{D}$  converges to a  $\delta$ -neighborhood of the uncorrupted (true) mean  $\boldsymbol{\mu}(\mathcal{D}_G) = \mathbb{E}_{\mathbf{x} \in \mathcal{D}_G} [\phi(\mathbf{x})]$  at the rate  $\mathcal{O}(1/k)$  such that:*

$$\delta^2 = \left\| \boldsymbol{\mu}_\epsilon^{\text{GM}}(\mathcal{D}) - \boldsymbol{\mu}(\mathcal{D}_G) \right\|^2 \leq \frac{8|\mathcal{D}_G|^2}{(|\mathcal{D}_G| - |\mathcal{D}_B|)^2} \sigma^2(\mathcal{D}_G) + \frac{2\epsilon^2}{(|\mathcal{D}_G| - |\mathcal{D}_B|)^2} \quad (18)$$

where,  $\sigma^2(\mathcal{D}_G) = \frac{1}{|\mathcal{D}_G|} \sum_{\mathbf{x} \in \mathcal{D}_G} \mathbb{E} \|\phi(\mathbf{x}) - \boldsymbol{\mu}(\mathcal{D}_G)\|^2$  denotes the variance of the uncorrupted samples.

This result suggests that, even under gross corruption, GM Matching converges to a neighborhood of the true mean, where the neighborhood radius depends on two terms – the first term depends on the variance of the uncorrupted samples and the second term depends on the approximation error in GM computation. Furthermore, GM Matching achieves a convergence rate of  $\mathcal{O}(1/k)$  — a quadratic improvement over random sampling  $\mathcal{O}(1/\sqrt{k})$ .

Simply put, as a straightforward consequence of Theorem 1, we have:

**Lemma 1.**

$$\Delta^2 = \left\| \boldsymbol{\mu}(\mathcal{D}_S) - \boldsymbol{\mu}(\mathcal{D}_G) \right\|^2 \leq \mathcal{O}\left(\frac{1}{k^2}\right) + \frac{16}{(1-\alpha)^2} \sigma_G^2 + \frac{4\epsilon^2}{|\mathcal{D}_G|^2(1-\alpha)^2} \quad (19)$$

where,  $\alpha = |\mathcal{D}_B|/|\mathcal{D}_G| < 1$  is the ratio of corrupted and clean samples.  $\boldsymbol{\mu}(\mathcal{D}_S)$  and  $\boldsymbol{\mu}(\mathcal{D}_G)$  denote the mean of the selected subset and the true uncorrupted mean respectively.

By matching  $\mu(\mathcal{D}_S)$  to  $\mu(\mathcal{D}_G)$ , we ensure that  $\mathcal{D}_S$  captures the uncorrupted distribution’s first moment in the RKHS. Specifically, because  $\phi(\cdot)$  is a *characteristic* feature map (Assumption 1), the **Maximum Mean Discrepancy (MMD)** (Gretton et al., 2012) between  $\hat{p}_S$  and the true underlying (uncorrupted) distribution  $p$  (Section 3) is given by:

$$\Lambda_{\text{MMD}}^2(\hat{p}_S, p) = \left\| \mathbb{E}_{\hat{p}_S}[\phi(\mathbf{x})] - \mathbb{E}_p[\phi(\mathbf{x})] \right\|_{\mathcal{H}}^2. \quad (20)$$

In our setting,

$$\mathbb{E}_{\hat{p}_S}[\phi(\mathbf{x})] = \mu(\mathcal{D}_S), \quad \mathbb{E}_p[\phi(\mathbf{x})] = \mu(\mathcal{D}_G). \quad (21)$$

Hence, bounding  $\|\mu(\mathcal{D}_S) - \mu(\mathcal{D}_G)\|$  immediately bounds  $\Lambda_{\text{MMD}}(\hat{p}_S, p)$ .

This implies that the subset  $\mathcal{D}_S$  – despite being drawn from a noisy mixture – induces a distribution  $\hat{p}_S$  that is close to  $p$  in MMD. In turn, *many well-behaved (e.g., Lipschitz or smooth) learning objectives exhibit similar performance when trained on  $\hat{p}_S$  as they would if trained on  $p$ , effectively mitigating the impact of the grossly corrupted samples.*

To complement our theoretical convergence guarantee, we empirically analyze the moment matching error under varying corruption levels in Figure 7. Specifically, we compare the convergence behavior of GM Matching with Kernel Herding and Random Sampling by plotting the squared moment discrepancy:  $\Delta^2 = \|\mu(\mathcal{D}_S) - \mu(\mathcal{D}_G)\|^2$  as a function of the subset size  $k = |\mathcal{D}_S|$ . In the clean setting (Figure 7(a)), both Kernel Herding and GM Matching exhibit the expected  $\mathcal{O}(1/k)$  convergence rate, with Kernel Herding marginally outperforming GM Matching due to its precise alignment with mean-based objectives. Random sampling, by contrast, converges more slowly, at the typical  $\mathcal{O}(1/\sqrt{k})$  rate. However, in the presence of corruption (Figure 7(b),(c)), the behavior diverges sharply. Kernel Herding’s performance degrades significantly as it becomes sensitive to outliers, and its convergence stalls beyond small subset sizes. Random sampling also fails to recover the clean mean, showing no systematic decay in error. In contrast, GM Matching continues to converge reliably—even under 40% corruption—exhibiting both stability and monotonic error reduction.

## 5.4 COMPUTATIONAL CONSIDERATIONS

Ensuring computational efficiency is of paramount importance for deploying robust  $k$ -subset selection methods in large-scale, real-world scenarios.

In this section, we first carefully dissect GM Matching into three primary cost components: first, the **computation of embeddings**, which transforms raw inputs into feature representations; second, the **estimation of the GM** — a robust measure that underpins our selection strategy — which is computed via iterative methods; and third, the **cost associated with sampling iterations**, where the algorithm progressively selects representative samples based on inner product computations. By thoroughly analyzing each of these components, we derive a comprehensive picture of the algorithm’s overall computational complexity.

Furthermore, building on this analysis, we propose practical modifications — as detailed in Algorithm 1 — that employ batching and sub-sampling techniques – *enabling efficient and parallel execution*. These enhancements not only mitigate computational overhead but also maintain high selection accuracy, thereby ensuring that the method remains scalable and effective even when processing large, noisy datasets.

### 5.4.1 GM MATCHING SCALING LAW

#### A. COMPUTE EMBEDDINGS

For inputs divided into  $L \approx \mathcal{O}(d)$  patches / tokens, the computational cost of computing CLIP ViT (Radford et al., 2021a)  $\phi(\cdot) : \mathbb{R}^d \rightarrow \mathbb{R}^s$  embedding is :

$$T^{\text{emb}} \approx \mathcal{O}(dh^2 + d^2h + dhs) \quad (22)$$

where,  $h$  is the hidden size of the encoder (Keles et al., 2023).

The  $\mathcal{O}(dh^2)$  term usually corresponds to the cost of the linear transformations that project the input tokens into the query, key, and value spaces (i.e., computing Q, K, and V). These projections typically

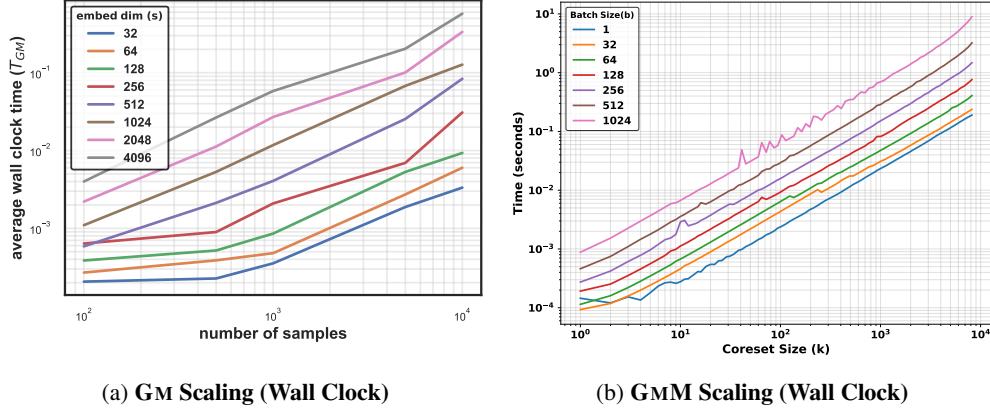


Figure 8: **SCALING LAWS (WALL CLOCK)**: This figure shows the scaling behavior for : **A. SCALING LAWS (WALL CLOCK) GM** computing the geometric median using Weiszfeld algorithm ( Algorithm 2) in terms of the wall clock time ( $T_{GM}$ ) as a function of population size. The x-axis represents the number of samples ( $n$ ) on a logarithmic scale, and the y-axis shows the average wall clock time ( $T_{GM}$ ) on a logarithmic scale. Each curve corresponds to a different embedding dimension ( $d$ ), ranging from 32 to 4096. The results were generated using synthetic data drawn from a standard normal distribution, with the geometric median computed iteratively until convergence (tolerance  $\epsilon = 10^{-5}$ , maximum iterations = 100). For each combination of  $n$  and  $s$ , wall clock time was averaged across 10 random seed. The computational cost increases with both  $n$  and  $s$ : for fixed  $n$ , the scaling with  $s$  is approximately linear, while for fixed  $s$ , scaling with  $n$  exhibits sub-linear to near-linear growth. These results emphasize the trade-offs in selecting  $n$  and  $s$  for practical applications. Experiments were run on a single-threaded CPU setup. These results confirm that the practical runtime aligns with the expected time complexity of  $\mathcal{O}(ns \log(1/\epsilon))$  in typical scenarios, showcasing the efficiency of Weiszfeld algorithm for high-dimensional data. **B. SCALING LAWS (WALL CLOCK) FOR BATCH GM MATCHING** as a function of coreset size ( $k$ ) across varying batch sizes. The log-log scale highlights the computational cost trends for batch sizes ranging from 1 to 1024.

involve matrix multiplications where the hidden size interacts quadratically, reflecting the cost of applying dense layers to each token.

The  $\mathcal{O}(d^2h)$  term is primarily associated with the multi-head attention mechanism itself, particularly the pairwise dot-product computations between tokens. In multi-head attention, each token’s query is compared against every token’s key, resulting in a quadratic dependency on the number of tokens or, more precisely, the per-head dimension after splitting the hidden dimension factors into these computations as well.

The  $\mathcal{O}(dhs)$  term typically arises from the final linear projection (or output projection) after the multi-head attention and other transformer layers.

## B. COMPUTE GM

We now discuss the computational complexity of GM computation over  $n$  points in  $\mathbb{R}^d$ :

Weiszfeld’s algorithm proceeds by iteratively updating the current estimate  $\mathbf{z}^{(k)}$  via a re-weighted average of the data points. Each iteration requires:

- *Distance evaluations*: Computing  $\|\mathbf{x}_i - \mathbf{z}^{(k)}\|$  for all  $i = 1, 2, \dots, n$ . Each distance in  $\mathbb{R}^d$  is evaluated in  $\mathcal{O}(d)$  time, so this step costs  $\mathcal{O}(nd)$  per iteration.
- *Update step*: Forming the weighted average  $\mathbf{z}^{(k+1)} = (\sum_i \frac{\mathbf{x}_i}{\|\mathbf{x}_i - \mathbf{z}^{(k)}\|}) / (\sum_i \frac{1}{\|\mathbf{x}_i - \mathbf{z}^{(k)}\|})$  also takes  $\mathcal{O}(nd)$  time.

Hence, each iteration costs  $\mathcal{O}(nd)$ .

Although Weiszfeld’s algorithm is guaranteed to converge under mild conditions, the *rate* of convergence depends on the geometric configuration of the data points:

- **Non-degenerate (typical) case**: If the geometric median  $\mu^{GM}$  lies strictly in the interior (i.e., it does *not* coincide with any  $\mathbf{x}_i$  and is at a positive distance from each data point), then Weiszfeld’s



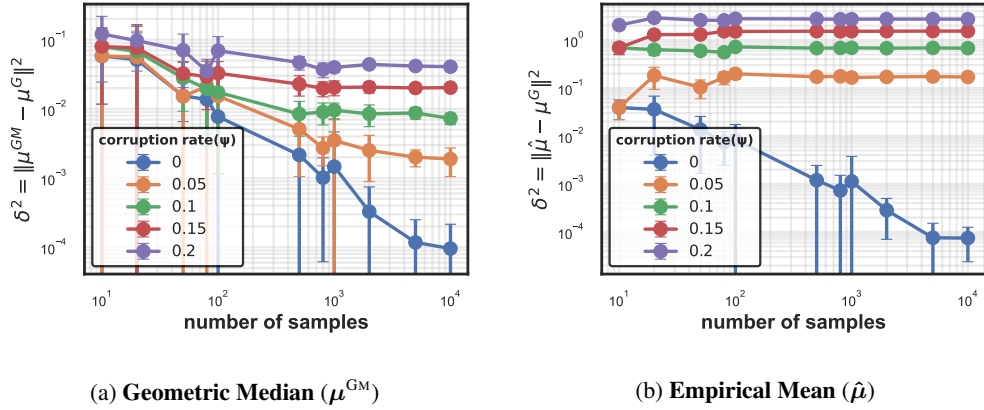


Figure 9: **GM SCALING LAW: CONVERGENCE IN MEAN ESTIMATION ERROR FOR RECOVERING ANISOTROPIC GAUSSIAN** : Comparison of Mean Estimation Error i.e. deviation from the oracle mean using Geometric Median (GM)  $\mu^{\text{GM}}$  and Empirical Mean (EM)  $\hat{\mu}$  as a function of sample size and amount of corruption. GM is computed using Weiszfeld Algorithm Algorithm 2. The  $x$ -axis represents the sample size i.e. the number of samples drawn i.i.d. from an anisotropic Gaussian, with a fraction  $0 \leq \psi < 1/2$  of them corrupted by an adversarially chosen distribution. The plots depict the convergence behavior of both methods across varying corruption rates, highlighting the robustness of GM in the presence of outliers. The plots further emphasize the effect of sample size on estimation error for both the estimators.

iteration converges *linearly* near the optimum. The number of iterations to achieve an  $\epsilon$ -accurate solution typically scales as  $\mathcal{O}(\log(1/\epsilon))$ .

- **Degenerate (worst) case:** If the geometric median coincides with (or lies extremely close to) some data point(s), the objective can lose strict convexity and the Weiszfeld update may progress more slowly. In the worst theoretical analyses, the iteration count can grow as  $\mathcal{O}(1/\epsilon)$ .

Putting it together, let  $K$  denote the iteration count required for an  $\epsilon$ -accurate estimate. We have:

$$T^{\text{GM}} = \begin{cases} \mathcal{O}\left(nd \log(1/\epsilon)\right) & \text{(typical, non-degenerate),} \\ \mathcal{O}\left(nd/\epsilon\right) & \text{(worst-case, degenerate).} \end{cases}$$

where, Time per iteration  $\mathcal{O}(nd)$ . Thus, the *overall time complexity* is either  $\mathcal{O}(nd \log(1/\epsilon))$  in the typical scenario or  $\mathcal{O}(nd(1/\epsilon))$  in the worst case. In practice, degeneracies are rare for generic data, and Weiszfeld's algorithm often converges quite rapidly to a high-accuracy solution. In Figure 8(a), we empirically validate the theoretical scaling behavior of the GM computation, demonstrating how the wall clock time  $T^{\text{GM}}$  scales with the number of samples  $n$  and embedding dimension  $s$ .

### C. SAMPLING ITERATIONS

Each iteration of GM Matching computes inner products between all points in  $\mathcal{D}$  and a direction vector  $\theta \in \mathbb{R}^s$  incurring  $\approx \mathcal{O}(nks)$  computation.

Thus, combining these results, we get the following computational complexity:

$$T \approx \mathcal{O}\left(n(dh^2 + d^2h + s/\epsilon + ks)\right) \quad (23)$$

Additionally, storing the embeddings gives rise to  $\mathcal{O}(ns)$  **space complexity**.

#### 5.4.2 COMPUTATIONAL IMPROVEMENTS

Deploying the robust GM Matching at scale requires addressing the computational costs associated with both the robust GM estimation and the iterative sampling procedure. To mitigate these issues,

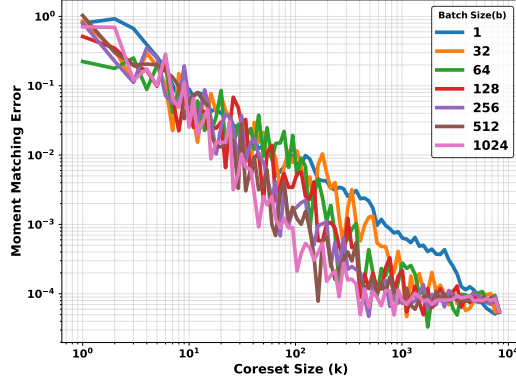


Figure 10: **GM Matching SCALING LAW (CONVERGENCE)**: We plot the moment matching error  $\|\mu(\mathcal{D}_G) - \mu(\mathcal{D}_S)\|^2$  versus the coreset size  $k = |\mathcal{D}_S|$  for the GM Matching algorithm under different batch sizes  $B \in \{1, 32, 64, 128, 256, 512, 1024\}$ . The error decreases as  $k$  grows for all batch sizes, confirming that larger coresets yield more accurate moment approximations. However, the rate of improvement and the final error plateau vary with  $B$ . When  $B = 1$ , the algorithm processes all  $k$  selections at once, resulting in a more pronounced error at smaller  $k$ . By contrast, moderate to large batch sizes (e.g.,  $B = 256$  or  $B = 512$ ) balance computational efficiency and convergence, generally achieving lower moment matching errors for the same  $k$ . This highlights the trade-off introduced by batching: larger  $B$  often provides more stable convergence but at an increased per-iteration computational cost, whereas smaller  $B$  may require more iterations (and potentially higher variance) to attain similar accuracy. Overall, the figure illustrates how careful tuning of  $B$  is critical to optimizing both the computational and statistical performance of GM Matching.

we propose two primary strategies: sub-sampling for GM and batched GM Matching, resulting in improved scalability.

Below we discuss this two-fold scaling strategy as outlined in Algorithm 1.

#### SUB SAMPLING FOR GM.

Computing the robust GM over the entire dataset can be computationally intensive, especially when  $|\mathcal{D}|$  is large. The idea behind sub-sampling is to randomly select a  $0 < \gamma_{GM} \leq 1$  fraction of the data points for the GM computation. This sub-sampling reduces the computational complexity to  $\mathcal{O}(n\gamma_{GM}s/\epsilon)$  in the worst case.

#### BATCHED MOMENT MATCHING.

Instead of selecting all  $k$  samples at once, we divide the iterations into  $B$  batches, selecting  $k/B$  samples per batch. This results in a linear reduction of inner product computations per iteration, lowering the complexity to  $\mathcal{O}(nsk/B)$ .

Furthermore, this also implies that we need to store only  $n/B$  embeddings at a time.

Incorporating these two ideas, we improve the efficiency as outlined in Lemma 2:

**Lemma 2 (GM Matching Computational Complexity).** *The overall time complexity of GM Matching (Algorithm 1) to select  $k$ -subset from  $n$  samples  $\in \mathbb{R}^d$  can be expressed as:*

$$T_{GMM} \approx \mathcal{O}\left(n(dh^2 + d^2h + ks/B + \gamma_{GM}s/\epsilon)\right) \quad (24)$$

where the GM is computed over a randomly chosen  $0 < \gamma_{GM} \leq 1$  fraction of the samples and the GM Matching iterations are performed in  $B$  batches.

Additionally, storing the embeddings of each batch results in  $\mathcal{O}(ks/B)$  **space complexity**.

Empirically, we observe near-linear gains in wall-clock speed when sub-sampling is used to compute the GM and batching is employed in the GM Matching selection process as illustrated in Figure 8.

#### VARIANCE CONSIDERATIONS.

In reducing computational costs, the use of sub-sampling for the robust GM, and batching in the GM Matching selection process inevitably introduces additional variance into the estimation and

selection outcomes. In this section, we dissect the variance implications of these strategies, stressing that any gain in efficiency incurs a trade-off with statistical precision—a quintessential *no free lunch* scenario: faster computation comes with the cost of reduced statistical precision.

Note that the deviation of GM from the true mean depends on the variance of the clean population (Theorem 1). This implies that, when estimating GM over a subset of the data, as the variance of the population increases :

$$\Delta(\sigma^2) \approx \mathcal{O}\left(\left(\frac{1 - \lambda_{\text{GM}}}{\lambda_{\text{GM}}}\right) \cdot \frac{\sigma^2(\mathcal{D}_G)}{n}\right) \quad (25)$$

Thus, while sub-sampling offers a significant computational speedup by reducing the number of points used, it also amplifies the estimation variance—a trade-off that must be carefully balanced by choosing an appropriate sub-sampling fraction relative to the intrinsic noise level of the data. In practice, however, we notice that for sufficiently large  $\gamma_{\text{GM}}$ , the variance increase is negligible compared to the savings as evidenced in Figure 9.

Similarly, batching in the GM Matching selection process, where the selection of the  $k$ -subset is partitioned into  $B$  smaller batches, inherently introduces additional error terms in the convergence. Firstly, for each batch, the herding convergence suffers a constant bias penalty because each batch only selects  $k/B$  samples instead of  $k$  samples, thereby incurring an error term on the order of  $\mathcal{O}(B/k)$ . Moreover, the overall estimate is formed as the mean of the batch estimates, which introduces an additional variance component arising from the averaging of independent errors across batches. This variance term scales as  $\mathcal{O}(1/\sqrt{B})$  i.e.

$$\left\| \mu(\mathcal{D}_S) - \mu_{\epsilon}^{\text{GM}}(\mathcal{D}) \right\| \leq \mathcal{O}\left(\frac{B}{k}\right) + \mathcal{O}\left(\frac{1}{\sqrt{B}}\right). \quad (26)$$

This implies that, while batching can result in significant speedups – too small a batch size can also slow down convergence. In practice, we find that, with a moderate batch size, this additional error is often negligible, while the speedup is substantial as demonstrated in Figure 10.

## 6 EXPERIMENTS

In this section, we outline our experimental setup, present our key empirical findings, and discuss deeper insights into the performance of GM Matching.

Our experiments are divided into three fundamental learning paradigms:

- *Approximating from Noisy Distributions* ( Section 6.2 )
- *Image Classification* ( Section 6.3 )
- *Image Generation* ( Section 6.4 )

By dividing the experiments into these categories, we ensure that GM Matching is tested across a wide spectrum of tasks, covering unsupervised, supervised, and generative learning scenarios. Detailed analyses in each paradigm help uncover not just the strengths of GM Matching but also potential limitations or areas where further improvements can be made. In each experiment, the performance of GM Matching is rigorously compared to established baselines, offering clear evidence of its competitive edge in handling noisy data, enhancing classification, and generating realistic outputs – demonstrating the practical applicability and versatility of GM Matching across a wide array of machine learning challenges.

### 6.1 BASELINES

We compare GM Matching (see Algorithm 1) against several baseline subset selection methods.

These baselines include:

- **Random:** Samples are selected uniformly at random. This approach serves as a **strong** baseline that does not incorporate any structure from the data – widely adopted in practical applications due to its simplicity and strong performance under idealized conditions.

CIFAR-100							
Method / Ratio	20%	30%	40%	60%	80%	100%	Mean ↑
Random	50.26±3.24	53.61±2.73	64.32±1.77	71.03±0.75	74.12±0.56	78.14±0.55	62.67
Herding	48.39±1.42	50.89±0.97	62.99±0.61	70.61±0.44	74.21±0.49	78.14±0.55	61.42
Forgetting	35.57±1.40	49.83±0.91	59.65±2.50	<b>73.34±0.39</b>	<b>77.50±0.53</b>	78.14±0.55	59.18
GraNd-score	42.65±1.39	53.14±1.28	60.52±0.79	69.70±0.68	74.67±0.79	78.14±0.55	60.14
EL2N-score	27.32±1.16	41.98±0.54	50.47±1.20	69.23±1.00	75.96±0.88	78.14±0.55	52.99
Optimization-based	42.16±3.30	53.19±2.14	58.93±0.98	68.93±0.70	75.62±0.33	78.14±0.55	59.77
Self-sup.-selection	44.45±2.51	54.63±2.10	62.91±1.20	70.70±0.82	75.29±0.45	78.14±0.55	61.60
Moderate-DS	51.83±0.52	57.79±1.61	64.92±0.93	71.87±0.91	75.44±0.40	78.14±0.55	64.37
<b>GM Matching</b>	<b>55.93± 0.48</b>	<b>63.08± 0.57</b>	<b>66.59± 1.18</b>	70.82± 0.59	74.63± 0.86	78.14± 0.55	<b>66.01</b>
Tiny ImageNet							
Method / Ratio	20%	30%	40%	60%	80%	100%	Mean ↑
Random	24.02±0.41	29.79±0.27	34.41±0.46	40.96±0.47	45.74±0.61	49.36±0.25	34.98
Herding	24.09±0.45	29.39±0.53	34.13±0.37	40.86±0.61	45.45±0.33	49.36±0.25	34.78
Forgetting	22.37±0.71	28.67±0.54	33.64±0.32	41.14±0.43	<b>46.77±0.31</b>	49.36±0.25	34.52
GraNd-score	23.56±0.52	29.66±0.37	34.33±0.50	40.77±0.42	45.96±0.56	49.36±0.25	34.86
EL2N-score	19.74±0.26	26.58±0.40	31.93±0.28	39.12±0.46	45.32±0.27	49.36±0.25	32.54
Optimization-based	13.88±2.17	23.75±1.62	29.77±0.94	37.05±2.81	43.76±1.50	49.36±0.25	29.64
Self-sup.-selection	20.89±0.42	27.66±0.50	32.50±0.30	39.64±0.39	44.94±0.34	49.36±0.25	33.13
Moderate-DS	25.29±0.38	30.57±0.20	34.81±0.51	41.45±0.44	46.06±0.33	49.36±0.25	35.64
<b>GM Matching</b>	<b>27.88±0.19</b>	<b>33.15±0.26</b>	<b>36.92±0.40</b>	<b>42.48±0.12</b>	46.75±0.51	49.36±0.25	<b>37.44</b>

Table 1: (CLEAN) IMAGE CLASSIFICATION: Comparing Downstream Test Accuracy (Top-1) (%) of several pruning algorithms (Section 6.1) on CIFAR-100 and Tiny-ImageNet in the uncorrupted setting. ResNet-50 is used both as proxy (pretrained) and for downstream classification.

- **Easy:** (Shah et al., 2020): This strategy selects samples that are closest to the centroid of the dataset. These “easy” samples are presumed to be representative of the core data distribution, but may under-represent the data’s diversity, especially in the presence of noise.
- **Hard:** (Joshi et al., 2009): This approach selects samples that are farthest from the centroid. While these “hard” samples may capture edge cases or outliers, they can also be overly sensitive to noise and may not adequately reflect the central structure of the clean distribution.
- **Moderate:** (Xia et al., 2022): This strategy selects samples that are closest to the median distance from the centroid. This approach aims to balance the representation of the data by avoiding the extremes of the distribution, thereby providing a more stable and robust subset.
- **Kernel Herding:** (Chen et al., 2010) kernel herding employs a greedy algorithm to select samples that minimize the discrepancy between the empirical distribution and the target distribution in a reproducing kernel Hilbert space which forms the basis of this work.
- **Forgetting** Toneva et al. (2018): Data points that are easily forgotten during optimization are chosen.
- **GraNd-score** Paul et al. (2021): Data points with larger loss gradient norms are included.
- **EL2N-score** Paul et al. (2021): This focuses on data points with larger norms of the error vector, which is the difference between the predicted class probabilities and the one-hot label encoding.
- **Optimization-based** Yang et al. (2022): This method uses the influence function Koh & Liang (2017) to select data points that minimize the generalization gap under strict constraints.
- **Self-sup.-selection** Sorscher et al. (2022): After self-supervised pre-training and clustering, data points are selected based on their distance to the nearest cluster centroid, with the number of clusters set to the number of classes to avoid tuning. Points with larger distances are chosen.

For GM Matching, the GM is approximated via Algorithm 2 (Weiszfeld, 1937). The optimization routine terminates, either when the GM approximation error is small  $\epsilon_0$  or after a maximum number of iterations  $T_{\max}$  is reached.  $\epsilon_0 = 10^{-8}$  and  $T_{\max} = 1000$  are used for all the experiments.

## 6.2 APPROXIMATING FROM NOISY DISTRIBUTIONS

We simulate a Gaussian Mixture Model (GMM) comprising both clean and adversarial components to evaluate robust moment estimation in noisy datasets. The clean and corrupt samples are drawn from two anisotropic Gaussian distributions:

$$p_{\text{clean}}(x) = \mathcal{N}(x; \mu, \Sigma), \quad p_{\text{adv}}(x) = \mathcal{N}(x; \mu', \Sigma'). \quad (27)$$

ImageNet-1k						
Method / Ratio	60%	70%	80%	90%	100%	Mean ↑
Random	87.91 ± 0.37	88.63 ± 0.95	89.52 ± 0.73	89.57 ± 0.60	90.86 ± 0.71	89.30
Herding	88.25 ± 2.16	88.81 ± 1.06	89.60 ± 0.58	90.41 ± 0.33	90.86 ± 0.71	89.59
Forgetting	88.83 ± 0.92	89.81 ± 0.97	89.94 ± 0.26	90.41 ± 0.58	90.86 ± 0.71	89.97
GraNd-score	88.48 ± 1.73	89.82 ± 2.07	89.94 ± 0.81	90.41 ± 0.62	90.86 ± 0.71	89.90
EL2N-score	88.48 ± 2.81	89.82 ± 1.14	90.34 ± 0.87	90.57 ± 0.46	90.86 ± 0.71	90.01
Self-sup.-selection	87.59 ± 2.61	89.56 ± 1.97	<b>90.74 ± 0.27</b>	90.49 ± 0.98	90.86 ± 0.71	89.49
Moderate-DS	89.23 ± 0.96	89.94 ± 0.74	90.65 ± 0.51	90.75 ± 0.35	90.86 ± 0.71	90.29
<b>GM Matching</b>	<b>90.28 ± 0.38</b>	<b>90.54 ± 0.19</b>	90.72 ± 0.26	<b>90.84 ± 0.32</b>	90.86 ± 0.71	<b>90.65</b>

Table 2: (CLEAN) IMAGE CLASSIFICATION: Downstream Test Accuracy (Top-5) (%) of a ResNet-50 trained on a 60%, 70%, 80%, and 90% subset of ImageNet-1k, where the subset is selected via several benchmark data pruning algorithms(Section 6.1). The best result in each case is in bold.

In our experiments, the two Gaussians are well-separated in the 2D plane, ensuring a clear notion of “clean” vs. “adversarial” clusters with means and covariances:

$$\boldsymbol{\mu} = \begin{bmatrix} 0 \\ 0 \end{bmatrix}, \boldsymbol{\Sigma} = \begin{bmatrix} 1 & -0.5 \\ -0.5 & 0.5 \end{bmatrix}, \boldsymbol{\mu}' = \begin{bmatrix} 10 \\ 6 \end{bmatrix}, \boldsymbol{\Sigma}' = \begin{bmatrix} 1 & 0.5 \\ 0.5 & 0.5 \end{bmatrix}. \quad (28)$$

Assuming that a fraction  $\psi$  of the data is corrupted, the input data is modeled as a mixture:

$$p_{\text{corrupt}}(x) = (1 - \psi)p_{\text{clean}}(x) + \psi p_{\text{adv}}(x). \quad (29)$$

The objective is to select a subset  $\mathcal{D}_S$  of samples such that the subset induced distribution  $p_S(x)$  is as close to the clean distribution  $p_{\text{clean}}(x)$ . We generate a total of  $n = 10^3$  samples, where  $\psi n$  samples are generated from  $p_{\text{adv}}(x)$  and the rest of the  $(1 - \psi)n$  samples are generated from  $p_{\text{clean}}(x)$ , and the sampling algorithms subset 10% of the samples.

#### ROBUSTNESS TO CORRUPTION.

Firstly, in **Figure 6**, we observe that as the fraction of adversarial samples  $\psi$  increases, the empirical mean of the noisy data set drifts noticeably towards the adversarial group. In contrast, GM remains anchored near the true uncorrupted mean  $\boldsymbol{\mu}$ . This divergence underscores the vulnerability of classical moment estimators to even modest levels of noise – a phenomenon well documented in robust statistics (Huber, 1992; Diakonikolas & Kane, 2019).

In our robust sampling experiments, we observe that when  $\psi = 0$  i.e. the no-corruption scenario, all methods trivially capture the clean distribution, but as soon as a fraction of the data is adversarial, many standard strategies fail to consistently filter out the adversarial cluster. However, as  $\psi$  increases as demonstrated in **Figure 2**. Methods like uniform sampling or even heuristic approaches (Easy, Hard, and Moderate), as well as standard Kernel Herding, begin to pick up an increasing number of adversarial points. Their selected subsets start to show a clear dual-group pattern, which results in a mixed empirical distribution that deviates from  $p_{\text{clean}}(x)$ .

In contrast, GM Matching yields a significantly more robust subset than these baseline methods, effectively filtering out adversarial noise while preserving the intrinsic structure of the clean data. The robustness of GM Matching becomes particularly prominent at high corruption levels ( $\psi = 0.4$ ,  $\psi = 0.45$ ) where most other methods fail. This demonstrates the potential of the proposed strategy to serve as a powerful tool for robust moment estimation in noisy and adversarial settings.

#### ABLATIONS WITH PROXY ENCODER

Next, we examine the impact of various kernel maps on the performance of GM Matching, particularly in the presence of data corruption. Using a Gaussian mixture model as our testbed, we empirically evaluated different kernels to understand their ability to capture the underlying data structure and robustness under noise.

In Figure 11, we experiment with polynomial kernels:

$$\omega(\mathbf{x}, \mathbf{x}') = (\langle \mathbf{x}, \mathbf{x}' \rangle + c)^d \quad (30)$$

where,  $c$  is a constant (typically set to 1) and  $d$  is the degree of the polynomial. We tried varying degrees  $d = \{1, 3, 5, 10\}$ , highlighting how increased degree improves representational capacity while potentially amplifying noise when data are corrupted 20% corruption.

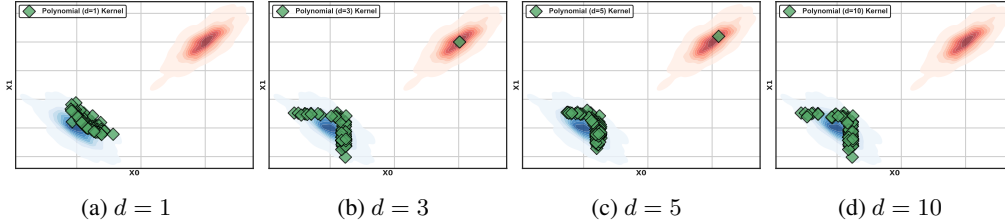


Figure 11: **POLYNOMIAL KERNEL**: GM Matching experiments under **20% corruption** using a polynomial kernel. Sub-figures (a)–(d) illustrate the effect of varying the polynomial degree (1, 3, 5, and 10, respectively) on the kernel mapping performance. The comparison highlights how increasing the degree can influence robustness and representational capacity in corrupted settings.

### 6.3 IMAGE CLASSIFICATION

This set of experiments evaluates the performance of GM Matching when applied to Image Classification tasks. To ensure reproducibility, our experimental setup – including baselines, neural architectures, and choice of hyper-parameters – is identical to (Xia et al., 2022).

#### 6.3.1 EXPERIMENTAL SETUP

We evaluate the performance of GM Matching against multiple popular data pruning baselines, namely Random selection, Moderate (Xia et al., 2022), Forgetting (Toneva et al., 2018), Kernel Herding (Chen et al., 2010), GraNd-score (Paul et al., 2021), EL2N-score (Paul et al., 2021), and Self-supervised Selection (Sorscher et al., 2022). These baselines are evaluated across both standard (uncorrupted) and robustness-focused experimental settings.

Our robust sampling experiments assess the resilience of each algorithm to a variety of data corruptions, measuring their generalization capabilities beyond conventional training conditions. Specifically, we investigate three key robustness scenarios: (1) direct corruptions applied to images (Section 6.3.3), (2) label noise (Section 6.3.4), and (3) adversarial attacks (Section 6.3.5) across different corruption intensities.

Additionally, we conduct a series of ablation studies to analyze the impact of incorporating a Proxy Encoder within the GM Matching pipeline. These studies examine how changes in network architecture and distribution shifts between the pretraining distribution (proxy) and downstream tasks affect pruning efficacy. These experiments provide deeper insights into the role of the Proxy Encoder and its influence on the overall performance of GM Matching.

We conduct experiments on widely used image classification benchmarks, including CIFAR-10/100 (Krizhevsky, 2009), Tiny-ImageNet (Le & Yang, 2015), and ImageNet-1K (Deng et al., 2009). Our study spans multiple popular neural network architectures, such as ResNet-18/50 (He et al., 2016), VGG-16 (Simonyan & Zisserman, 2014), ShuffleNet (Ma et al., 2018), SENet (Hu et al., 2018), EfficientNet-B0 (Tan & Le, 2019), and ViT-S (Dosovitskiy et al., 2020; Lee et al., 2021).

For CIFAR-10/100 datasets, the training configuration consists of a batch size of 128, SGD optimizer with momentum (0.9), weight decay of  $5 \times 10^{-4}$ , and an initial learning rate of 0.1. The learning rate undergoes step-wise decay by a factor of 5 at epochs 60, 120, and 160, totaling 200 epochs. Data augmentation strategies incorporate random cropping and random horizontal flipping.

For Tiny-ImageNet and ImageNet-1k experiments, we use a batch size of 256, SGD optimizer with momentum (0.9), weight decay of  $1 \times 10^{-4}$ , and an initial learning rate of 0.1. The learning rate decreases by a factor of 10 at epochs 30 and 60, across 90 total epochs, employing random horizontal flipping for data augmentation.

For computational practicality, particularly due to the scale of datasets and the complexity of geometric median computation, we employ the approximate Weiszfeld solver (Algorithm 2) for estimating the GM. Specifically, to further enhance computational efficiency without significant performance compromise, the solver computes the median over a randomly selected subset consisting of 50% of the training data points.

CIFAR-100							
Method / Ratio	20%	30%	40%	60%	80%	100%	Mean ↑
<b>5% Feature Corruption</b>							
Random	43.14±3.04	54.19±2.92	64.21±2.39	69.50±1.06	72.90±0.52	77.26±0.39	60.79
Herding	42.50±1.27	53.88±3.07	60.54±0.94	69.15±0.55	73.47±0.89	77.26±0.39	59.81
Forgetting	32.42±0.74	49.72±1.64	54.84±2.20	70.22±2.00	75.19±0.40	77.26±0.39	56.48
GraNd-score	42.24±0.57	53.48±0.76	60.17±1.66	69.16±0.81	73.35±0.81	77.26±0.39	59.68
EL2N-score	26.13±1.75	39.01±1.42	49.89±1.87	68.36±1.41	73.10±0.36	77.26±0.39	51.30
Optimization-based	38.25±3.04	50.88±6.07	57.26±0.93	68.02±0.39	73.77±0.56	77.26±0.39	57.64
Self-sup.-selection	44.24±0.48	55.99±1.21	61.03±0.59	69.96±1.07	74.56±1.17	77.26±0.39	61.16
Moderate-DS	46.78±1.90	57.36±1.22	65.40±1.19	71.46±0.19	<b>75.64±0.61</b>	77.26±0.39	63.33
<b>GM Matching</b>	<b>49.50±0.72</b>	<b>60.23±0.88</b>	<b>66.25±0.51</b>	<b>72.91±0.26</b>	75.10±0.29	77.26±0.39	<b>64.80</b>
<b>10% Feature Corruption</b>							
Random	43.27±3.01	53.94±2.78	62.17±1.29	68.41±1.21	73.50±0.73	76.50±0.63	60.26
Herding	44.34±1.07	53.31±1.49	60.13±0.38	68.20±0.74	74.34±1.07	76.50±0.63	60.06
Forgetting	30.43±0.70	47.50±1.43	53.16±0.44	70.36±0.82	75.11±0.71	76.50±0.63	55.31
GraNd-score	36.36±1.06	52.26±0.66	60.22±1.39	68.96±0.62	72.78±0.51	76.50±0.63	58.12
EL2N-score	21.75±1.56	30.80±2.23	41.06±1.23	64.82±1.48	73.47±1.30	76.50±0.63	46.38
Optimization-based	37.22±0.39	48.92±1.38	56.88±1.48	67.33±2.15	72.94±1.90	76.50±0.63	56.68
Self-sup.-selection	42.01±1.31	54.47±1.19	61.37±0.68	68.52±1.24	74.73±0.36	76.50±0.63	60.22
Moderate-DS	47.02±0.66	55.60±1.67	62.18±1.86	71.83±0.78	<b>75.66±0.66</b>	76.50±0.63	62.46
<b>GM Matching</b>	<b>48.86±1.02</b>	<b>60.15±0.43</b>	<b>66.92±0.28</b>	<b>72.03±0.38</b>	73.71±0.19	76.50±0.63	<b>64.33</b>
<b>20% Feature Corruption</b>							
Random	40.99±1.46	50.38±1.39	57.24±0.65	65.21±1.31	71.74±0.28	74.92±0.88	57.11
Herding	44.42±0.46	53.57±0.31	60.72±1.78	69.09±1.73	73.08±0.98	74.92±0.88	60.18
Forgetting	26.39±0.17	40.78±2.02	49.95±2.31	65.71±1.12	73.67±1.12	74.92±0.88	51.30
GraNd-score	36.33±2.66	46.21±1.48	55.51±0.76	64.59±2.40	70.14±1.36	74.92±0.88	54.56
EL2N-score	21.64±2.03	23.78±1.66	35.71±1.17	56.32±0.86	69.66±0.43	74.92±0.88	41.42
Optimization-based	33.42±1.60	45.37±2.81	54.06±1.74	65.19±1.27	70.06±0.83	74.92±0.88	54.42
Self-sup.-selection	42.61±2.44	54.04±1.90	59.51±1.22	68.97±0.96	72.33±0.20	74.92±0.88	60.01
Moderate-DS	42.98±0.87	55.80±0.95	61.84±1.96	70.05±1.29	73.67±0.30	74.92±0.88	60.87
<b>GM Matching</b>	<b>47.12±0.64</b>	<b>59.17±0.92</b>	<b>63.45±0.34</b>	<b>71.70±0.60</b>	<b>74.60±1.03</b>	74.92±0.88	<b>63.21</b>

Table 3: **(FEATURE CORRUPTION) IMAGE CLASSIFICATION ( CIFAR 100 )**: Comparing the downstream test accuracy of various pruning methods when 5%, 10%, and 20% of images are corrupted. Results are reported across different selection ratios (20%-100%) using **ResNet-50** as both the proxy and downstream classifier. GM Matching consistently outperforms all baselines, demonstrating superior robustness to corrupted data, with increasing performance gains at higher corruption levels.

To account for variability and ensure statistical robustness, each experimental configuration is independently replicated across five distinct random seeds. Performance metrics are reported with variance to transparently capture and reflect the consistency of each method.

### 6.3.2 IDEAL (NO CORRUPTION) SCENARIO:

Our initial set of experiments evaluates the effectiveness of different data pruning strategies under an ideal, uncorrupted setting. We systematically prune datasets at selection ratios ranging from 20% to 80%, assessing the downstream classification performance across two widely used benchmarks: CIFAR-100 and Tiny ImageNet. The corresponding results, presented in Table 1, demonstrate that despite being designed with robustness-oriented applications in mind, GM Matching surpasses existing strong baselines even in the standard, clean setting.

Across both datasets, GM Matching achieves an average improvement of over 2% compared to prior methods. Notably, its performance gains are particularly pronounced in the low-data selection regime (20%-40%), where it significantly outperforms competing pruning techniques. In Table 2, we observe similar improvements with GM Matching on ImageNet-1k. This suggests that GM Matching is especially effective in scenarios where data efficiency is critical, making it a promising approach for resource-constrained settings.

Tiny ImageNet							
Method / Ratio	20%	30%	40%	60%	80%	100%	Mean ↑
<b>5% Feature Corruption</b>							
Random	23.51±0.22	28.82±0.72	32.61±0.68	39.77±0.35	44.37±0.34	49.02±0.35	33.82
Herding	23.09±0.53	28.67±0.37	33.09±0.32	39.71±0.31	45.04±0.15	49.02±0.35	33.92
Forgetting	21.36±0.28	27.72±0.43	33.45±0.21	40.92±0.45	45.99±0.51	49.02±0.35	33.89
GraNd-score	22.47±0.23	28.85±0.83	33.81±0.24	40.40±0.15	44.86±0.49	49.02±0.35	34.08
EL2N-score	18.98±0.72	25.96±0.28	31.07±0.63	38.65±0.36	44.21±0.68	49.02±0.35	31.77
Optimization-based	13.65±1.26	24.02±1.35	29.65±1.86	36.55±1.84	43.64±0.71	49.02±0.35	29.50
Self-sup.-selection	19.35±0.57	26.11±0.31	31.90±0.37	38.91±0.29	44.43±0.42	49.02±0.35	32.14
Moderate-DS	24.63±0.78	30.27±0.16	34.84±0.24	40.86±0.42	45.60±0.31	49.02±0.35	35.24
<b>GM Matching</b>	<b>27.46±1.22</b>	<b>33.14±0.61</b>	<b>35.76±1.14</b>	<b>41.62±0.71</b>	<b>46.83±0.56</b>	49.02±0.35	<b>36.96</b>
<b>10% Feature Corruption</b>							
Random	22.67±0.27	28.67±0.52	31.88±0.30	38.63±0.36	43.46±0.20	48.40±0.32	33.06
Herding	22.01±0.18	27.82±0.11	31.82±0.26	39.37±0.18	44.18±0.27	48.40±0.32	33.04
Forgetting	20.06±0.48	27.17±0.36	32.31±0.22	40.19±0.29	45.51±0.48	48.40±0.32	33.05
GraNd-score	21.52±0.48	26.98±0.43	32.70±0.19	40.03±0.26	44.87±0.35	48.40±0.32	33.22
EL2N-score	18.59±0.13	25.23±0.18	30.37±0.22	38.44±0.32	44.32±1.07	48.40±0.32	31.39
Optimization-based	14.05±1.74	29.18±1.77	29.12±0.61	36.28±1.88	43.52±0.31	48.40±0.32	29.03
Self-sup.-selection	19.47±0.26	26.51±0.55	31.78±0.14	38.87±0.54	44.69±0.29	48.40±0.32	32.26
Moderate-DS	23.79±0.16	29.56±0.16	34.60±0.12	40.36±0.27	45.10±0.23	48.40±0.32	34.68
<b>GM Matching</b>	<b>27.41±0.23</b>	<b>32.84±0.98</b>	<b>36.27±0.68</b>	<b>41.85±0.29</b>	<b>46.35±0.44</b>	48.40±0.32	<b>36.94</b>
<b>20% Feature Corruption</b>							
Random	19.99±0.42	25.93±0.53	30.83±0.44	37.98±0.31	42.96±0.62	46.68±0.43	31.54
Herding	19.46±0.14	24.47±0.33	29.72±0.39	37.50±0.59	42.28±0.30	46.68±0.43	30.86
Forgetting	18.47±0.46	25.53±0.23	31.17±0.24	39.35±0.44	44.55±0.67	46.68±0.43	31.81
GraNd-score	20.07±0.49	26.68±0.40	31.25±0.40	38.21±0.49	42.84±0.72	46.68±0.43	30.53
EL2N-score	18.57±0.30	24.42±0.44	30.04±0.15	37.62±0.44	42.43±0.61	46.68±0.43	30.53
Optimization-based	13.71±0.26	23.33±1.84	29.15±2.84	36.12±1.86	42.94±0.52	46.88±0.43	29.06
Self-sup.-selection	20.22±0.23	26.90±0.50	31.93±0.49	39.74±0.52	44.27±0.10	46.68±0.43	32.61
Moderate-DS	23.27±0.33	29.06±0.36	33.48±0.11	40.07±0.36	44.73±0.39	46.68±0.43	34.12
<b>GM Matching</b>	<b>27.19±0.92</b>	<b>31.70±0.78</b>	<b>35.14±0.19</b>	<b>42.04±0.31</b>	<b>45.12±0.28</b>	46.68±0.43	<b>36.24</b>

Table 4: (FEATURE CORRUPTION) IMAGE CLASSIFICATION (TINY IMAGENET): Comparison of downstream test accuracy for various pruning methods when 5%, 10%, and 20% of images are corrupted. Results are reported across different selection ratios (20%-100%) using **ResNet-50** as both the proxy and downstream classifier. GM Matching consistently outperforms all baselines, demonstrating stronger resilience to image corruption, with increasing performance advantages at higher corruption levels.

### 6.3.3 ROBUSTNESS TO IMAGE CORRUPTION:

In real-world applications, machine learning models are often deployed in environments where the input data is imperfect, degraded, or subject to various forms of corruption. This degradation can stem from sensor noise, environmental conditions, transmission artifacts, or adversarial perturbations.

To systematically evaluate the robustness of data pruning strategies under such conditions, we introduce structured image corruptions into the dataset and assess the downstream test accuracy across varying levels of pruning.

Specifically, we adopt the following practical perturbation types, drawing from established robustness benchmarks (Hendrycks & Dietterich, 2019; Szegedy et al., 2013) as -

- *Gaussian Noise*: Models real-world sensor noise by adding random perturbations sampled from a standard normal distribution.
- *Random Occlusion*: Mimics missing or occluded regions in images by replacing random patches with black or noisy pixels.
- *Resolution Reduction*: Simulates low-quality images by applying aggressive down-sampling and up-sampling, introducing pixelation artifacts.
- *Fog*: Emulates atmospheric distortions by overlaying a simulated fog effect – resulting in reduced contrast and visibility.
- *Motion Blur*: Models dynamic distortions caused by camera motion or moving objects during exposure.



Method / Ratio	CIFAR-100 (Label noise)		Tiny ImageNet (Label noise)		Mean ↑
	20%	30%	20%	30%	
<b>20% Label Noise</b>					
Random	34.47±0.64	43.26±1.21	17.78±0.44	23.88±0.42	29.85
Herding	42.29±1.75	50.52±3.38	18.98±0.44	24.23±0.29	34.01
Forgetting	36.53±1.11	45.78±1.04	13.20±0.38	21.79±0.43	29.33
GraNd-score	31.72±0.67	42.80±0.30	18.28±0.32	23.72±0.18	28.05
EL2N-score	29.82±1.19	33.62±2.35	13.93±0.69	18.57±0.31	23.99
Optimization-based	32.79±0.62	41.80±1.14	14.77±0.95	22.52±0.77	27.57
Self-sup.-selection	31.08±0.78	41.87±0.63	15.10±0.73	21.01±0.36	27.27
Moderate-DS	40.25±0.12	48.53±1.60	19.64±0.40	24.96±0.30	31.33
<b>GM Matching</b>	<b>52.64±0.72</b>	<b>61.01±0.47</b>	<b>25.80±0.37</b>	<b>31.71±0.24</b>	<b>42.79</b>
<b>35% Label Noise</b>					
Random	24.51±1.34	32.26±0.81	14.64±0.29	19.41±0.45	22.71
Herding	29.42±1.54	37.50±2.12	15.14±0.45	20.19±0.45	25.56
Forgetting	29.48±1.98	38.01±2.21	11.25±0.90	17.07±0.66	23.14
GraNd-score	23.03±1.05	34.83±2.01	13.68±0.46	19.51±0.45	22.76
EL2N-score	21.95±1.08	31.63±2.84	10.11±0.25	13.69±0.32	19.39
Optimization-based	26.77±0.15	35.63±0.92	12.37±0.68	18.52±0.90	23.32
Self-sup.-selection	23.12±1.47	34.85±0.68	11.23±0.32	17.76±0.69	22.64
Moderate-DS	28.45±0.53	36.55±1.26	15.27±0.31	20.33±0.28	25.15
<b>GM Matching</b>	<b>43.33± 1.02</b>	<b>58.41± 0.68</b>	<b>23.14± 0.92</b>	<b>27.76± 0.40</b>	<b>38.16</b>

Table 5: (LABEL NOISE) IMAGE CLASSIFICATION: Comparing (Test Accuracy) pruning methods on CIFAR-100 and TinyImageNet datasets, under 20% and 35% Symmetric Label Corruption, at 20% and 30% selection ratio. ResNet-50 is used both as proxy and for downstream classification.

To introduce diverse corruption across the dataset while ensuring a balanced distribution, we apply each corruption type uniformly at random to the corrupted samples. Instead of assigning fixed partitions, this approach ensures that each sample has an equal probability of being affected by any of the five corruption types. This stochastic allocation results in a heterogeneous mix of corruptions, compelling models to generalize across multiple degradation patterns rather than overfitting to a specific type of distortion.

The results of our experiments, presented in Tables 3 and 4, evaluate the impact of increasing corruption levels (5%, 10%, and 20%) on various pruning methods. Across both CIFAR-100 and Tiny ImageNet, GM Matching consistently outperforms all baselines, achieving an average accuracy improvement of  $\approx 3\%$  over the next-best approach.

This performance gap is amplified at higher corruption levels, where GM Matching maintains superior test accuracy. Moreover, the gains are also significant at aggressive pruning ratios (20%-40%), where GM Matching improves test accuracy by 2-4% over baselines. This trend aligns with its strong performance in data-scarce settings, reinforcing its ability to preserve robustness even when training data is significantly reduced.

Among baselines, Random Selection exhibits a steady performance drop with increasing corruption, confirming its inability to retain robustness. Herding and Moderate-DS, while effective in standard settings, struggle under high corruption levels. Forgetting and Optimization-based methods show inconsistent results, likely due to their reliance on training dynamics that become unstable when corrupted samples are introduced. GraNd-score and EL2N-score, which prioritize loss-based selection, perform well in clean settings but degrade significantly under corruption, suggesting vulnerability to adversarial perturbations. Self-supervised Selection remains competitive but fails to match GM Matching, particularly at higher corruption intensities.

### 6.3.4 ROBUSTNESS TO LABEL CORRUPTION:

Next, we consider label noise – a prevalent issue in real-world datasets, where obtaining perfectly annotated data is impractical due to human labeling errors, dataset aggregation inconsistencies, or adversarial data manipulations. Consequently, it is crucial to assess the ability of data pruning methods to select informative samples while filtering out mislabeled examples, ensuring robustness to noisy annotations.

Tiny ImageNet (Label Noise)							
Method / Ratio	20%	30%	40%	60%	80%	100%	Mean $\uparrow$
Random	17.78 $\pm$ 0.44	23.88 $\pm$ 0.42	27.97 $\pm$ 0.39	34.88 $\pm$ 0.51	38.47 $\pm$ 0.40	44.42 $\pm$ 0.47	28.60
Herdling	18.98 $\pm$ 0.44	24.23 $\pm$ 0.29	27.28 $\pm$ 0.31	34.36 $\pm$ 0.29	39.00 $\pm$ 0.49	44.42 $\pm$ 0.47	28.87
Forgetting	13.20 $\pm$ 0.38	21.79 $\pm$ 0.43	27.89 $\pm$ 0.22	36.03 $\pm$ 0.24	40.60 $\pm$ 0.31	44.42 $\pm$ 0.47	27.50
GraNd-score	18.28 $\pm$ 0.32	23.72 $\pm$ 0.18	27.34 $\pm$ 0.33	34.91 $\pm$ 0.19	39.45 $\pm$ 0.45	44.42 $\pm$ 0.47	28.34
EL2N-score	13.93 $\pm$ 0.69	18.57 $\pm$ 0.31	24.56 $\pm$ 0.34	32.14 $\pm$ 0.49	37.64 $\pm$ 0.41	44.42 $\pm$ 0.47	25.37
Optimization-based	14.77 $\pm$ 0.95	22.52 $\pm$ 0.77	25.62 $\pm$ 0.90	34.18 $\pm$ 0.79	38.49 $\pm$ 0.69	44.42 $\pm$ 0.47	27.12
Self-sup.-selection	15.10 $\pm$ 0.73	21.01 $\pm$ 0.36	26.62 $\pm$ 0.22	33.93 $\pm$ 0.36	39.22 $\pm$ 0.12	44.42 $\pm$ 0.47	27.18
Moderate-DS	19.64 $\pm$ 0.40	24.96 $\pm$ 0.30	29.56 $\pm$ 0.21	35.79 $\pm$ 0.36	39.93 $\pm$ 0.23	44.42 $\pm$ 0.47	30.18
<b>GM Matching</b>	<b>25.80<math>\pm</math>0.37</b>	<b>31.71<math>\pm</math>0.24</b>	<b>34.87<math>\pm</math>0.21</b>	<b>39.76<math>\pm</math>0.71</b>	<b>41.94<math>\pm</math>0.23</b>	44.42 $\pm$ 0.47	<b>34.82</b>

Table 6: (LABEL NOISE) IMAGE CLASSIFICATION (TINY IMAGENET): Comparing downstream classification performance of pruning methods under 20% Symmetric Label Corruption across wide array of selection ratio (20%-100%). ResNet-50 is used both as proxy and for downstream classification.

To systematically evaluate pruning methods under label noise, we introduce synthetically injected symmetric label noise, a widely used corruption paradigm in robust learning (Li et al., 2022; Patrini et al., 2017; Xia et al., 2020). In this setting, a fraction of training labels is randomly flipped to a different class, simulating annotation errors encountered in large-scale weakly labeled datasets. We experiment with two corruption levels (20% and 35% label noise) and report test accuracy across different pruning ratios.

Interestingly, in both CIFAR-100 and Tiny ImageNet, training ResNet50 in a subset selected by GM Matching outperforms all competing methods by a large margin (Table 5,6). For instance, at 20% label noise, when selecting 30% of samples from CIFAR-100, GM Matching achieves 61.01% accuracy, compared to 48.53% (Moderate-DS) and 45.78% (Forgetting). At 35% label noise, the performance gap widens, with GM Matching achieving 58.41%, while the closest baseline (Moderate-DS) lags behind at 36.55%. Similar trends hold for Tiny ImageNet, where GM Matching outperforms the best baseline by 4-6% across different noise levels. Overall, on average GM Matching outperforms the baselines by  $\approx 12\%$  when selecting a small 20 – 30%. Moreover, when Vision Transformers are trained on a 20% subset of CIFAR-10 data chosen by GM Matching, they achieve  $\approx 10\%$  improvement over previous robust data selection algorithms (Table 8).

Since mislabeled examples originate from random class assignments, they tend to be spatially dissimilar from their intended class distributions. As a result, GM Matching is less likely to select such noisy examples, leading to improved generalization despite high noise levels.

### 6.3.5 ROBUSTNESS TO ADVERSARIAL ATTACKS:

Adversarial attacks pose a fundamental challenge to the reliability of deep learning models, as they introduce imperceptible but highly effective perturbations to input samples, forcing misaligned predictions (Szegedy et al., 2013; Huang et al., 2010).

To assess the robustness of data pruning methods in adversarial settings, we experiment with two widely used attack techniques:

- *Projected Gradient Descent (PGD)* (Madry et al., 2017): A strong iterative attack that optimizes perturbations by taking multiple gradient ascent steps, maximizing the model’s loss function.
- *Gradient Sign Attack (GS)* (Goodfellow et al., 2014): A single-step adversarial attack that perturbs the input along the gradient of the loss function, often serving as a computationally efficient alternative to PGD.

Using these attack methods, we generate adversarial examples from models trained on CIFAR-100 and Tiny ImageNet. We then apply different data pruning strategies to these adversarial datasets and retrain models on the curated subsets to analyze their effectiveness in retaining robustness. The results with ResNet-50 are summarized in Table 7, and the experiments with ViT are presented in Table 8.

Similar to other corruption scenarios, across both datasets and attack types, GM Matching consistently outperforms all baseline pruning methods, yielding an average accuracy improvement of 3% over the next-best approach. Specifically, under PGD attacks on CIFAR-100, GM Matching achieves 45.41% accuracy at 20% selection, compared to 43.60% (Moderate-DS) and 40.87% (GraNd-score).

CIFAR-100 (PGD Attack)		CIFAR-100 (GS Attack)		Mean $\uparrow$	
Method / Ratio	20%	30%	20%		30%
Random	43.23 $\pm$ 0.31	52.86 $\pm$ 0.34	44.23 $\pm$ 0.41	53.44 $\pm$ 0.44	48.44
Herding	40.21 $\pm$ 0.72	49.62 $\pm$ 0.65	39.92 $\pm$ 1.03	50.14 $\pm$ 0.15	44.97
Forgetting	35.90 $\pm$ 1.30	47.37 $\pm$ 0.99	37.55 $\pm$ 0.53	46.88 $\pm$ 1.91	41.93
GraNd-score	40.87 $\pm$ 0.84	50.13 $\pm$ 0.30	40.77 $\pm$ 1.11	49.88 $\pm$ 0.83	45.41
EL2N-score	26.61 $\pm$ 0.58	34.50 $\pm$ 1.02	26.72 $\pm$ 0.66	35.55 $\pm$ 1.30	30.85
Optimization-based	38.29 $\pm$ 1.77	46.25 $\pm$ 1.82	41.36 $\pm$ 0.92	49.10 $\pm$ 0.81	43.75
Self-sup.-selection	40.53 $\pm$ 1.15	49.95 $\pm$ 0.50	40.74 $\pm$ 1.66	51.23 $\pm$ 0.25	45.61
Moderate-DS	43.60 $\pm$ 0.97	51.66 $\pm$ 0.39	44.69 $\pm$ 0.68	53.71 $\pm$ 0.37	48.42
<b>GM Matching</b>	<b>45.41 <math>\pm</math>0.86</b>	<b>51.80 <math>\pm</math>1.01</b>	<b>49.78 <math>\pm</math>0.27</b>	<b>55.50 <math>\pm</math>0.31</b>	<b>50.62</b>

Tiny ImageNet (PGD Attack)		Tiny ImageNet (GS Attack)		Mean $\uparrow$	
Method / Ratio	20%	30%	20%		30%
Random	20.93 $\pm$ 0.30	26.60 $\pm$ 0.98	22.43 $\pm$ 0.31	26.89 $\pm$ 0.31	24.21
Herding	21.61 $\pm$ 0.36	25.95 $\pm$ 0.19	23.04 $\pm$ 0.28	27.39 $\pm$ 0.14	24.50
Forgetting	20.38 $\pm$ 0.47	26.12 $\pm$ 0.19	22.06 $\pm$ 0.31	27.21 $\pm$ 0.21	23.94
GraNd-score	20.76 $\pm$ 0.21	26.34 $\pm$ 0.32	22.56 $\pm$ 0.30	27.52 $\pm$ 0.40	24.30
EL2N-score	16.67 $\pm$ 0.62	22.36 $\pm$ 0.42	19.93 $\pm$ 0.57	24.65 $\pm$ 0.32	20.93
Optimization-based	19.26 $\pm$ 0.77	24.55 $\pm$ 0.92	21.26 $\pm$ 0.24	25.88 $\pm$ 0.37	22.74
Self-sup.-selection	19.23 $\pm$ 0.46	23.92 $\pm$ 0.51	19.70 $\pm$ 0.20	24.73 $\pm$ 0.39	21.90
Moderate-DS	21.81 $\pm$ 0.37	27.11 $\pm$ 0.20	23.20 $\pm$ 0.13	28.89 $\pm$ 0.27	25.25
<b>GM Matching</b>	<b>25.98 <math>\pm</math>1.12</b>	<b>30.77 <math>\pm</math>0.25</b>	<b>29.71 <math>\pm</math>0.45</b>	<b>32.88 <math>\pm</math>0.73</b>	<b>29.84</b>

Table 7: (ADVERSARIAL ATTACKS) IMAGE CLASSIFICATION: Comparing (Test Accuracy) pruning methods under PGD and GS attacks. ResNet-50 is used both as proxy and for downstream classification.

CIFAR-100 (ViT-S)					
Method	No Corruption	Noisy Feature	Label Noise	Adv. Attack	Mean $\uparrow$
Random	33.80 $\pm$ 0.54	31.29 $\pm$ 0.61	26.67 $\pm$ 0.54	31.01 $\pm$ 0.45	30.19
Herding	32.16 $\pm$ 0.37	31.75 $\pm$ 0.22	32.27 $\pm$ 0.53	31.28 $\pm$ 0.66	31.37
Forgetting	33.52 $\pm$ 0.73	24.45 $\pm$ 0.29	26.24 $\pm$ 1.07	28.26 $\pm$ 1.95	28.12
GraNd-score	22.49 $\pm$ 0.47	18.40 $\pm$ 0.11	22.13 $\pm$ 0.90	19.27 $\pm$ 1.27	20.07
EL2N-score	26.15 $\pm$ 0.21	23.27 $\pm$ 0.68	24.80 $\pm$ 0.72	20.26 $\pm$ 1.68	23.12
Optimization-based	31.84 $\pm$ 0.63	30.12 $\pm$ 0.73	30.12 $\pm$ 0.70	29.36 $\pm$ 0.75	30.36
Self-sup.-selection	33.35 $\pm$ 0.31	30.72 $\pm$ 0.90	29.16 $\pm$ 0.27	28.49 $\pm$ 0.56	30.93
Moderate-DS	34.43 $\pm$ 0.32	32.73 $\pm$ 0.35	31.86 $\pm$ 0.49	32.61 $\pm$ 0.40	32.91
<b>GM Matching</b>	<b>40.81<math>\pm</math>0.87</b>	<b>38.26<math>\pm</math>0.68</b>	<b>42.11<math>\pm</math>0.36</b>	<b>39.45<math>\pm</math>0.82</b>	<b>40.66</b>

Table 8: IMAGE CLASSIFICATION (ViT-S): We compare the downstream test accuracy of various data selection methods on simulated CIFAR-100 (using ViT-S) under different corruption types: No Corruption, Noisy Feature, Label Noise, and Adversarial Attack. All experiments are performed with a fixed selection ratio of 20%, using ResNet-50 as both the proxy and downstream classifier. Our method, GM Matching, consistently outperforms all baselines—demonstrating superior robustness to corrupted data, with larger performance gains at higher corruption levels. Mean and standard deviation (%) are reported over multiple runs. The best result in each case is highlighted in **bold**.

Similarly, in Tiny ImageNet under GS attacks, GM Matching maintains the highest mean accuracy of 29.84%, outperforming Moderate-DS (25.25%) and Self-supervised Selection (21.90%).

### 6.3.6 ABLATIONS WITH PROXY ENCODER

Since the input features (e.g. images) often reside on a non-separable manifold, data pruning strategies rely on proxy models to map raw input samples into a separable embedding space, where importance scores can be assigned more effectively.

#### A. IDEALIZED SETTING.

In the standard setting, the proxy model used for sample selection is identical to the model used for downstream training—both in terms of architecture and dataset. This represents an idealized scenario, where the feature representations used to evaluate sample importance remain consistent throughout training. Since the proxy and final models are identical, performance differences between pruning methods directly reflect the effectiveness of sample selection, rather than being confounded by architectural mismatches. Since no external factors (such as domain shifts) interfere, the results from this setup serve as a benchmark for understanding the best-case scenario for sample selection.

Method / Ratio	ResNet-50→SENet		ResNet-50→EfficientNet-B0		Mean ↑
	20%	30%	20%	30%	
Random	34.13±0.71	39.57±0.53	32.88±1.52	39.11±0.94	36.42
Herding	34.86±0.55	38.60±0.68	32.21±1.54	37.53±0.22	35.80
Forgetting	33.40±0.64	39.79±0.78	31.12±0.21	38.38±0.65	35.67
GraNd-score	35.12±0.54	41.14±0.42	33.20±0.67	40.02±0.35	37.37
EL2N-score	31.08±1.11	38.26±0.45	31.34±0.49	36.88±0.32	34.39
Optimization-based	33.18±0.52	39.42±0.77	32.16±0.90	38.52±0.50	35.82
Self-sup.-selection	31.74±0.71	38.45±0.39	30.99±1.03	37.96±0.77	34.79
Moderate-DS	36.04±0.15	41.40±0.20	34.26±0.48	39.57±0.29	37.82
<b>GM Matching</b>	<b>37.93±0.23</b>	<b>42.59±0.29</b>	<b>36.31±0.67</b>	<b>41.03±0.41</b>	<b>39.47</b>

Method / Ratio	ResNet-50→VGG-16		ResNet-50→ShuffleNet		Mean ↑
	20%	30%	20%	30%	
Random	29.63±0.43	35.38±0.83	32.40±1.06	39.13±0.81	34.96
Herding	31.05±0.22	36.27±0.57	33.10±0.39	38.65±0.22	35.06
Forgetting	27.53±0.36	35.61±0.39	27.82±0.56	36.26±0.51	32.35
GraNd-score	29.93±0.95	35.61±0.39	29.56±0.46	37.40±0.38	33.34
EL2N-score	26.47±0.31	33.19±0.51	28.18±0.27	35.81±0.29	31.13
Optimization-based	25.92±0.64	34.82±1.29	31.37±1.14	38.22±0.78	32.55
Self-sup.-selection	25.16±1.10	33.30±0.94	29.47±0.56	36.68±0.36	31.45
Moderate-DS	31.45±0.32	37.89±0.36	33.32±0.41	39.68±0.34	35.62
<b>GM Matching</b>	<b>35.86±0.41</b>	<b>40.56±0.22</b>	<b>35.51±0.32</b>	<b>40.30±0.58</b>	<b>38.47</b>

Table 9: **NETWORK TRANSFER (NO CORRUPTION) PROXY ENCODER:** (Tiny-ImageNet) Model Transfer Results. A ResNet-50 proxy is used to find important samples which are then used to train SENet and EfficientNet.

All the experiments reported in Tables 3–7 follow this framework: We perform data pruning on CIFAR-100 and Tiny ImageNet, using ResNet-50 as both the proxy model (for selecting samples) and the downstream classifier (for final training). The proxy model assigns importance scores to training samples, and a subset is selected accordingly. A new ResNet-50 is then trained from scratch on the pruned dataset, ensuring that no information leakage occurs between sample selection and final training. This methodology remains consistent across clean data, label noise, feature corruption, and adversarial attack settings, providing a direct comparison of how pruning strategies perform across diverse learning conditions.

By maintaining this controlled setup, we isolate the true impact of different pruning strategies, ensuring that their ability to retain the most valuable and generalizable training samples is the sole factor influencing performance. This establishes a strong foundation before extending the analysis to more complex settings involving distribution shifts and network mismatches.

However, a critical question remains:

*How well do samples selected by a proxy model generalize when trained on a different architecture or dataset?*

In real-world applications, the model used for data selection (proxy model) is often different from the final model used for training due to hardware constraints, deployment considerations, or domain shifts. An ideal pruning strategy should ensure that the selected subset remains highly effective, even when the final model differs from the one used during selection.

To investigate this, we perform comprehensive ablation studies across multiple proxy selection scenarios, evaluating the robustness to distribution shifts and network mismatches i.e. to say that samples selected via a proxy network should generalize well when trained on unseen (during sample selection) networks / domains.

## B. GENERALIZATION TO UNSEEN NETWORK.

In this setting, the proxy model and downstream classifier are trained on the same dataset, meaning there is no distribution shift. However, the proxy model’s architecture differs from the final training model, testing whether a pruned subset remains useful across different network designs. This scenario simulates practical constraints where a proxy model is used for data selection, but the final model needs to be optimized for different architectural properties (e.g., mobile-friendly architectures).

Method / Ratio	ResNet-50→ VGG-16		ResNet-50→ ShuffleNet		Mean ↑
	20%	30%	20%	30%	
<b>Label Corruption</b>					
Random	23.29±1.12	28.18±1.84	25.08±1.32	31.44±1.21	27.00
Herding	23.99±0.36	28.57±0.40	26.25±0.47	30.73±0.28	27.39
Forgetting	14.52±0.66	21.75±0.23	15.70±0.29	22.31±0.35	18.57
GraNd-score	22.44±0.46	27.95±0.29	23.64±0.10	30.85±0.21	26.22
EL2N-score	15.15±1.25	23.36±0.30	18.01±0.44	24.68±0.34	20.30
Optimization-based	22.93±0.58	24.92±2.50	25.82±1.70	30.19±0.48	25.97
Self-sup.-selection	18.39±1.30	25.77±0.87	22.87±0.54	29.80±0.36	24.21
Moderate-DS	23.68±0.19	28.93±0.19	28.82±0.33	32.39±0.21	28.46
<b>GM Matching</b>	<b>28.77±0.77</b>	<b>34.87±0.23</b>	<b>32.05±0.93</b>	<b>37.43±0.25</b>	<b>33.28</b>
<b>Feature Corruption</b>					
Random	26.33±0.88	31.57±1.31	29.15±0.83	34.72±1.00	30.44
Herding	18.03±0.33	25.77±0.34	23.33±0.43	31.73±0.38	24.72
Forgetting	19.41±0.57	28.35±0.16	18.44±0.57	31.09±0.61	24.32
GraNd-score	23.59±0.19	30.69±0.13	23.15±0.56	31.58±0.95	27.25
EL2N-score	24.60±0.81	31.49±0.33	26.62±0.34	33.91±0.56	29.16
Optimization-based	25.12±0.34	30.52±0.89	28.87±1.25	34.08±1.92	29.65
Self-sup.-selection	26.33±0.21	33.23±0.26	26.48±0.37	33.54±0.46	29.90
Moderate-DS	29.65±0.68	35.89±0.53	32.30±0.38	38.66±0.29	34.13
<b>GM Matching</b>	<b>33.45±1.02</b>	<b>39.46±0.44</b>	<b>35.14±0.21</b>	<b>39.89±0.98</b>	<b>36.99</b>
<b>PGD Attack</b>					
Random	26.12±1.09	31.98±0.78	28.28±0.90	34.59±1.18	30.24
Herding	26.76±0.59	32.56±0.35	28.87±0.48	35.43±0.22	30.91
Forgetting	24.55±0.57	31.83±0.36	23.32±0.37	31.82±0.15	27.88
GraNd-score	25.19±0.33	31.46±0.54	26.03±0.66	33.22±0.24	28.98
EL2N-score	21.73±0.47	27.66±0.32	22.66±0.35	29.89±0.64	25.49
Optimization-based	26.02±0.36	31.64±1.75	27.93±0.47	34.82±0.96	30.10
Self-sup.-selection	22.36±0.30	28.56±0.50	25.35±0.27	32.57±0.13	27.21
Moderate-DS	27.24±0.36	32.90±0.31	29.06±0.28	35.89±0.53	31.27
<b>GM Matching</b>	<b>27.96±1.60</b>	<b>35.76±0.82</b>	<b>34.11±0.65</b>	<b>40.91±0.84</b>	<b>34.69</b>

Table 10: **NETWORK TRANSFER (CORRUPTED) PROXY ENCODER**: A ResNet-50 proxy (pretrained on TinyImageNet) is used to find important samples from Tiny-ImageNet; which is then used to train a VGGNet-16 and ShuffleNet. We repeat the experiment across multiple corruption settings - clean; 20% Feature / Label Corruption and PGD attack when 20% and 30% samples are selected.

In Table 9, we use a ResNet-50 proxy trained on TinyImageNet (no corruption) to select samples from the same dataset for downstream training. Instead of using ResNet-50 for final training, we train with different architectures on the pruned subset:

- SENet – A model optimized for channel-wise attention mechanisms, which enhances feature selection by adaptively recalibrating channel-wise responses.
- EfficientNet-B0 – A lightweight model designed for mobile and resource-efficient inference, using a combination of depthwise convolutions and width scaling to optimize performance while maintaining parameter efficiency.
- VGG-16 – A deep convolutional network with uniform architecture, known for its simple yet effective design, using fixed-size convolution filters and max pooling layers.
- ShuffleNet – A model specifically designed for speed and efficiency, utilizing group convolutions and channel shuffling to maximize accuracy while maintaining low computational overhead.

In Table 10, we also experiment with similar network mismatch scenarios, in the presence of various types and levels of corruption.

Both sets of experiments demonstrate that GM Matching consistently outperforms all pruning baselines, ensuring that selected samples remain informative and transferable across different network architectures. SENet and EfficientNet-B0 benefit the most from pruning, likely due to their adaptive feature recalibration and efficiency optimizations, while VGG-16 and ShuffleNet show greater sensitivity to pruning and corruption, struggling more under distribution shifts. Under corruption,

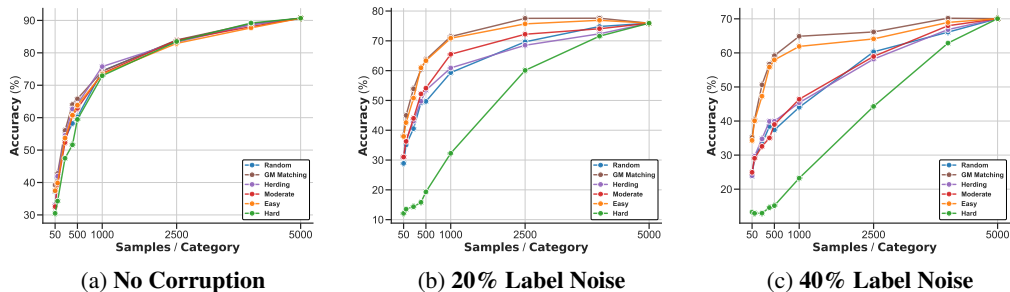


Figure 12: **DOMAIN TRANSFER ( IMAGENET-1K → CIFAR-10 ) PROXY ENCODER:** CIFAR10, corrupted with label noise is pruned using a (proxy) ResNet-18 pretrained on ImageNet-1k. A ResNet-18 is trained from scratch on the subset. We compare our method GM MATCHING with geometric pruning baselines: UNIFORM, EASY, HARD, MODERATE, HERDING.

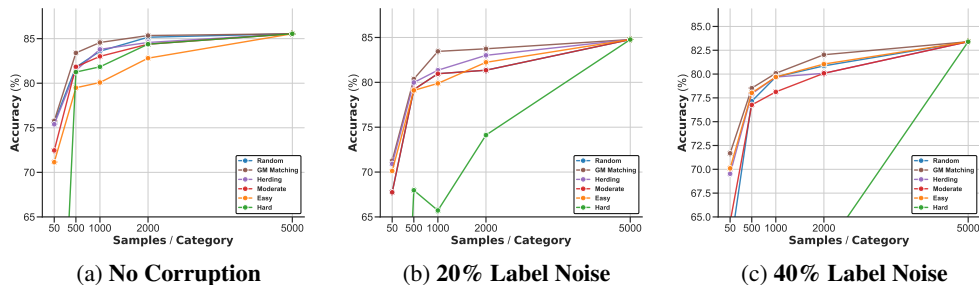


Figure 13: **DOMAIN TRANSFER ( IMAGENET-1K → CIFAR-10 ) PROXY ENCODER :** We train a Linear Classifier on CIFAR10; over embeddings obtained from a frozen ResNet-18 pretrained on ImageNet-1k. The dataset was pruned using the same encoder. We compare GM Matching with several geometric pruning baselines ( Section 6.1): Uniform, Easy, Hard, Moderate, Herding across no corruption, 20% and 30% label noise settings.

loss-based selection methods (GraNd, EL2N) degrade significantly, whereas representative selection methods (Moderate-DS, Herding) hold up better under mild corruption but fail under severe noise.

These results highlight the importance of selecting subsets that generalize well, not only across different architectures but also under varying levels of corruption, reinforcing GM Matching as a highly robust and adaptable pruning strategy suitable for diverse deployment scenarios.

### C. GENERALIZATION TO UNSEEN DOMAIN.

In many real-world applications, deep learning models are pretrained on large-scale datasets (e.g., ImageNet) before being adapted to a different, often smaller, target dataset (e.g., CIFAR-10). This introduces a distribution shift between the dataset used for proxy-based sample selection and the dataset used for final training. If a pruning method is truly effective, it should be able to identify robust samples that generalize well across different data distributions, ensuring that the selected subset remains informative even if the proxy model was never explicitly trained on the target dataset.

To investigate this, we conduct experiments where the proxy model and downstream classifier share the same architecture, but the proxy model is pretrained on a different dataset, introducing a distribution shift. By keeping the architecture constant, we isolate the impact of dataset shift while avoiding confounding factors related to network differences.

In Figure 12, a ResNet-18 pretrained on ImageNet is used to select samples from CIFAR-10, which are then used to train a new ResNet-18 from scratch. This setup closely mirrors real-world transfer learning scenarios, where large-scale pretraining is leveraged to prune or curate training data for a smaller, domain-specific dataset before training a new model. The key objective is to determine whether the subset selected by a proxy trained on a different dataset remains informative and structurally representative of the target dataset when used for full downstream training.

CIFAR-10 (ViT-B/32 → ResNet-18)				
Method / Size	10	100	1000	Mean ↑
<b>No Corruption</b>				
Random	23.2 ± 3.9	42.4 ± 2.3	86.8 ± 0.7	50.8
Easy	27.4 ± 0.4	42.5 ± 0.5	84.2 ± 0.3	51.4
Hard	19.8 ± 1.7	39.7 ± 1.0	86.1 ± 0.2	48.5
Herding	24.9 ± 1.6	45.7 ± 0.6	86.8 ± 0.4	52.5
Moderate	24.0 ± 1.8	44.5 ± 2.7	86.1 ± 1.3	51.5
GM Matching	<b>25.6 ± 0.2</b>	<b>47.6 ± 1.9</b>	<b>86.9 ± 0.3</b>	<b>53.4</b>
<b>20% Label Noise</b>				
Random	18.0 ± 2.4	36.4 ± 0.9	75.5 ± 0.7	43.3
Easy	24.2 ± 0.6	40.7 ± 1.1	76.5 ± 1.9	47.1
Hard	13.1 ± 1.9	22.7 ± 0.7	67.2 ± 0.5	34.3
Herding	22.7 ± 0.3	38.5 ± 1.5	76.6 ± 1.3	45.9
Moderate	23.0 ± 1.3	39.8 ± 1.3	75.9 ± 1.3	46.2
GM Matching	<b>26.0 ± 0.9</b>	<b>41.1 ± 1.8</b>	<b>77.8 ± 0.4</b>	<b>48.3</b>
<b>40% Label Noise</b>				
Random	16.8 ± 2.0	28.3 ± 2.2	66.2 ± 0.8	37.1
Easy	22.5 ± 1.5	34.1 ± 1.5	70.5 ± 1.1	42.4
Hard	12.8 ± 1.3	16.5 ± 1.6	51.4 ± 1.9	26.9
Herding	18.0 ± 1.4	30.1 ± 0.9	65.1 ± 1.4	37.7
Moderate	20.2 ± 1.3	34.0 ± 1.7	67.8 ± 1.5	40.7
GM Matching	<b>23.3 ± 1.8</b>	<b>36.8 ± 1.4</b>	<b>71.0 ± 1.3</b>	<b>43.7</b>

Table 11: **NETWORK AND DOMAIN TRANSFER - PROXY ENCODER:** A pretrained CLIP ViT-B/32 proxy encoder is used to find (10, 100, 1000) samples per class from CIFAR-10. Consequently, a ResNet-18 is trained on the selected subset. We perform the experiment across - clean; 20% and 40% Label Noise.

Furthermore, in Figure 13, we introduce an even more challenging setting by freezing the pretrained (on ImageNet) ResNet-18 and training only a linear classifier on top of the extracted CIFAR-10 features. Unlike the full fine-tuning approach, this method eliminates any feature adaptation between datasets, forcing the classifier to rely entirely on the quality of the selected samples. This makes it a more rigorous test of how well the pruned subsets inherently align with robust, transferable representations, ensuring that the selected data itself is informative, rather than merely benefiting from feature adaptation during training.

The results from Figure 12 13 demonstrate that GM Matching consistently outperforms all baselines, ensuring that selected samples remain highly informative and transferable despite the distribution shift. When fully fine-tuned, models trained on GM Matching pruned subsets achieve higher accuracy than those trained on subsets selected by other methods, indicating that it effectively identifies structurally important and generalizable samples. In the frozen feature setting, performance gaps between pruning strategies become even more pronounced, with Hard and Easy pruning strategies performing significantly worse, highlighting their reliance on feature adaptation rather than inherently meaningful sample selection. Loss-based methods (GraNd-score, EL2N-score) degrade under dataset shifts, suggesting that they may over-prioritize easy-to-learn samples that do not generalize well across domains. These findings emphasize that effective pruning strategies must go beyond dataset-specific heuristics and instead focus on selecting robust, transferable samples that remain useful even under feature extraction constraints, reinforcing the advantage of GM Matching in real-world transfer learning applications.

#### D. GENERALIZATION TO BOTH UNSEEN DOMAIN AND NETWORK.

In many real-world scenarios, both domain and architecture mismatches occur simultaneously — a setting where the data selection model differs from the downstream training model both in terms of dataset and architecture. For instance, models like CLIP (Radford et al., 2021a) are often used as frozen, large-scale pretrained encoders on generic web-scale data (e.g., YFCC), whereas final deployment models may be lightweight CNNs (e.g., ResNet-18) trained from scratch on task-specific datasets like CIFAR.

To assess the robustness of pruning strategies in this challenging setting, we construct an experiment where a frozen CLIP ViT-B/32 encoder — pretrained on a generic dataset — is used as a proxy to

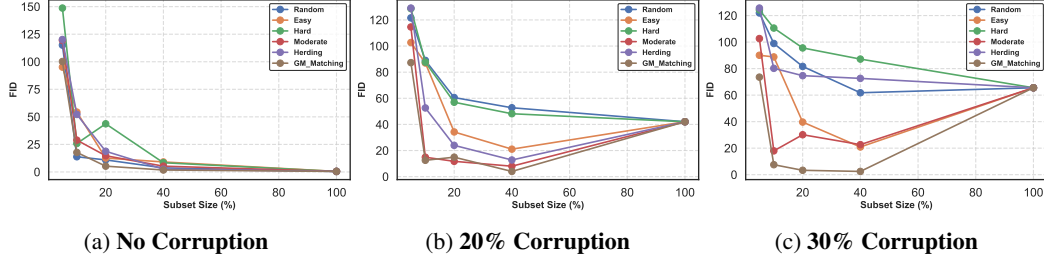


Figure 14: **DIFFUSION (FID)**: We train DDPM on MNIST across different sampling fraction and corruption rates using different sampling strategies. GM Matching consistently outperformed other approaches especially under corruption.

embed CIFAR-10 samples and perform subset selection via GM Matching. A ResNet-18 model is then trained from scratch on the selected subset using only CIFAR-10 labels. This setup introduces both a *domain shift* (CLIP never trained on CIFAR-10) and a *network shift* (ViT to ResNet).

We evaluate performance across multiple corruption regimes: a clean dataset, as well as with 20% and 40% label noise. Table 11 presents the results across three subset sizes (10, 100, 1000 samples per class), showing the classification accuracy of ResNet-18 trained on these subsets.

Across all corruption levels and subset sizes, GM Matching consistently outperforms all baselines. For instance, in the 40% label noise setting, GM Matching achieves 43.7% mean accuracy — a full 3% higher than the next best method (Moderate, 40.7%). Notably, the advantage of GM Matching is particularly prominent at smaller subset sizes (e.g., 10 samples/class), suggesting that it is more effective at isolating informative, transferable samples even when the proxy encoder and downstream model differ significantly.

These findings highlight a key strength of GM Matching: its ability to select subsets that retain semantic structure and predictive utility, even when selected in a drastically different representation space than where the model is ultimately trained. By anchoring the selection process on the geometric median — a robust estimator that captures the core of the data distribution — GM Matching exhibits strong generalization under simultaneous domain and architecture shifts, making it a practical and principled choice for real-world deployment settings involving large-scale, black-box, or frozen proxy encoders.

## 6.4 UNCONDITIONAL IMAGE GENERATION

To further validate our approach, we conduct experiments on an unconditional image generation task using a diffusion model. Specifically, we train a U-Net on the MNIST dataset, with Denoising Diffusion Probabilistic Models (DDPM) (Ho et al., 2020), which learns to generate images through a gradual denoising process. We perform sample selection with CLIP ViT-B/32 (Radford et al., 2021a) embeddings as demonstrated in Figure 4.

The fundamental idea behind diffusion models is to learn the reverse of a gradual noise corruption process applied to training images. This forward diffusion process progressively adds Gaussian noise to an image across a sequence of time-steps  $t = 1, \dots, T$ , following the Markovian formulation:

$$q(x_t|x_{t-1}) = \mathcal{N}(x_t; \sqrt{1 - \beta_t}x_{t-1}, \beta_t I), \quad (31)$$

where,  $x_t$  represents the image at timestep  $t$  and  $\beta_t \in (0, 1)$  denotes the noise variance at timestep  $t$ , following a predefined schedule. The generative process aims to learn a function  $p_\theta(x_{t-1}|x_t)$  that can reverse this diffusion, thereby reconstructing clean images from noise. The learned denoising function is parameterized using a deep neural network that predicts the noise component in a given sample, enabling the recovery of realistic image distributions.

To evaluate the quality of the generated samples, we use the Fréchet Inception Distance (FID), which measures the Wasserstein-2 distance between the feature distributions of real and generated images:

$$\text{FID} = \left\| \mu_r - \mu_g \right\|^2 + \text{Tr} \left( \Sigma_r + \Sigma_g - 2(\Sigma_r \Sigma_g)^{1/2} \right) \quad (32)$$



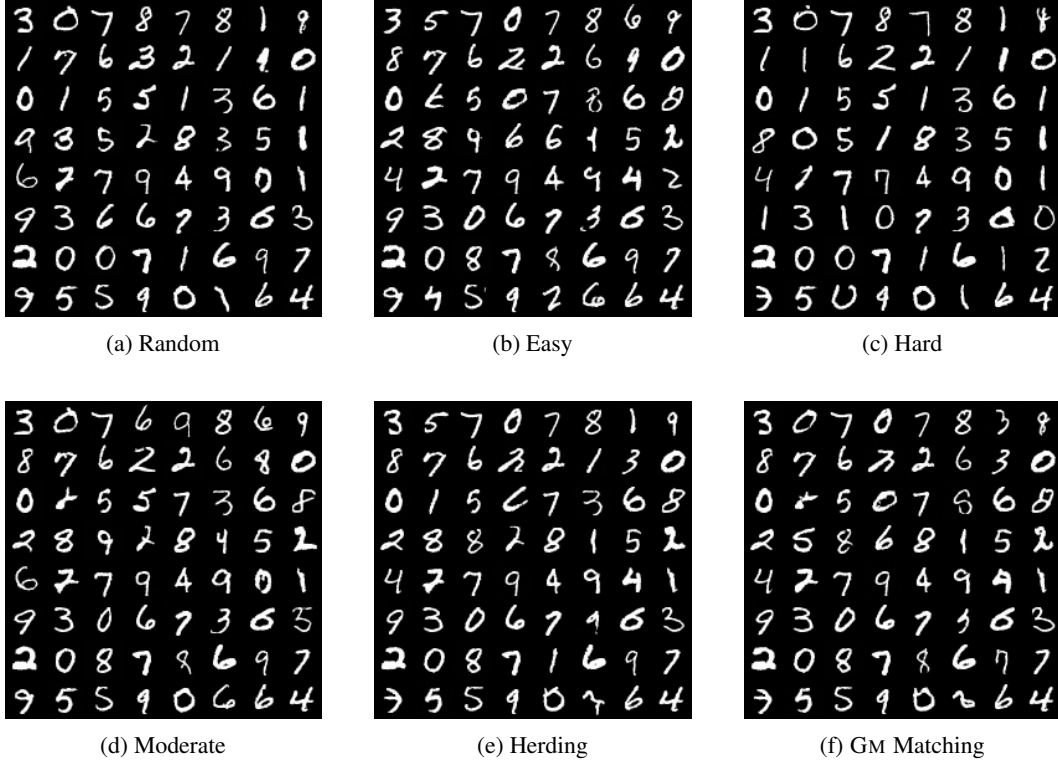


Figure 15: (No Corruption) Visualization of Generated Samples 40% sampling

where  $(\mu_r, \Sigma_r)$  and  $(\mu_g, \Sigma_g)$  are the mean and covariance of the real and generated feature distributions respectively, and  $\text{Tr}(\cdot)$  denotes the trace operator. Lower FID values indicate that the generated images more closely resemble the real data distribution.

## EXPERIMENTAL SETUP.

For training stability and optimal convergence, we adopt specific hyperparameter settings. The batch size is set to 128 to ensure efficient mini-batch updates. The learning rate is fixed at  $1 \times 10^{-4}$ , tuned for stable convergence. We use the AdamW optimizer due to its adaptive learning rate properties and weight decay regularization. The number of diffusion time-steps is set to 1000, providing sufficient granularity for high-resolution generative refinement. A linear noise schedule is applied where  $\beta_t$  increases linearly over time-steps, preventing abrupt changes in noise levels. To ensure robustness in our conclusions, we conduct multiple training runs with different random seeds, mitigating the impact of initialization biases and training variability.

Our experiments involve running the model across multiple random seeds to ensure statistical robustness. Results are compared using FID scores to determine the effectiveness of different data selection strategies in training the diffusion model. We compare GM Matching against multiple baseline geometric subset selection strategies(Section 6.1): Random, Easy, Hard, Moderate, and Kernel Herding.

To further stress-test these selection methods, we introduce structured perturbations into the training data, simulating realistic noise and adversarial conditions. These perturbations include Gaussian noise, which applies additive white noise pixel-wise; uniform noise, which perturbs pixel intensities randomly; random patches, which corrupt localized regions with random pixel values; cutout augmentations, which mask out rectangular sections of images; and completely random images, which introduce purely random noise samples into training batches. Visual examples of these corrupted data samples are presented in Figure 3.

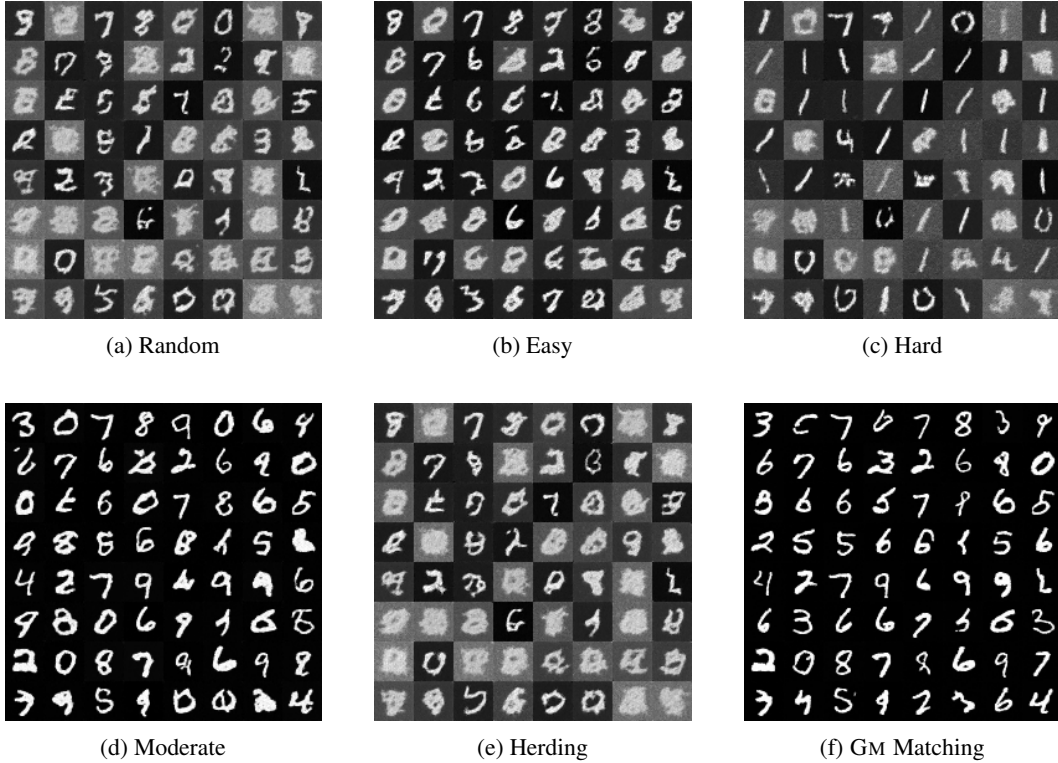


Figure 16: (30% Corruption) Visualization of Generated Samples 40% sampling

## DISCUSSION.

Figure 14 depicts the generative performance of the diffusion model when trained on the selected subset. Evidently, GM Matching consistently achieves FID scores across all subset sizes and corruption scenarios, clearly demonstrating its superior performance in terms of generating high-quality samples. *In the clean (no corruption) setting*, at smaller subset sizes (10%-20%), GM Matching substantially outperforms the baseline methods. While all methods eventually converge to similar performance levels at full dataset size (100%), the early advantage of GM Matching highlights its efficiency in selecting representative subsets. *Under moderate (20%) corruption*, GM Matching maintains a significant performance advantage, especially at smaller subset sizes (10%-40%). This result suggests that GM Matching effectively identifies high-quality training subsets even in the presence of moderately corrupted data, thereby preserving generative quality. *At higher (30%) corruption rates*, GM Matching demonstrates remarkable robustness against higher corruption levels. In contrast, methods such as "Hard" sampling significantly degrade in performance due to sensitivity to corrupted data. GM Matching, however, remains stable and consistently achieves superior FID scores, emphasizing its robustness in more challenging scenarios.

Visual analyses provide additional insights into the effectiveness of GM Matching, particularly when comparing subsets of clean versus noisy training data. In Figure 15, we present visualizations of generated samples obtained from the UNet trained via DDPM on a 40% subset of MNIST. All subset selection methods produce visually comparable and clear digit images under these clean conditions, demonstrating that, in an ideal scenario without data corruption, the impact of different subset selection methods on visual quality is minimal. However, Figure 16 highlights significant differences in generated samples when the same model is trained on a 40% subset derived from data subjected to severe corruption (30%). Baseline methods, such as Random, Easy, and Hard selection, result in samples with substantial visual distortion and ambiguity. In contrast, GM Matching notably produces clear and well-defined digit representations, emphasizing its superior robustness and capability to effectively mitigate the adverse effects of corrupted data during training. Collectively, these visual results reinforce our quantitative findings (Figure 14), clearly underscoring the suitability and robustness of GM Matching in challenging data corruption scenarios for training diffusion models.

## 7 CONCLUSION AND LIMITATIONS

We introduced GM Matching, a robust data pruning algorithm that selects a  $k$ -subset whose mean approximates the geometric median of a noisy dataset. Unlike prior approaches that degrade under corruption, GM Matching is resilient to adversarial noise, as supported by both theoretical analysis and empirical results across diverse tasks. While promising, GM Matching has limitations. Its performance depends on accurate geometric median estimation, which can be computationally challenging or unstable in degenerate or high-dimensional settings. Moreover, its effectiveness is influenced by the choice of embedding space, and may deteriorate when encoders are biased or poorly calibrated. Future work could explore scalable, structure-aware approximations of the geometric median, and adaptive selection strategies that account for uncertainty in the embedding representation.

### References

- Acharya, A., Hashemi, A., Jain, P., Sanghavi, S., Dhillon, I. S., and Topcu, U. Robust training in high dimensions via block coordinate geometric median descent. In Camps-Valls, G., Ruiz, F. J. R., and Valera, I. (eds.), *Proceedings of The 25th International Conference on Artificial Intelligence and Statistics*, volume 151 of *Proceedings of Machine Learning Research*, pp. 11145–11168. PMLR, 28–30 Mar 2022. URL <https://proceedings.mlr.press/v151/acharya22a.html>.
- Agarwal, P. K., Har-Peled, S., Varadarajan, K. R., et al. Geometric approximation via coresets. *Combinatorial and computational geometry*, 52(1), 2005.
- Bach, F., Lacoste-Julien, S., and Obozinski, G. On the equivalence between herding and conditional gradient algorithms. *arXiv preprint arXiv:1203.4523*, 2012.
- Bajaj, C. The algebraic degree of geometric optimization problems. *Discrete & Computational Geometry*, 3:177–191, 1988.
- Balcan, M.-F., Broder, A., and Zhang, T. Margin based active learning. In *International Conference on Computational Learning Theory*, pp. 35–50. Springer, 2007.
- Boyd, S. and Vandenberghe, L. *Convex optimization*. Cambridge university press, 2004.
- Brown, T., Mann, B., Ryder, N., Subbiah, M., Kaplan, J. D., Dhariwal, P., Neelakantan, A., Shyam, P., Sastry, G., Askell, A., et al. Language models are few-shot learners. *Advances in neural information processing systems*, 33:1877–1901, 2020.
- Campbell, T. and Broderick, T. Bayesian coreset construction via greedy iterative geodesic ascent. In *International Conference on Machine Learning*, pp. 698–706. PMLR, 2018.
- Chen, T., Kornblith, S., Norouzi, M., and Hinton, G. A simple framework for contrastive learning of visual representations. In *International conference on machine learning*, pp. 1597–1607. PMLR, 2020.
- Chen, Y. and Welling, M. Parametric herding. In *Proceedings of the Thirteenth International Conference on Artificial Intelligence and Statistics*, pp. 97–104. JMLR Workshop and Conference Proceedings, 2010.
- Chen, Y., Welling, M., and Smola, A. Super-samples from kernel herding. In *Proceedings of the Twenty-Sixth Conference on Uncertainty in Artificial Intelligence*, pp. 109–116, 2010.
- Chen, Y., Su, L., and Xu, J. Distributed statistical machine learning in adversarial settings: Byzantine gradient descent. *Proceedings of the ACM on Measurement and Analysis of Computing Systems*, 1(2):1–25, 2017.
- Cho, Y. and Saul, L. Kernel methods for deep learning. *Advances in neural information processing systems*, 22, 2009.
- Cohen, M. B., Lee, Y. T., Miller, G., Pachocki, J., and Sidford, A. Geometric median in nearly linear time. In *Proceedings of the forty-eighth annual ACM symposium on Theory of Computing*, pp. 9–21, 2016.

- Davies, P. and Gather, U. The breakdown point—examples and counterexamples. *REVSTAT Statistical Journal*, 5(1):1–17, 2007.
- Deng, J., Dong, W., Socher, R., Li, L.-J., Li, K., and Fei-Fei, L. Imagenet: A large-scale hierarchical image database. In *2009 IEEE conference on computer vision and pattern recognition*, pp. 248–255. Ieee, 2009.
- Diakonikolas, I. and Kane, D. M. Recent advances in algorithmic high-dimensional robust statistics. *arXiv preprint arXiv:1911.05911*, 2019.
- Diakonikolas, I., Kamath, G., Kane, D., Li, J., Moitra, A., and Stewart, A. Robust estimators in high-dimensions without the computational intractability. *SIAM Journal on Computing*, 48(2): 742–864, 2019.
- Donoho, D. L. and Huber, P. J. The notion of breakdown point. *A festschrift for Erich L. Lehmann*, 157184, 1983.
- Dosovitskiy, A., Beyer, L., Kolesnikov, A., Weissenborn, D., Zhai, X., Unterthiner, T., Dehghani, M., Minderer, M., Heigold, G., Gelly, S., et al. An image is worth 16x16 words: Transformers for image recognition at scale. *arXiv preprint arXiv:2010.11929*, 2020.
- Dwivedi, R. and Mackey, L. Generalized kernel thinning. *arXiv preprint arXiv:2110.01593*, 2021.
- Feige, U. A threshold of  $\ln n$  for approximating set cover. *Journal of the ACM (JACM)*, 45(4): 634–652, 1998.
- Feldman, D. Core-sets: Updated survey. In *Sampling techniques for supervised or unsupervised tasks*, pp. 23–44. Springer, 2020.
- Feldman, D. and Langberg, M. A unified framework for approximating and clustering data. In *Proceedings of the forty-third annual ACM symposium on Theory of computing*, pp. 569–578, 2011.
- Feldman, V. and Zhang, C. What neural networks memorize and why: Discovering the long tail via influence estimation. *Advances in Neural Information Processing Systems*, 33:2881–2891, 2020.
- Goodfellow, I. J., Shlens, J., and Szegedy, C. Explaining and harnessing adversarial examples. *arXiv preprint arXiv:1412.6572*, 2014.
- Gretton, A., Borgwardt, K. M., Rasch, M. J., Schölkopf, B., and Smola, A. A kernel two-sample test. *The Journal of Machine Learning Research*, 13(1):723–773, 2012.
- Har-Peled, S. *Geometric approximation algorithms*. Number 173. American Mathematical Soc., 2011.
- Har-Peled, S., Roth, D., and Zimak, D. Maximum margin coresets for active and noise tolerant learning. In *Proceedings of the 20th international joint conference on Artificial intelligence*, pp. 836–841, 2007.
- He, K., Zhang, X., Ren, S., and Sun, J. Deep residual learning for image recognition. In *Proceedings of the IEEE conference on computer vision and pattern recognition*, pp. 770–778, 2016.
- Hendrycks, D. and Dietterich, T. Benchmarking neural network robustness to common corruptions and perturbations. *arXiv preprint arXiv:1903.12261*, 2019.
- Hestness, J., Narang, S., Ardalani, N., Diamos, G., Jun, H., Kianinejad, H., Patwary, M., Ali, M., Yang, Y., and Zhou, Y. Deep learning scaling is predictable, empirically. *arXiv preprint arXiv:1712.00409*, 2017.
- Ho, J., Jain, A., and Abbeel, P. Denoising diffusion probabilistic models. *Advances in neural information processing systems*, 33:6840–6851, 2020.
- Hofmann, T., Schölkopf, B., and Smola, A. J. Kernel methods in machine learning. 2008.

- Hu, J., Shen, L., and Sun, G. Squeeze-and-excitation networks. In *Proceedings of the IEEE conference on computer vision and pattern recognition*, pp. 7132–7141, 2018.
- Huang, S.-J., Jin, R., and Zhou, Z.-H. Active learning by querying informative and representative examples. *Advances in neural information processing systems*, 23, 2010.
- Huber, P. J. Robust estimation of a location parameter. In *Breakthroughs in statistics*, pp. 492–518. Springer, 1992.
- Jiang, L., Zhou, Z., Leung, T., Li, L.-J., and Fei-Fei, L. Mentornet: Learning data-driven curriculum for very deep neural networks on corrupted labels. In *International conference on machine learning*, pp. 2304–2313. PMLR, 2018.
- Joshi, A. J., Porikli, F., and Papanikolopoulos, N. Multi-class active learning for image classification. In *2009 IEEE conference on computer vision and pattern recognition*, pp. 2372–2379. IEEE, 2009.
- Joshi, S. and Mirzasoleiman, B. Data-efficient contrastive self-supervised learning: Most beneficial examples for supervised learning contribute the least. In *International conference on machine learning*, pp. 15356–15370. PMLR, 2023.
- Kaplan, J., McCandlish, S., Henighan, T., Brown, T. B., Chess, B., Child, R., Gray, S., Radford, A., Wu, J., and Amodei, D. Scaling laws for neural language models. *arXiv preprint arXiv:2001.08361*, 2020.
- Katharopoulos, A. and Fleuret, F. Not all samples are created equal: Deep learning with importance sampling. In *International conference on machine learning*, pp. 2525–2534. PMLR, 2018.
- Keles, F. D., Wijewardena, P. M., and Hegde, C. On the computational complexity of self-attention. In *International conference on algorithmic learning theory*, pp. 597–619. PMLR, 2023.
- Kemperman, J. The median of a finite measure on a banach space. *Statistical data analysis based on the L1-norm and related methods (Neuchâtel, 1987)*, pp. 217–230, 1987.
- Koh, P. W. and Liang, P. Understanding black-box predictions via influence functions. In *International conference on machine learning*, pp. 1885–1894. PMLR, 2017.
- Krizhevsky, A. Learning multiple layers of features from tiny images. *Technical Report*, 2009.
- Lamport, L., SHOSTAK, R., and PEASE, M. The byzantine generals problem. *ACM Transactions on Programming Languages and Systems*, 4(3):382–401, 1982.
- Le, Y. and Yang, X. Tiny imagenet visual recognition challenge. In *CS 231N*, 2015.
- Lee, S. H., Lee, S., and Song, B. C. Vision transformer for small-size datasets. *arXiv preprint arXiv:2112.13492*, 2021.
- Li, L., Xu, W., Chen, T., Giannakis, G. B., and Ling, Q. Rsa: Byzantine-robust stochastic aggregation methods for distributed learning from heterogeneous datasets. In *Proceedings of the AAAI Conference on Artificial Intelligence*, volume 33, pp. 1544–1551, 2019.
- Li, S., Xia, X., Ge, S., and Liu, T. Selective-supervised contrastive learning with noisy labels. In *Proceedings of the IEEE/CVF conference on computer vision and pattern recognition*, pp. 316–325, 2022.
- Lopuhaa, H. P., Rousseeuw, P. J., et al. Breakdown points of affine equivariant estimators of multivariate location and covariance matrices. *The Annals of Statistics*, 19(1):229–248, 1991.
- Ma, N., Zhang, X., Zheng, H.-T., and Sun, J. Shufflenet v2: Practical guidelines for efficient cnn architecture design. In *Proceedings of the European conference on computer vision (ECCV)*, pp. 116–131, 2018.
- Madry, A., Makelov, A., Schmidt, L., Tsipras, D., and Vladu, A. Towards deep learning models resistant to adversarial attacks. *arXiv preprint arXiv:1706.06083*, 2017.

- Minsker, S. et al. Geometric median and robust estimation in banach spaces. *Bernoulli*, 21(4): 2308–2335, 2015.
- Mirzasoleiman, B., Bilmes, J., and Leskovec, J. Coresets for data-efficient training of machine learning models. In *International Conference on Machine Learning*, pp. 6950–6960. PMLR, 2020.
- Muthukrishnan, S. et al. Data streams: Algorithms and applications. *Foundations and Trends® in Theoretical Computer Science*, 1(2):117–236, 2005.
- Needell, D., Ward, R., and Srebro, N. Stochastic gradient descent, weighted sampling, and the randomized kaczmarz algorithm. *Advances in neural information processing systems*, 27, 2014.
- Nemhauser, G. L., Wolsey, L. A., and Fisher, M. L. An analysis of approximations for maximizing submodular set functions—i. *Mathematical programming*, 14:265–294, 1978.
- Olive, D. J. High breakdown analogs of the trimmed mean. *Statistics & probability letters*, 51(1): 87–92, 2001.
- Park, D., Choi, S., Kim, D., Song, H., and Lee, J.-G. Robust data pruning under label noise via maximizing re-labeling accuracy. *Advances in Neural Information Processing Systems*, 36, 2024.
- Patrini, G., Rozza, A., Krishna Menon, A., Nock, R., and Qu, L. Making deep neural networks robust to label noise: A loss correction approach. In *Proceedings of the IEEE conference on computer vision and pattern recognition*, pp. 1944–1952, 2017.
- Paul, M., Ganguli, S., and Dziugaite, G. K. Deep learning on a data diet: Finding important examples early in training. *Advances in Neural Information Processing Systems*, 34:20596–20607, 2021.
- Pleiss, G., Zhang, T., Elenberg, E., and Weinberger, K. Q. Identifying mislabeled data using the area under the margin ranking. *Advances in Neural Information Processing Systems*, 33:17044–17056, 2020.
- Qian, C., Shi, J.-C., Yu, Y., Tang, K., and Zhou, Z.-H. Subset selection under noise. *Advances in neural information processing systems*, 30, 2017.
- Radford, A., Narasimhan, K., Salimans, T., Sutskever, I., et al. Improving language understanding by generative pre-training. 2018.
- Radford, A., Kim, J. W., Hallacy, C., Ramesh, A., Goh, G., Agarwal, S., Sastry, G., Askell, A., Mishkin, P., Clark, J., Krueger, G., and Sutskever, I. Learning transferable visual models from natural language supervision. In *ICML*, 2021a.
- Radford, A., Kim, J. W., Hallacy, C., Ramesh, A., Goh, G., Agarwal, S., Sastry, G., Askell, A., Mishkin, P., Clark, J., et al. Learning transferable visual models from natural language supervision. In *International conference on machine learning*, pp. 8748–8763. PMLR, 2021b.
- Shah, V., Wu, X., and Sanghavi, S. Choosing the sample with lowest loss makes sgd robust. In *International Conference on Artificial Intelligence and Statistics*, pp. 2120–2130. PMLR, 2020.
- Shen, Y. and Sanghavi, S. Learning with bad training data via iterative trimmed loss minimization. In *International Conference on Machine Learning*, pp. 5739–5748. PMLR, 2019.
- Simonyan, K. and Zisserman, A. Very deep convolutional networks for large-scale image recognition. *arXiv preprint arXiv:1409.1556*, 2014.
- Sorscher, B., Geirhos, R., Shekhar, S., Ganguli, S., and Morcos, A. Beyond neural scaling laws: beating power law scaling via data pruning. *Advances in Neural Information Processing Systems*, 35:19523–19536, 2022.
- Sriperumbudur, B. K., Gretton, A., Fukumizu, K., Schölkopf, B., and Lanckriet, G. R. Hilbert space embeddings and metrics on probability measures. *The Journal of Machine Learning Research*, 11: 1517–1561, 2010.
- Sugiyama, M. and Kawanabe, M. *Machine learning in non-stationary environments: Introduction to covariate shift adaptation*. MIT press, 2012.

- Szegedy, C., Zaremba, W., Sutskever, I., Bruna, J., Erhan, D., Goodfellow, I., and Fergus, R. Intriguing properties of neural networks. *arXiv preprint arXiv:1312.6199*, 2013.
- Tan, M. and Le, Q. Efficientnet: Rethinking model scaling for convolutional neural networks. In *International conference on machine learning*, pp. 6105–6114. PMLR, 2019.
- Thompson, R. Robust subset selection. *arXiv preprint arXiv:2005.08217*, 2022.
- Toneva, M., Sordoni, A., Combes, R. T. d., Trischler, A., Bengio, Y., and Gordon, G. J. An empirical study of example forgetting during deep neural network learning. *arXiv preprint arXiv:1812.05159*, 2018.
- Touvron, H., Lavril, T., Izacard, G., Martinet, X., Lachaux, M.-A., Lacroix, T., Rozière, B., Goyal, N., Hambro, E., Azhar, F., et al. Llama: Open and efficient foundation language models. *arXiv preprint arXiv:2302.13971*, 2023.
- Van der Maaten, L. and Hinton, G. Visualizing data using t-sne. *Journal of machine learning research*, 9(11), 2008.
- Vardi, Y. and Zhang, C.-H. The multivariate 11-median and associated data depth. *Proceedings of the National Academy of Sciences*, 97(4):1423–1426, 2000.
- Vert, J.-P., Tsuda, K., and Schölkopf, B. A primer on kernel methods. *Kernel methods in computational biology*, 47:35–70, 2004.
- Weber, A., Friedrich, C. J., et al. *Alfred Weber’s theory of the location of industries*. The University of Chicago Press, 1929.
- Weiszfeld, E. Sur le point pour lequel la somme des distances de n points donnés est minimum. *Tohoku Mathematical Journal, First Series*, 43:355–386, 1937.
- Welling, M. Herding dynamical weights to learn. In *Proceedings of the 26th Annual International Conference on Machine Learning*, pp. 1121–1128, 2009.
- Wu, Z., Ling, Q., Chen, T., and Giannakis, G. B. Federated variance-reduced stochastic gradient descent with robustness to byzantine attacks. *IEEE Transactions on Signal Processing*, 68:4583–4596, 2020.
- Xia, X., Liu, T., Han, B., Gong, C., Wang, N., Ge, Z., and Chang, Y. Robust early-learning: Hindering the memorization of noisy labels. In *International conference on learning representations*, 2020.
- Xia, X., Liu, J., Yu, J., Shen, X., Han, B., and Liu, T. Moderate coreset: A universal method of data selection for real-world data-efficient deep learning. In *The Eleventh International Conference on Learning Representations*, 2022.
- Xu, Y., Zhao, S., Song, J., Stewart, R., and Ermon, S. A theory of usable information under computational constraints. *arXiv preprint arXiv:2002.10689*, 2020.
- Xu, Y.-H., Qian, C., and Tang, K. Pareto optimization with robust evaluation for noisy subset selection. *arXiv preprint arXiv:2501.06813*, 2025.
- Yang, S., Xie, Z., Peng, H., Xu, M., Sun, M., and Li, P. Dataset pruning: Reducing training data by examining generalization influence. *arXiv preprint arXiv:2205.09329*, 2022.
- Zhang, Z. and Sabuncu, M. Generalized cross entropy loss for training deep neural networks with noisy labels. *Advances in neural information processing systems*, 31, 2018.

# Supplementary Material for GM Matching

## A NOTATIONS AND ABBREVIATIONS

$a$	A scalar (integer or real)
$\mathbf{a}$	A vector
$\mathbf{A}$	A matrix
$a$	A scalar random variable
$\mathbf{a}$	A vector-valued random variable
$\mathbb{A}, \mathcal{A}$	A set
$[a, b]$	The real interval including $a$ and $b$
$\mathbb{A} \setminus \mathbb{B}$	Set subtraction, i.e., the set containing the elements of $\mathbb{A}$ that are not in $\mathbb{B}$
$a_i$	Element $i$ of the random vector $\mathbf{a}$
$P(\mathbf{a})$	A probability distribution over a discrete variable
$p(\mathbf{a})$	A probability distribution over a continuous variable, or over a variable whose type has not been specified
$f : \mathbb{A} \rightarrow \mathbb{B}$	The function $f$ with domain $\mathbb{A}$ and range $\mathbb{B}$
$f \circ g$	Composition of the functions $f$ and $g$
$f(\mathbf{x}; \boldsymbol{\theta})$	A function of $\mathbf{x}$ parametrized by $\boldsymbol{\theta}$ . (Sometimes we write $f(\mathbf{x})$ and omit the argument $\boldsymbol{\theta}$ to lighten notation)
$\ \mathbf{x}\ _p$	$L^p$ norm of $\mathbf{x}$
$\mathbf{1}(\text{condition})$	is 1 if the condition is true, 0 otherwise
GM Matching	Geometric Median Matching



## B ADDITIONAL DEFINITIONS

**Definition 5 (Multivariate Gaussian).** A Multivariate Gaussian (or normal) distribution for a random vector  $\mathbf{x} \in \mathbb{R}^d$  with mean  $\boldsymbol{\mu}$  and covariance matrix  $\boldsymbol{\Sigma}$  has the probability density function:

$$p(\mathbf{x}) = \frac{1}{(2\pi)^{d/2} |\boldsymbol{\Sigma}|^{1/2}} \exp\left(-\frac{1}{2}(\mathbf{x} - \boldsymbol{\mu})^\top \boldsymbol{\Sigma}^{-1}(\mathbf{x} - \boldsymbol{\mu})\right) \quad (33)$$

**Definition 6 (Isotropic Gaussian).** A Gaussian distribution is said to be isotropic if its covariance matrix is a scalar multiple of the identity matrix:

$$\boldsymbol{\Sigma} = \sigma^2 \mathbf{I} \quad (34)$$

where,  $\sigma^2 > 0$  is the variance (common to all dimensions) and  $\mathbf{I}$  is the  $d \times d$  identity matrix.

In this case, the density function simplifies to:

$$p(\mathbf{x}) = \frac{1}{(2\pi\sigma^2)^{d/2}} \exp\left(-\frac{1}{2\sigma^2} \|\mathbf{x} - \boldsymbol{\mu}\|^2\right) \quad (35)$$

**Key characteristics:**

- Equal variance in all directions: Every component of  $\mathbf{x}$  has the same variance  $\sigma^2$ .
- No correlations: The off-diagonal elements of the covariance matrix are zero.
- Circular (or spherical in higher dimensions): Level sets of the density (i.e., contours) are circles (or spheres) centered at  $\boldsymbol{\mu}$ .

**Definition 7 (Anisotropic Gaussian).** A Gaussian distribution is anisotropic if its covariance matrix is a general symmetric positive definite matrix that is not a scalar multiple of the identity:

$$\boldsymbol{\Sigma} \neq \sigma^2 \mathbf{I} \quad (36)$$

In this case, the full density function remains:

$$p(\mathbf{x}) = \frac{1}{(2\pi)^{d/2} |\boldsymbol{\Sigma}|^{1/2}} \exp\left(-\frac{1}{2}(\mathbf{x} - \boldsymbol{\mu})^\top \boldsymbol{\Sigma}^{-1}(\mathbf{x} - \boldsymbol{\mu})\right). \quad (37)$$

**Key characteristics:**

- Different variances along different axes: The eigenvalues of  $\boldsymbol{\Sigma}$  determine the variance along the corresponding eigen-directions.
- Possible correlations: Off-diagonal entries may be nonzero, indicating correlations between components.
- Elliptical contours: The level sets of the density are ellipsoids, which can be elongated in some directions and compressed in others.

**Definition 8 (Discrete Derivative).** For a set function  $f : 2^{\mathbb{E}} \rightarrow \mathbb{R}$ ,  $\mathbb{S} \subseteq \mathbb{E}$ ,  $e \in \mathbb{E} \setminus \mathbb{S}$  the discrete derivative or the marginal gain of  $f$  at  $\mathbb{S}$  with respect to  $e$  is defined as:

$$\Delta_f(e|\mathbb{S}) = f(\mathbb{S} \cup \{e\}) - f(\mathbb{S}) \quad (38)$$

**Definition 9 (Submodularity).** A set function  $f : 2^{\mathbb{E}} \rightarrow \mathbb{R}$  is submodular if  $\forall \mathbb{A} \subseteq \mathbb{B} \subseteq \mathbb{E}$  and  $e \in \mathbb{E} \setminus \mathbb{B}$  the following holds:

$$\Delta_f(e|\mathbb{A}) \geq \Delta_f(e|\mathbb{B}) \quad (39)$$

It can be shown that it is equivalent to the following condition:

$$f(\mathbb{A}) + f(\mathbb{B}) \geq f(\mathbb{A} \cap \mathbb{B}) + f(\mathbb{A} \cup \mathbb{B}) \quad (40)$$

### C LEMMA 3 : VULNERABILITY OF IMPORTANCE SCORE BASED PRUNING

In the ideal setting, given a batch of i.i.d samples  $\mu_y = \mu_y^{\mathcal{G}} = \mathbb{E}_{\mathbf{x} \sim \mathcal{D}_{\mathcal{G}}}(\mathbf{x})$ . However, the presence of even a single grossly corrupted sample can cause the centroid estimate to deviate arbitrarily from the true mean. Consider a single grossly corrupt sample  $(\mathbf{x}_i^{\mathcal{B}}, y_i)$  such that :

$$\mathbf{x}_i^{\mathcal{B}} = \sum_{(\mathbf{x}_i, y_i) \in \mathcal{D}} \mathbf{1}(y_i = y) \mu_y^{\mathcal{B}} - \sum_{(\mathbf{x}_i, y_i) \in \mathcal{D} \setminus (\mathbf{x}_i^{\mathcal{B}}, y_i)} \mathbf{1}(y_i = y) \mathbf{x}_i \quad (41)$$

resulting in shifting the estimated centroid  $\Delta \mu_y = \mu_y^{\mathcal{B}} - \mu_y^{\mathcal{G}}$

**Lemma 3.** *A single gross corrupted sample (41) causes the importance scores to deviate arbitrarily:*

$$\Delta d(\mathbf{x}_i, y_i) = \|\Delta \mu_y\|^2 - 2 \left( \mathbf{x}_i - \mu_y^{\mathcal{G}} \right)^T \Delta \mu_y \quad (42)$$

*Implying, these methods yield the lowest possible asymptotic breakdown of 0.*

#### C.1 PROOF OF LEMMA 3

*Proof.* The original importance score without the corrupted sample is:

$$d(\mathbf{x}_i, y_i) = \|\mathbf{x}_i - \mu_y^{\mathcal{G}}\|_2^2 \quad (43)$$

The importance score with the corrupted sample affecting the centroid is:

$$d'(\mathbf{x}_i, y_i) = \|\mathbf{x}_i - \mu_y^{\mathcal{B}}\|_2^2 \quad (44)$$

We can calculate the deviation as:

$$\begin{aligned} \Delta d(\mathbf{x}_i, y_i) &= d(\mathbf{x}_i, y_i) - d'(\mathbf{x}_i, y_i) \\ &= \left( \mathbf{x}_i - \mu_y^{\mathcal{B}} \right)^T \left( \mathbf{x}_i - \mu_y^{\mathcal{B}} \right) - \left( \mathbf{x}_i - \mu_y^{\mathcal{G}} \right)^T \left( \mathbf{x}_i - \mu_y^{\mathcal{G}} \right) \end{aligned}$$

The result follows by expanding and defining  $\Delta \mu_y = \mu_y^{\mathcal{B}} - \mu_y^{\mathcal{G}}$  ■

## D PROOF OF THEOREM 1

We restate the theorem for convenience:

**Theorem 1** Given a set of Grossly-corrupted samples  $\mathcal{D} = \mathcal{D}_G \cup \mathcal{D}_B$  (Definition 1) and an  $\epsilon$  approx. GM( $\cdot$ ) oracle (11). Further assume that  $\|\mathbf{x}\| \leq R \forall \mathbf{x} \in \mathcal{D}$  for some constant  $R$ . Then, GM Matching guarantees that the mean of the selected  $k$ -subset  $\mathcal{D}_S \subseteq \mathcal{D}$  converges to a  $\delta$ -neighborhood of the uncorrupted (true) mean  $\boldsymbol{\mu}(\mathcal{D}_G) = \mathbb{E}_{\mathbf{x} \in \mathcal{D}_G}(\mathbf{x})$  at the rate  $\mathcal{O}(\frac{1}{k})$  such that:

$$\delta^2 = \mathbb{E} \left\| \boldsymbol{\mu}_\epsilon^{\text{GM}}(\mathcal{D}) - \boldsymbol{\mu}(\mathcal{D}_G) \right\|^2 \leq \frac{8|\mathcal{D}_G|}{(|\mathcal{D}_G| - |\mathcal{D}_B|)^2} \sum_{\mathbf{x} \in \mathcal{D}_G} \mathbb{E} \left\| \mathbf{x} - \boldsymbol{\mu}(\mathcal{D}_G) \right\|^2 + \frac{2\epsilon^2}{(|\mathcal{D}_G| - |\mathcal{D}_B|)^2} \quad (45)$$

*Proof.* For notational simplicity, WLOG we will assume that the samples are already in RKHS i.e. we drop the notation  $\phi(\cdot)$  for the proof i.e. we assume that  $\mathbf{x}_i$  is already projected on the positive definite kernel space using a characteristic mapping  $\phi(\cdot)$ . We prove Theorem 1 in two main steps:

### D.1 BOUNDING ESTIMATION ERROR FROM APPROXIMATE GEOMETRIC MEDIAN

We will first establish the following result which follows from the definition of GM; see also (Lopuhaa et al., 1991; Minsker et al., 2015; Cohen et al., 2016; Chen et al., 2017; Li et al., 2019; Wu et al., 2020; Acharya et al., 2022) for similar adaptations.

**Lemma 4.** *Given a set of  $\alpha$ -corrupted samples  $\mathcal{D} = \mathcal{D}_G \cup \mathcal{D}_B$  (Definition 1), and an  $\epsilon$ -approx. GM( $\cdot$ ) oracle (11), then we have:*

$$\mathbb{E} \left\| \boldsymbol{\mu}_\epsilon^{\text{GM}}(\mathcal{D}) - \boldsymbol{\mu}(\mathcal{D}_G) \right\|^2 \leq \frac{8|\mathcal{D}_G|}{(|\mathcal{D}_G| - |\mathcal{D}_B|)^2} \sum_{\mathbf{x} \in \mathcal{D}_G} \mathbb{E} \left\| \mathbf{x} - \boldsymbol{\mu}(\mathcal{D}_G) \right\|^2 + \frac{2\epsilon^2}{(|\mathcal{D}_G| - |\mathcal{D}_B|)^2} \quad (46)$$

where,  $\boldsymbol{\mu}_\epsilon^{\text{GM}}(\mathcal{D})$  is the  $\epsilon$ -approximate GM over the entire ( $\alpha$ -corrupted) dataset; and  $\boldsymbol{\mu}(\mathcal{D}_G) = \frac{1}{|\mathcal{D}_G|} \sum_{\mathbf{x}_i \in \mathcal{D}_G} \mathbf{x}_i$  denotes the mean of the (underlying) uncorrupted set.

Now we prove this bound:

Note that, by using the triangle inequality, we can write:

$$\sum_{\mathbf{x}_i \in \mathcal{D}} \left\| \boldsymbol{\mu}_\epsilon^{\text{GM}}(\mathcal{D}) - \mathbf{x}_i \right\| \geq \sum_{\mathbf{x}_i \in \mathcal{D}_B} \left( \left\| \mathbf{x}_i \right\| - \left\| \boldsymbol{\mu}_\epsilon^{\text{GM}}(\mathcal{D}) \right\| \right) + \sum_{\mathbf{x}_i \in \mathcal{D}_G} \left( \left\| \boldsymbol{\mu}_\epsilon^{\text{GM}}(\mathcal{D}) \right\| - \left\| \mathbf{x}_i \right\| \right) \quad (47)$$

$$= \left( \sum_{\mathbf{x}_i \in \mathcal{D}_G} - \sum_{\mathbf{x}_i \in \mathcal{D}_B} \right) \left\| \boldsymbol{\mu}_\epsilon^{\text{GM}}(\mathcal{D}) \right\| + \sum_{\mathbf{x}_i \in \mathcal{D}_B} \left\| \mathbf{x}_i \right\| - \sum_{\mathbf{x}_i \in \mathcal{D}_G} \left\| \mathbf{x}_i \right\| \quad (48)$$

$$= \left( |\mathcal{D}_G| - |\mathcal{D}_B| \right) \left\| \boldsymbol{\mu}_\epsilon^{\text{GM}}(\mathcal{D}) \right\| + \sum_{\mathbf{x}_i \in \mathcal{D}} \left\| \mathbf{x}_i \right\| - 2 \sum_{\mathbf{x}_i \in \mathcal{D}_G} \left\| \mathbf{x}_i \right\|. \quad (49)$$

Now, by definition (13); we have that:

$$\sum_{\mathbf{x}_i \in \mathcal{D}} \left\| \boldsymbol{\mu}_\epsilon^{\text{GM}}(\mathcal{D}) - \mathbf{x}_i \right\| \leq \inf_{\mathbf{z} \in \mathcal{H}} \sum_{\mathbf{x}_i \in \mathcal{D}} \left\| \mathbf{z} - \mathbf{x}_i \right\| + \epsilon \leq \sum_{\mathbf{x}_i \in \mathcal{D}} \left\| \mathbf{x}_i \right\| + \epsilon \quad (50)$$

Combining these two inequalities, we get:

$$\left( |\mathcal{D}_G| - |\mathcal{D}_B| \right) \left\| \boldsymbol{\mu}_\epsilon^{\text{GM}}(\mathcal{D}) \right\| \leq \sum_{\mathbf{x}_i \in \mathcal{D}} \left\| \mathbf{x}_i \right\| - \sum_{\mathbf{x}_i \in \mathcal{D}} \left\| \mathbf{x}_i \right\| + 2 \sum_{\mathbf{x}_i \in \mathcal{D}_G} \left\| \mathbf{x}_i \right\| + \epsilon \quad (51)$$

This implies:

$$\left\| \boldsymbol{\mu}_\epsilon^{\text{GM}}(\mathcal{D}) \right\| \leq \frac{2}{\left( |\mathcal{D}_G| - |\mathcal{D}_B| \right)} \sum_{\mathbf{x}_i \in \mathcal{D}_G} \left\| \mathbf{x}_i \right\| + \frac{\epsilon}{\left( |\mathcal{D}_G| - |\mathcal{D}_B| \right)} \quad (52)$$

Squaring both sides,

$$\left\| \boldsymbol{\mu}_\epsilon^{\text{GM}}(\mathcal{D}) \right\|^2 \leq \left[ \frac{2}{(|\mathcal{D}_G| - |\mathcal{D}_B|)} \sum_{\mathbf{x}_i \in \mathcal{D}_G} \left\| \mathbf{x}_i \right\| + \frac{\epsilon}{(|\mathcal{D}_G| - |\mathcal{D}_B|)} \right]^2 \quad (53)$$

$$\leq 2 \left[ \frac{2}{(|\mathcal{D}_G| - |\mathcal{D}_B|)} \sum_{\mathbf{x}_i \in \mathcal{D}_G} \left\| \mathbf{x}_i \right\|^2 \right] + 2 \left[ \frac{\epsilon}{(|\mathcal{D}_G| - |\mathcal{D}_B|)} \right]^2 \quad (54)$$

Where the last step is a well-known consequence of the triangle inequality and AM-GM inequality.

Taking expectation on both sides, we have:

$$\mathbb{E} \left\| \boldsymbol{\mu}_\epsilon^{\text{GM}}(\mathcal{D}) \right\|^2 \leq \frac{8|\mathcal{D}_G|}{(|\mathcal{D}_G| - |\mathcal{D}_B|)^2} \sum_{\mathbf{x}_i \in \mathcal{D}_G} \mathbb{E} \left\| \mathbf{x}_i \right\|^2 + \frac{2\epsilon^2}{(|\mathcal{D}_G| - |\mathcal{D}_B|)^2} \quad (55)$$

Since, GM is **translation equivariant**, we can write:

$$\mathbb{E} \left[ \text{GM} \left( \left\{ \mathbf{x}_i - \boldsymbol{\mu}(\mathcal{D}_G) \mid \mathbf{x}_i \in \mathcal{D} \right\} \right) \right] = \mathbb{E} \left[ \text{GM} \left( \left\{ \mathbf{x}_i \mid \mathbf{x}_i \in \mathcal{D} \right\} \right) - \boldsymbol{\mu}(\mathcal{D}_G) \right] \quad (56)$$

Consequently, we have that :

$$\mathbb{E} \left\| \boldsymbol{\mu}_\epsilon^{\text{GM}}(\mathcal{D}) - \boldsymbol{\mu}(\mathcal{D}_G) \right\|^2 \leq \frac{8|\mathcal{D}_G|}{(|\mathcal{D}_G| - |\mathcal{D}_B|)^2} \sum_{\mathbf{x}_i \in \mathcal{D}_G} \mathbb{E} \left\| \mathbf{x}_i - \boldsymbol{\mu}(\mathcal{D}_G) \right\|^2 + \frac{2\epsilon^2}{(|\mathcal{D}_G| - |\mathcal{D}_B|)^2}$$

This concludes the proof of Lemma 4

## D.2 CONVERGENCE OF THE GREEDY UPDATES

We will now show that GM Matching converges to  $\boldsymbol{\mu}_\epsilon^{\text{GM}}(\mathcal{D})$  at  $\mathcal{O}(\frac{1}{k})$ .

It suffices to show that the error  $\delta = \left\| \boldsymbol{\mu}_\epsilon^{\text{GM}}(\mathcal{D}) - \frac{1}{k} \sum_{\mathbf{x}_i \in \mathcal{S}} \mathbf{x}_i \right\| \rightarrow 0$  asymptotically. We will follow the proof technique in (Chen et al., 2010) mutatis-mutandis to prove this result. We also assume that  $\mathcal{D}$  contains the support of the resulting noisy distribution.

We start by defining a GM-centered marginal polytope as the convex hull –

$$\mathcal{M}_\epsilon := \text{conv} \left\{ \mathbf{x} - \boldsymbol{\mu}_\epsilon^{\text{GM}}(\mathcal{D}) \mid \mathbf{x} \in \mathcal{D} \right\} \quad (57)$$

Then, we can rewrite the update equation (16) as:

$$\boldsymbol{\theta}_{t+1} = \boldsymbol{\theta}_t + \boldsymbol{\mu}_\epsilon^{\text{GM}}(\mathcal{D}) - \mathbf{x}_{t+1} \quad (58)$$

$$= \boldsymbol{\theta}_t - (\mathbf{x}_{t+1} - \boldsymbol{\mu}_\epsilon^{\text{GM}}(\mathcal{D})) \quad (59)$$

$$= \boldsymbol{\theta}_t - \left( \arg \max_{\mathbf{x} \in \mathcal{D}} \langle \boldsymbol{\theta}_t, \mathbf{x} \rangle - \boldsymbol{\mu}_\epsilon^{\text{GM}}(\mathcal{D}) \right) \quad (60)$$

$$= \boldsymbol{\theta}_t - \arg \max_{\mathbf{m} \in \mathcal{M}_\epsilon} \langle \boldsymbol{\theta}_t, \mathbf{m} \rangle \quad (61)$$

$$= \boldsymbol{\theta}_t - \mathbf{m}_t \quad (62)$$

Now, squaring both sides we get :

$$\|\boldsymbol{\theta}_{t+1}\|^2 = \|\boldsymbol{\theta}_t\|^2 + \|\mathbf{m}_t\|^2 - 2\langle \boldsymbol{\theta}_t, \mathbf{m}_t \rangle \quad (63)$$

Rearranging the terms we get:

$$\|\boldsymbol{\theta}_{t+1}\|^2 - \|\boldsymbol{\theta}_t\|^2 = \|\mathbf{m}_t\|^2 - 2\langle \boldsymbol{\theta}_t, \mathbf{m}_t \rangle \quad (64)$$

$$= \|\mathbf{m}_t\|^2 - 2\|\mathbf{m}_t\| \|\boldsymbol{\theta}_t\| \left\langle \frac{\boldsymbol{\theta}_t}{\|\boldsymbol{\theta}_t\|}, \frac{\mathbf{m}_t}{\|\mathbf{m}_t\|} \right\rangle \quad (65)$$

$$= 2\|\mathbf{m}_t\| \left( \frac{1}{2}\|\mathbf{m}_t\| - \|\boldsymbol{\theta}_t\| \left\langle \frac{\boldsymbol{\theta}_t}{\|\boldsymbol{\theta}_t\|}, \frac{\mathbf{m}_t}{\|\mathbf{m}_t\|} \right\rangle \right) \quad (66)$$

Assume that  $\|\mathbf{x}_i\| \leq r \forall \mathbf{x}_i \in \mathcal{D}$ . Then we note that,

$$\|\mathbf{x}_i - \boldsymbol{\mu}_\epsilon^{\text{GM}}(\mathcal{D})\| \leq \|\mathbf{x}_i\| + \|\boldsymbol{\mu}_\epsilon^{\text{GM}}(\mathcal{D})\| \leq 2r$$

Plugging this in, we get:

$$\|\boldsymbol{\theta}_{t+1}\|^2 - \|\boldsymbol{\theta}_t\|^2 \leq 2\|\mathbf{m}_t\| \left( r - \|\boldsymbol{\theta}_t\| \left\langle \frac{\boldsymbol{\theta}_t}{\|\boldsymbol{\theta}_t\|}, \frac{\mathbf{m}_t}{\|\mathbf{m}_t\|} \right\rangle \right) \quad (67)$$

Recall that,  $\boldsymbol{\mu}_\epsilon^{\text{GM}}(\mathcal{D})$  is guaranteed to be in the relative interior of  $\text{conv}\{\mathbf{x} \mid \mathbf{x} \in \mathcal{D}\}$  (Lopuhaa et al., 1991; Minsker et al., 2015). Consequently,  $\exists \kappa$ -ball around  $\boldsymbol{\mu}_\epsilon^{\text{GM}}(\mathcal{D})$  contained inside  $\mathcal{M}$  and we have  $\forall t > 0$

$$\left\langle \frac{\boldsymbol{\theta}_t}{\|\boldsymbol{\theta}_t\|}, \frac{\mathbf{m}_t}{\|\mathbf{m}_t\|} \right\rangle \geq \kappa > 0 \quad (68)$$

This implies,  $\forall t > 0$

$$\|\boldsymbol{\theta}_t\| \leq \frac{r}{\kappa} \quad (69)$$

Expanding the value of  $\boldsymbol{\theta}_t$ , we have:

$$\|\boldsymbol{\theta}_k\| = \left\| \boldsymbol{\theta}_0 + k\boldsymbol{\mu}_\epsilon^{\text{GM}}(\mathcal{D}) - \sum_{i=1}^k \mathbf{x}_k \right\| \leq \frac{r}{\kappa} \quad (70)$$

Apply Cauchy-Schwarz inequality:

$$\left\| k\boldsymbol{\mu}_\epsilon^{\text{GM}}(\mathcal{D}) - \sum_{i=1}^k \mathbf{x}_k \right\| \leq \|\boldsymbol{\theta}_0\| + \frac{r}{\kappa} \quad (71)$$

Normalizing both sides by the number of iterations  $k$

$$\left\| \boldsymbol{\mu}_\epsilon^{\text{GM}}(\mathcal{D}) - \frac{1}{k} \sum_{i=1}^k \mathbf{x}_k \right\| \leq \frac{1}{k} \left( \|\boldsymbol{\theta}_0\| + \frac{r}{\kappa} \right) \quad (72)$$

Thus, we have that GM Matching converges to  $\boldsymbol{\mu}_\epsilon^{\text{GM}}$  at the rate  $\mathcal{O}(\frac{1}{k})$ .

Combining this with Lemma 4, completes the proof of Theorem 1. ■

## E PROOF OF LEMMA 1

We restate the lemma for convenience:

**Lemma 1:** Suppose that we are given a set of grossly corrupted samples  $\mathcal{D} = \mathcal{D}_G \cup \mathcal{D}_B$  (Definition 1), an  $\epsilon$  approx. GM( $\cdot$ ) oracle (11) and bounded, characteristic feature map  $\phi(\cdot) : \mathbb{R}^d \rightarrow \mathcal{H}$  (Assumption 1). Then, GM Matching guarantees that:

$$\Delta^2 = \left\| \boldsymbol{\mu}(\mathcal{D}_S) - \boldsymbol{\mu}(\mathcal{D}_G) \right\|^2 \leq \mathcal{O}\left(\frac{1}{k^2}\right) + \frac{16}{(1-\alpha)^2} \sigma_G^2 + \frac{4\epsilon^2}{|\mathcal{D}_G|^2(1-\alpha)^2} \quad (73)$$

where,  $\alpha = |\mathcal{D}_B|/|\mathcal{D}_G| < 1$  is the ratio of corrupted and clean samples.  $\boldsymbol{\mu}(\mathcal{D}_S)$  and  $\boldsymbol{\mu}(\mathcal{D}_G)$  denote the mean of the selected subset and the true uncorrupted mean respectively.

*Proof.* We begin by decomposing the overall error using the triangle inequality:

$$\Delta^2 = \left\| \boldsymbol{\mu}(\mathcal{D}_S) - \boldsymbol{\mu}(\mathcal{D}_G) \right\|^2 \quad (74)$$

$$= \left\| \left( \boldsymbol{\mu}(\mathcal{D}_S) - \boldsymbol{\mu}_\epsilon^{\text{GM}}(\mathcal{D}) \right) + \left( \boldsymbol{\mu}_\epsilon^{\text{GM}}(\mathcal{D}) - \boldsymbol{\mu}(\mathcal{D}_G) \right) \right\|^2 \quad (75)$$

$$\leq 2 \left\| \boldsymbol{\mu}(\mathcal{D}_S) - \boldsymbol{\mu}_\epsilon^{\text{GM}}(\mathcal{D}) \right\|^2 + 2 \left\| \boldsymbol{\mu}_\epsilon^{\text{GM}}(\mathcal{D}) - \boldsymbol{\mu}(\mathcal{D}_G) \right\|^2 \quad (76)$$

**Bounding the first term.** The herding-style greedy procedure is designed to iteratively reduce the discrepancy between the empirical mean of the selected subset and the robust target moment  $\boldsymbol{\mu}_\epsilon^{\text{GM}}(\mathcal{D})$ . Standard results from the analysis of kernel herding imply that

$$\left\| \boldsymbol{\mu}(\mathcal{D}_S) - \boldsymbol{\mu}_\epsilon^{\text{GM}}(\mathcal{D}) \right\| = \mathcal{O}\left(\frac{1}{k}\right) \quad (77)$$

Thus, there exists a constant  $C_1 > 0$  such that

$$\left\| \boldsymbol{\mu}(\mathcal{D}_S) - \boldsymbol{\mu}_\epsilon^{\text{GM}}(\mathcal{D}) \right\|^2 \leq \frac{C_1}{k^2}. \quad (78)$$

**Bounding the second term.** By Theorem 1, the robust estimator  $\boldsymbol{\mu}_\epsilon^{\text{GM}}(\mathcal{D})$  satisfies

$$\left\| \boldsymbol{\mu}_\epsilon^{\text{GM}}(\mathcal{D}) - \boldsymbol{\mu}(\mathcal{D}_G) \right\|^2 \leq \frac{8|\mathcal{D}_G|^2}{(|\mathcal{D}_G| - |\mathcal{D}_B|)^2} \sigma^2(\mathcal{D}_G) + \frac{2\epsilon^2}{(|\mathcal{D}_G| - |\mathcal{D}_B|)^2}. \quad (79)$$

Since  $|\mathcal{D}_G| - |\mathcal{D}_B| = |\mathcal{D}_G|(1-\alpha)$  with  $\alpha = |\mathcal{D}_B|/|\mathcal{D}_G| < 1$ , we can rewrite the bound as

$$\left\| \boldsymbol{\mu}_\epsilon^{\text{GM}}(\mathcal{D}) - \boldsymbol{\mu}(\mathcal{D}_G) \right\|^2 \leq \frac{8}{(1-\alpha)^2} \sigma^2(\mathcal{D}_G) + \frac{2\epsilon^2}{|\mathcal{D}_G|^2(1-\alpha)^2}. \quad (80)$$

Multiplying both sides by 2 yields:

$$2 \left\| \boldsymbol{\mu}_\epsilon^{\text{GM}}(\mathcal{D}) - \boldsymbol{\mu}(\mathcal{D}_G) \right\|^2 \leq \frac{16}{(1-\alpha)^2} \sigma^2(\mathcal{D}_G) + \frac{4\epsilon^2}{|\mathcal{D}_G|^2(1-\alpha)^2}. \quad (81)$$

**Combining the bounds.** Substituting the bounds from (78) and (81) into (76), we obtain

$$\Delta^2 \leq \frac{2C_1}{k^2} + \frac{16}{(1-\alpha)^2} \sigma^2(\mathcal{D}_G) + \frac{4\epsilon^2}{|\mathcal{D}_G|^2(1-\alpha)^2}.$$

Since the constant  $2C_1$  can be absorbed into the  $\mathcal{O}(1/k^2)$  term, we conclude that

$$\Delta^2 \leq \mathcal{O}\left(\frac{1}{k^2}\right) + \frac{16}{(1-\alpha)^2} \sigma^2(\mathcal{D}_G) + \frac{4\epsilon^2}{|\mathcal{D}_G|^2(1-\alpha)^2}.$$

This completes the proof. ■

## F COMPUTING GEOMETRIC MEDIAN

As discussed earlier, we adopt the Weiszfeld algorithm( Algorithm 2) to compute the  $\epsilon$  approximate GM. Here, we provide the derivation and modifications to ensure numerical stability.

Recall the definition of GM (Definition 4):

$$\boldsymbol{\mu}^{\text{GM}} = \arg \min_{\mathbf{z} \in \mathcal{H}} \left[ \rho(\mathbf{z}) := \sum_{i=1}^n \left\| \mathbf{z} - \phi(\mathbf{x}_i) \right\| \right] \quad (82)$$

Note that the subgradient of  $\rho(\mathbf{z})$  at any point  $\mathbf{z}$  is given by:

$$\partial \rho(\mathbf{z}) = \sum_{i=1}^n \frac{\mathbf{z} - \mathbf{x}_i}{\|\mathbf{x}_i - \mathbf{z}\|}. \quad (83)$$

Let  $f(\mathbf{z}) = \|\mathbf{z} - \mathbf{x}_i\|$ , where:

$$f(\mathbf{z}) = \sqrt{(\mathbf{z} - \mathbf{x}_i)^\top (\mathbf{z} - \mathbf{x}_i)}.$$

The Euclidean norm can be expressed as:

$$\|\mathbf{z} - \mathbf{x}_i\| = \sqrt{\sum_{j=1}^d (z_j - x_{ij})^2}.$$

Define  $g(\mathbf{z}) = (\mathbf{z} - \mathbf{x}_i)^\top (\mathbf{z} - \mathbf{x}_i)$ , so:

$$f(\mathbf{z}) = \sqrt{g(\mathbf{z})}.$$

Using the chain rule, the gradient of  $f(\mathbf{z})$  with respect to  $\mathbf{z}$  is:

$$\nabla_{\mathbf{z}} f(\mathbf{z}) = \frac{1}{2\sqrt{g(\mathbf{z})}} \nabla_{\mathbf{z}} g(\mathbf{z}).$$

The function  $g(\mathbf{z})$  is given by:

$$g(\mathbf{z}) = (\mathbf{z} - \mathbf{x}_i)^\top (\mathbf{z} - \mathbf{x}_i),$$

and its gradient is:

$$\nabla_{\mathbf{z}} g(\mathbf{z}) = 2(\mathbf{z} - \mathbf{x}_i).$$

Substituting  $\nabla_{\mathbf{z}} g(\mathbf{z})$  into the chain rule:

$$\nabla_{\mathbf{z}} f(\mathbf{z}) = \frac{1}{2\sqrt{g(\mathbf{z})}} \cdot 2(\mathbf{z} - \mathbf{x}_i).$$

Since  $\sqrt{g(\mathbf{z})} = \|\mathbf{z} - \mathbf{x}_i\|$ , we have:

$$\nabla_{\mathbf{z}} \|\mathbf{z} - \mathbf{x}_i\| = \frac{\mathbf{z} - \mathbf{x}_i}{\|\mathbf{z} - \mathbf{x}_i\|}.$$

thus we have that the subgradient of the Euclidean norm  $\|\mathbf{z} - \mathbf{x}_i\|$  with respect to  $\mathbf{z}$  is:

$$\nabla_{\mathbf{z}} \|\mathbf{z} - \mathbf{x}_i\| = \frac{\mathbf{z} - \mathbf{x}_i}{\|\mathbf{z} - \mathbf{x}_i\|}.$$

To find the optimal solution  $\mathbf{z}^*$ , we can solve the condition:

$$\mathbf{0} \in \partial \rho(\mathbf{z}^*)$$

Substituting  $\mathbf{z} = \mathbf{z}^*$  and re-arranging the terms, we get:

$$\mathbf{z}^* = \frac{\sum_{i=1}^n \frac{\mathbf{x}_i}{\|\mathbf{x}_i - \mathbf{z}^*\|}}{\sum_{i=1}^n \frac{1}{\|\mathbf{x}_i - \mathbf{z}^*\|}}.$$

Since this equation is non-linear in  $\mathbf{z}^*$ , solving it directly is infeasible. Instead, the Weiszfeld algorithm approximates  $\mathbf{z}^*$  iteratively using the update:

$$\mathbf{z}^{(k+1)} = \frac{\sum_{i=1}^n \frac{\mathbf{x}_i}{\|\mathbf{x}_i - \mathbf{z}^{(k)}\|}}{\sum_{i=1}^n \frac{1}{\|\mathbf{x}_i - \mathbf{z}^{(k)}\|}}$$

where  $\mathbf{z}^{(k)}$  is the estimate at the  $k$ -th iteration.

This update step can be interpreted as a re-weighted average, where the weights are inversely proportional to the distance of each point  $\mathbf{x}_i$  from the current estimate  $\mathbf{z}^{(k)}$ . Points closer to  $\mathbf{z}^{(k)}$  contribute most to the next estimate.

### Handling Non-Differentiability :

At points where  $\mathbf{z}^{(k)} = \mathbf{x}_i$  i.e. the current estimate coincides with one of the observations, the term  $\|\mathbf{x}_i - \mathbf{z}^{(k)}\| = 0$  results in division by zero. To address this, the algorithm excludes the term corresponding to  $\mathbf{x}_i$  from the summation. Alternatively, the subgradient of  $\|\mathbf{x}_i - \mathbf{z}\|$  at  $\mathbf{z} = \mathbf{x}_i$  can be defined as:

$$\partial\|\mathbf{x}_i - \mathbf{z}\| = \begin{cases} \frac{\mathbf{z} - \mathbf{x}_i}{\|\mathbf{x}_i - \mathbf{z}\|} & \text{if } \mathbf{z} \neq \mathbf{x}_i, \\ \{\mathbf{g} : \|\mathbf{g}\| \leq 1\} & \text{if } \mathbf{z} = \mathbf{x}_i. \end{cases}$$

### Convergence and Regularization:

Notably, the Weiszfeld algorithm converges under mild conditions if the initial point  $\mathbf{z}^{(0)}$  is not chosen at one of the data points. Convergence can be shown using fixed-point theory or by analyzing the decrease in the objective function  $\rho(\mathbf{z})$  at each iteration. However, convergence is only guaranteed to a local minimum if the data points  $\mathbf{x}_i$  are not in general position (e.g., collinear points in  $\mathbb{R}^2$ ). To handle singularities, we modify the denominator to avoid division by zero:

$$\mathbf{z}^{(k+1)} = \frac{\sum_{i=1}^n \frac{\mathbf{x}_i}{\|\mathbf{x}_i - \mathbf{z}^{(k)}\| + \delta}}{\sum_{i=1}^n \frac{1}{\|\mathbf{x}_i - \mathbf{z}^{(k)}\| + \delta}}$$

where  $\delta > 0$  is a small regularization term.